

Physics of adherent cells

Ulrich S. Schwarz

*BioQuant and Institute for Theoretical Physics,
Heidelberg University,
Philosophenweg 19,
69120 Heidelberg,
Germany*

Samuel A. Safran

*Department of Materials and Interfaces,
Weizmann Institute, Rehovot 76100,
Israel*

(Dated: September 12, 2013)

One of the most unique physical features of cell adhesion to external surfaces is the active generation of mechanical force at the cell-material interface. This includes pulling forces generated by contractile polymer bundles and networks, and pushing forces generated by the polymerization of polymer networks. These forces are transmitted to the substrate mainly by focal adhesions, which are large, yet highly dynamic adhesion clusters. Tissue cells use these forces to sense the physical properties of their environment and to communicate with each other. The effect of forces is intricately linked to the material properties of cells and their physical environment. Here we review recent progress in our understanding of the role of forces in cell adhesion from the viewpoint of theoretical soft matter physics and in close relation to the relevant experiments.

CONTENTS

I. Introduction	1	VII. Cell assemblies	46
II. Physics background	3	A. Matrix-mediated cell interactions	46
A. Soft matter in biological systems	3	B. Elastic interactions of force dipoles	47
B. Liquid crystals	4	C. Myofibril registry modulated by substrate elasticity	47
C. Semi-flexible polymers	5		
D. Polymer gels	6	VIII. Conclusions and outlook	49
E. Elements of elasticity	7	IX. Acknowledgements	51
F. Adhesion of vesicles and capsules	9	References	52
III. Biology Background	11		
A. Actin cytoskeleton and cell adhesion	11		
B. Actin filaments and their assemblies	14		
C. Actomyosin contractility	16		
D. Focal adhesions	17		
IV. Physics of cell-matrix adhesions	19		
A. Physical motivation	19		
B. Stability of stationary adhesion clusters under force	20		
C. Adhesion between moving surfaces	22		
D. Load localization and fracture in adhesions	24		
E. Adsorption kinetics for growing adhesions	25		
F. Force-induced growth of adhesions	27		
V. Cell shape and forces	29		
A. Physical motivation	29		
B. Contour-models for cell shape	30		
C. Whole-cell models	32		
D. Force from shape	35		
VI. Active response of cells	35		
A. Mechanical response of force dipoles	35		
B. Force dipoles and their interactions	37		
C. Elastic model for cells on a substrate	38		
D. Cell polarization guided by substrate rigidity	40		
E. Single cell response to rigidity gradients	41		
F. Dynamical response of cells to mechanical stress	42		

I. INTRODUCTION

Observations of swimming bacteria, crawling animal cells or developing organisms dramatically indicate that physical force and movement are central to the behavior of biological systems (Huang and Ingber, 1999; Kollmannsberger *et al.*, 2011; Lecuit and Lenne, 2007; Thompson, 1992). The functions of cells have evolved in the context of very specific physical environments leading to a close coupling between cells and their surroundings (Alberts *et al.*, 2007; Phillips *et al.*, 2008). This is especially true for animal cells, which have evolved in the controlled environment provided by multi-cellular organisms and therefore appear to be more sensitive to environmental cues than *e.g.*, uni-cellular organisms that can sometimes live in very harsh surroundings. Therefore it is an essential element of understanding animal cells to consider their physical interactions with the environment.

During recent years, it has become increasingly clear that the cell-material interface determines the behaviour and fate of biological cells to a much larger extent than

was formerly appreciated (De *et al.*, 2010; Discher *et al.*, 2009, 2005; Geiger *et al.*, 2009; Hoffman *et al.*, 2011; Janmey *et al.*, 2009; Ladoux and Nicolas, 2012; Mitragotri and Lahann, 2009; Schwarz and Bischofs, 2005; Schwarz and Gardel, 2012; Vogel and Sheetz, 2006). For example, it has been shown that the differentiation of stem cells can be guided by the mechanical or adhesive properties of the substrate (Engler *et al.*, 2006; Fu *et al.*, 2010; Kilian *et al.*, 2010). Such observations can lead the way to exciting new applications for regenerative medicine and tissue engineering, because physical signals are easier to control and can be more permanent than biochemical or genetic manipulations. On the scientific side, however, the fundamentals of these processes are puzzling and not yet well understood, despite their importance in development, health and disease (DuFort *et al.*, 2011; Janmey and Miller, 2011).

From a physical point of view, the most important aspect of the cellular response to the physical properties of the environment is the observation that cells show a controlled response only if they are able to actively generate force and to transmit this force to the surroundings. This finding makes sense because cells must actively sense the passive properties of their environment. For rigidity sensing, for example, cells must actively strain their surroundings to probe their elastic properties (similar to a bat that senses the geometry of its environment by sending out ultrasound). Cells have evolved special sensory systems for this purpose. For example, it has been found that the size of the contacts between cells and their environment grow with physical force (Balaban *et al.*, 2001; Choquet *et al.*, 1997; Chrzanowska-Wodnicka and Burridge, 1996; Colombelli *et al.*, 2009; Paul *et al.*, 2008; Riveline *et al.*, 2001; Tan *et al.*, 2003; Trichet *et al.*, 2012). Although this finding makes sense from a biological viewpoint, it is at the same time puzzling to the physicist, since in materials science, force usually disrupts adhesion contacts.

Physicists have traditionally been reluctant to study living systems due to their molecular complexity. However, this has recently changed in many ways. An important development that has led to physics approaches to describe cells and tissue is the maturation of soft matter physics into an independent and very active field of research. Soft matter physics traditionally has focused on the properties of liquid crystals, colloidal dispersions, emulsions, fluid membranes, polymer gels and other complex fluids (Chaikin and Lubensky, 2000; de Gennes, 1992; Jones, 2002; Safran, 2003). These systems are *soft* since the interaction energies are of the same order as the thermal energy. They are thus very sensitive to thermal fluctuations and concepts from both mechanics and statistical mechanics must be employed to understand phenomena such as, *e.g.*, conformational changes of membranes (Powers, 2010; Seifert, 1997) or deformations of polymer networks (Bausch and Kroy, 2006; Chen *et al.*,

2010b). While soft matter physics has established a firm physical basis of the building blocks of biological cells, their behavior critically depends on additional elements, most prominently active remodeling controlled by genetic and signaling networks. Meeting the challenge of combining the physics of soft matter physics with active processes to describe *active matter* will enable insight into many biological processes, guide the design of new types of materials and further extend the range of phenomena that can be analyzed by concepts and methods from physics (Fletcher and Geissler, 2009; Gonzalez-Rodriguez *et al.*, 2012; Huber *et al.*, 2013; MacKintosh and Schmidt, 2010; Marchetti *et al.*, 2013; Ramaswamy, 2010).

To understand the physical aspects of cell adhesion, soft matter physics provides useful model reference systems, such as the wetting of substrates by droplets (de Gennes, 1985), adhesion of vesicles made of fluid membranes (Seifert, 1997) or the adhesion of capsules that comprise thin polymer shells (Pozrikidis and Pozrikidis, 2003). The challenge is to combine these reference systems with the molecularly specific and active processes that they support at the cell-material interface, such as force generation by polymerization (Mogilner, 2006) or the binding and unbinding of transmembrane adhesion receptors (Evans and Calderwood, 2007). Over the last decade, several soft matter systems have been revisited with a focus on this particular point of view. The physical understanding of the properties of active materials is rapidly growing; particular attention has been paid to active membranes (Gov, 2004; Manneville *et al.*, 2001) and active gels (Julicher *et al.*, 2007; Kruse *et al.*, 2004; Liverpool and Marchetti, 2003; Marchetti *et al.*, 2013).

Cell adhesion is a multi-scale problem because the molecular processes at the cell-material interface are dramatically amplified on the scale of cells. Cellular processes such as spreading, adhesion, migration and proliferation are in turn dramatically amplified on the scale of tissues (Gonzalez-Rodriguez *et al.*, 2012). Interestingly, similar concepts have been successfully applied to different levels in this hierarchy. In order to address the role of cellular forces in the context of connective tissue, whose mechanical properties are dominated by the extracellular matrix, one can build on traditional approaches from condensed matter physics for force-generating centers in a continuum matrix, such as the theory of elastic defects and their interactions (Eshelby, 1957, 1959; Lau and Kohn, 1977; Safran and Hamann, 1979; Siems, 1968; Wagner and Horner, 1974). Motivated by experimental measurements of cellular traction patterns (Butler *et al.*, 2002; Dembo and Wang, 1999; Schwarz *et al.*, 2002), it has been suggested that the contractile activity of cells can be modeled as anisotropic force contraction dipoles (Schwarz *et al.*, 2002; Schwarz and Safran, 2002) and that cell orientation and positioning can be predicted by minimizing the energy invested by the cell into straining its environment for a given level of force generation (Bischofs

et al., 2004; Bischofs and Schwarz, 2003). Similar concepts have been used to predict the contractile action of molecular motors in the cytoskeleton (Dasanayake *et al.*, 2011; Silva *et al.*, 2011), the orientation response of single cells to externally applied stress (De *et al.*, 2007), the collective response of contractile cells in an elastic medium (Zemel *et al.*, 2006), the polarization and registry of cells as a function of external rigidity (Friedrich and Safran, 2011, 2012; Zemel *et al.*, 2010b), and the growth of tissue where dividing cells correspond to force dipoles (Ranft *et al.*, 2010). Thus the concept of force dipoles is very general, with applications to molecular, cellular and tissue scales. However, the details of these different applications strongly depend on the biological situation of interest.

For epithelial tissue dominated by direct cell-cell contacts, other approaches are adequate, most prominently vertex models starting from the fact that cell walls are strongly contractile (Aegerter-Wilmsen *et al.*, 2010; Aliee *et al.*, 2012; Canelas-Xandri *et al.*, 2011; Farhadifar *et al.*, 2007; Hufnagel *et al.*, 2007; Landsberg *et al.*, 2009; Rauzi *et al.*, 2008). Although this situation is somehow reminiscent of foams, due to the presence of cell proliferation and death we are dealing with an active material (Basan *et al.*, 2009; Ranft *et al.*, 2010; Shraiman, 2005). This shows again that within the overarching framework of active materials, different physics concepts have to be used depending on the biological context.

Because biological systems are very complex, meaningful mathematical models must be selective and focus on phenomena that can be treated in a tractable manner in order to yield physical insight. The role of forces at the cell-material interface is certainly a phenomenon which can be only be fully understood with concepts and tools from physics. For future progress, it is essential to choose the appropriate parameters and formulate models that are sufficiently simple to be analysed in detail, but predictive enough to be verified or falsified by experiments. A theoretical analysis has many benefits. Apart from providing deeper insight and quantitative predictions, it usually reveals relations between quantities or phenomena that would go unnoticed without a theoretical model. For example, the interplay between cell adhesion and mechanics leads to interesting predictions regarding the coupling of cell shape and forces (Bar-Ziv *et al.*, 1999; Bischofs *et al.*, 2008, 2009; Deshpande *et al.*, 2006; Guthardt Torres *et al.*, 2012). A major focus of this review is to point out the relations between cell shape, structure, adhesion, and force as they emerge from our growing physical understanding of the role of physical forces at the cell-material interface.

This review is organized as follows. We start with a survey of the relevant soft matter physics that describes and quantifies those parts of cells that are involved in force transmission. In particular, we review the properties of liquid crystals, flexible and semi-flexible chains

and gels, and elements of elasticity theory, for both bulk systems such as elastic solids as well as for finite-sized systems such as vesicles and capsules. We then present the minimally required cell biology background, including a general discussion of the cytoskeleton and the properties of actin polymers and networks, myosin molecular motors that endow these networks with active contractility, and the membrane-based adhesion structures that connect cells to their environment. The main part of this review then covers recent developments in the physics of adherent cells. In the spirit of a multiscale approach, we start on a relatively small scale with simple models for the physics of adhesion clusters. We then progress to models for cell shape and structure, which in turn form the basis for coarse-grained models for entire cells as force dipoles. In particular, we use this framework to discuss cell response to mechanical stress as well as actin network polarization and its dependence on the elasticity of the underlying matrix. Finally we address the physics of matrix-mediated cell assemblies from the viewpoint of cellular forces. We close with some conclusions and an outlook on future perspectives.

II. PHYSICS BACKGROUND

A. Soft matter in biological systems

The present review on physical forces at the cell-material interface focuses on a view of animal cells as complex, composite, soft materials comprising fluid membranes that are coupled to two types of elastic and often contractile polymer networks. Inside the cell, there exists a highly crosslinked and entangled network of three different types of polymers (actin filaments, microtubules and intermediate filaments) collectively called the *cytoskeleton* (CSK). On the outside, the cell is coupled to another multi-component, gel-like network (including fibrous protein components such as collagen or fibronectin) called the *extracellular matrix* (ECM). If subjected to mechanical forces, the biological material initially responds like a passive elastic body; thus elasticity theory is an essential element of the physics of cells and tissues. At longer time scales, the cell can respond to mechanical perturbations by actively reorganizing the structure of its CSK (and to a certain extent, its ECM as well).

Experiments suggest that cells in solution respond elastically up to times on the order of a few seconds (Wottawah *et al.*, 2005). The same is true for tissue on a timescale of seconds and minutes (Gonzalez-Rodriguez *et al.*, 2012). The deformation of an elastic body induces both stress and strain. For example, for a simple, one dimensional stretch of an elastic slab, the stress σ is the force per area applied to the slab on its top and bottom faces, while the strain ϵ is the resulting relative change in length (for a more detailed introduction to the tensorial

theory of elasticity see below). The simplest constitutive relation that relates stress and strain is a linear one in which $\sigma = E\epsilon$. The elastic constant E introduced in this way is known as *Young's modulus* and is often called the *stiffness* or *rigidity*. The larger the Young's modulus, the more stress is required to stretch the material to the same extent. Because strain ϵ is dimensionless, the Young's modulus has the same physical dimensions as stress σ , that is $\text{N/m}^2 = \text{Pa}$. Physically, this means that the elastic modulus is a measure of the mechanical energy density of the system. The corresponding spring constant $k = EA/L_0$ also depends on two geometrical quantities: the cross-sectional area A and the rest length L_0 of the spring.

For much of our discussion of cell elasticity, it is essential to note that the elastic modulus of a typical tissue cell is in the range of 10 kPa (comparable to very soft cheese or toothpaste). This should be contrasted with the much higher values of crystal moduli of 100 GPa. With a typical size of the supramolecular assembly of 10 nm, simple scaling predicts that the typical energy scale for cells is in the range of $10\text{kPa}(10\text{nm})^3 = 10^{-20}\text{J}$, which is close to the thermal energy scale $k_B T = 4.1 \cdot 10^{-21}\text{J} = 4.1 \text{ pN nm}$ (here we have used $T = 300\text{K}$ since most of biology operates at room or body temperature). Although somehow simplistic, this argument nevertheless correctly indicates that the cohesive interactions that stabilize cells are weak. These are mainly electrostatic attractions between charges or charge distributions (mainly dipoles) that are screened by water and relatively high salt concentration (100 mM corresponding to a Debye screening length of about 1 nm), hydrogen bridges, hydrophobic interactions due to the special properties of water, and entropic forces such as depletion interactions, all of which operate on an energy scale of a few $k_B T$ (Dill and Bromberg, 2010; Israelachvili, 2011).

The relatively weak cohesive energies are also related to the large length scales that characterize soft matter, since it is often the energy density (energy per unit volume) that is relevant. For example, the large-scale structures of linear macromolecules (polymers) in solution can be described by disordered, blob-like structures where the typical blob size can be hundreds of Angstroms (de Gennes, 1979). Water-amphiphile dispersions can exhibit disordered, sponge-like structures consisting of bilayer sheets of amphiphilic molecules whose sizes can be a hundred times the size of an individual molecule (Safran, 2003; Schwarz and Gompper, 2002). Even those soft materials that show solid-like elasticity, such as gels (Boal, 2012; de Gennes, 1979) or colloidal crystals (Pieranski, 1983), have mesh or lattice constants that are in the range of hundreds to thousands of Angstrom. In addition, the overall weak nature of the interactions (*e.g.*, gels with dilute crosslinks separated by large distances, colloidal particles with small surface charges), results in shear elastic constants that can be many orders of mag-

nitude weaker than those of hard-matter. The weak, non-covalent nature of the interactions in soft matter often compete with the entropy of the system and leads to large responses and variations in the structures and phases as the temperature or composition is varied. The soft matter topics that are most closely related to cellular forces are liquid crystals, polymers and gels, elasticity and the adhesion of fluid drops, amphiphilic vesicles and polymerized capsules.

In practice, the mechanical properties of cells are described by linear elasticity only in a limited regime, and there exists a hierarchy of length and energy scales that determine how cells respond to force. In fact, the viscoelastic response of cells has been measured using various techniques, in different situations and over a large range of frequencies (Fung, 1993). These measurements show that cells share many of the features of the viscoelasticity of *in vitro*, reconstituted networks of biopolymers (Bausch and Kroy, 2006; Chen *et al.*, 2010b).

While synthetic soft matter systems are subject and sensitive to thermal disorder, biological cells exhibit far more noisy behavior (Pearson, 2008) due to the stochastic nature of many of the biomolecular processes that take place; in our context such non-thermal noise occurs mainly in the context of force generation by molecular motors (Howard, 2001) and actin polymerization (Mogilner, 2006). If these processes are correlated only on molecular length and time scales, we can regard them as *active white noise* with regard to modeling cellular behavior on much longer scales. In that case, the molecular processes can be approximated as being delta correlated in both space and time the results of which (Haken, 1983) resemble an *effective temperature* that determines the width of a Boltzmann-like distribution. However, this cannot not be generalized to the role of an effective temperature in a true thermodynamic sense (Ben-Isaac *et al.*, 2011). In particular, the fluctuation-dissipation theorem (Chaikin and Lubensky, 2000) is not obeyed (Mizuno *et al.*, 2007) as it is in thermal systems. With these caveats firmly in mind, we shall use the concept of effective temperature and the resulting Boltzmann distribution of cellular energies in situations in which the molecular noise can be regarded as delta-correlated.

B. Liquid crystals

We begin our review of relevant physical systems with liquid crystals, which comprise anisotropic (*e.g.*, rod-like) molecules that can show orientational (*nematic*) order, but not necessarily positional (translational) order (de Gennes and Prost, 1995). At lower temperatures, nematically ordered systems can show a type of one-dimensional (*smectic*) order in which the molecules form well-defined layers with the molecular axis oriented parallel to the layer normal (*smectic A*). The layers them-

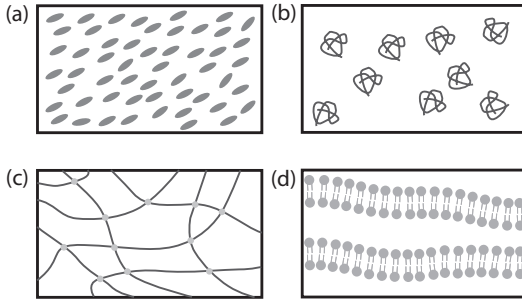


FIG. 1 Passive bulk soft matter examples that are important model systems for the understanding of the material properties of cells and tissues. (a) Liquid crystals often form nematic phases, with no positional but orientational order. (b) In a dilute polymer solution, each polymer forms a globule that is well separated from the other polymers. (c) A cross-linked polymer gel can behave like an elastic solid but with much weaker rigidity. (d) Lipids self-assemble into fluid bilayers, that at high concentration in turn tend to self-assemble into stacks, the so-called lamellar phase.

selves are fluid with no translational, in-plane order. The relevance of liquid crystal ordering to cells lies in the fact that under external forces (shear flow or elastic deformation) or in elastic environments of appropriate rigidity, the polymer networks inside cells can show nematic and even smectic order; these applications are discussed later on and here we outline the relevant liquid crystal physics.

The cooperative, orientational interactions between rod-like molecules can give rise to phase transitions in which they all align in a given direction, as in Fig. 1(a) (de Gennes and Prost, 1995). Such nematic ordering transitions can arise when the temperature is lowered in systems governed by microscopic interactions that promote order. Microscopically, each molecule is characterized by its thermally fluctuating orientation angle θ where the z axis that defines the angle can be defined by convention or by some macroscopic, symmetry breaking field such as the (non-spherical) shape of the system. Because the rod-like molecules have up-down symmetry, the interaction energy cannot be an odd function of the angle since that changes sign when the rod is flipped. Instead, the energies must be even functions of θ .

These symmetry considerations allow the definition of the local value of the nematic order parameter, S_i , of a given molecule labelled by i as:

$$S_i = \frac{1}{2} (3 \cos \theta_i^2 - 1) \quad (1)$$

A simple mean-field theory for nematic ordering was formulated by Maier and Saupe (Maier and Saupe, 1959). The Hamiltonian of the interacting system of rods in which the energy depends on the local orientations of nearby molecules is replaced by a one-body approximation, U_{ms} in which the energy of a given molecule is proportional to the product of its order parameter with the

thermal average of the average order parameter of the system, $\langle S \rangle$. The mean-field nature of this assumption lies in the fact that the orientations of neighboring, interacting molecules is approximated by the average order parameter

$$U_{ms} = B \langle S \rangle \sum_i S_i \quad (2)$$

where B is a constant that characterizes the interactions. The order parameter is determined self-consistently from the statistical mechanical definition of the thermal average in which the probability distribution is proportional to the Boltzmann factor, $\exp[-U_{ms}/k_B T]$:

$$\langle S \rangle = \frac{1}{Z} \int d\Omega S_i \exp[-B \langle S \rangle S_i / k_B T] \quad (3)$$

where Ω is the solid angle and the normalization Z is the average of the $\exp[-U_{ms}/k_B T]$ over all solid angles.

This approximation correctly predicts a first order phase transition at which the average order parameter $\langle S \rangle$ jumps from a value of zero to a value of approximately 0.4 when $B/k_B T = 4.6$. As the temperature is lowered, the order parameter increases till it reaches its saturation value of unity. The molecules are still in the fluid state; there is no translational order, but only orientational order.

C. Semi-flexible polymers

Semi-flexible polymers (also known as *worm-like chains*) (Marko and Siggia, 1995; Nobuhiko Sait and Yunoki, 1967) are long, one-dimensional chains of N molecules (monomeric units) whose intermolecular bonds resist bending; this is in contrast to flexible chains (de Gennes, 1979) where there is no energetic penalty for bending (at scales that are comparable to the size of a monomer) and which are completely governed by entropy. Both types of polymers form globules, as in Fig. 1(b), but with different typical sizes. The physics of flexible chains are well known (Doi, 1996; de Gennes, 1979; Rubinstein and Colby, 2003) and their resistance to changes of their “size” (end-to-end distance or radius of gyration, R) away from their “random walk” or Gaussian conformation where $R \sim N^{1/2}$ is characterized in a mean-field treatment by a free energy per chain

$$f = \frac{3k_B T}{2} \frac{R^2}{Na^2} \quad (4)$$

where N is the number of monomers in the chain and a is the monomer size. Self-avoidance of the chain due to excluded volume interactions among the monomers leads to additional interactions and in a mean-field treatment the scaling of R with N is modified so that $R \sim N^{3/5}$. Many biopolymers including DNA and various cytoskeletal filaments such as actin and microtubules discussed later

on, are semi-flexible, and only bend on length scales of 50 nm (DNA) through micrometers (actin) or even millimeters (microtubules), while synthetic polymers such as polystyrene in organic solvents are flexible and easily bend on nanometric scales.

On a coarse-grained, continuum level, the bending resistance of a semi-flexible polymer is similar to that of an elastic rod (Landau and Lifshitz, 1970). Bending is geometrically characterized by the curvature of the position vector of the rod, $\vec{R}(s)$ which is a function of the monomer distance, s , along the contour ($0 \leq s \leq L$, where L is the contour length of the rod). For systems where positive and negative curvatures are equivalent by symmetry, there can be no terms in the energy that are linear in curvature, so that in a small curvature expansion (appropriate when the radius of curvature is much larger than a monomer size), the energy, H_b , is quadratic in the chain curvature (Landau and Lifshitz, 1970):

$$H_b = \frac{\kappa}{2} \int_0^L ds \left(\frac{d^2 \vec{R}}{ds^2} \right)^2 \quad (5)$$

where κ is the bending modulus that characterizes the elastic resistance to bending. The lowest energy deformations of the rod are the bending modes that do not result in an overall volume change of the rod and involve only relative extension and compression of its upper and lower surfaces (Landau and Lifshitz, 1970). For most purposes one assumes that the rod is inextensible and neglects any stretching of the center of mass distances between molecules. This is expressed by the inextensibility constraint that leaves the rod length unchanged:

$$L = \int_0^L ds \left| \frac{d\vec{R}}{ds} \right| \quad (6)$$

and is equivalent to the requirement that the tangent vector given by $d\vec{R}/ds$ is a unit vector.

In equilibrium, a semi-flexible polymer represented by such a rod undergoes thermally driven motion that is resisted by the bending energy. The inextensibility constraint makes this problem difficult to treat exactly (Marko and Siggia, 1995; Nobuhiko Sait and Yunoki, 1967; Rubinstein and Colby, 2003). For small deformations of a chain oriented in the z direction, one can approximate $s \approx z$ and describe the chain position by $\vec{R} = (X(z), Y(z), z)$. The deformations can be resolved into their Fourier components $X(q) = \int dz X(z) e^{iqz}$ that are the normal modes which diagonalize the bending Hamiltonian. Using the equipartition theorem one finds that $\langle |X(q)|^2 \rangle = k_B T / (\kappa q^4)$ and one can show that the tangent vectors $\hat{t} = d\vec{R}/dz$ of neighboring points are nearly equal with:

$$\langle (\hat{t}(z) - \hat{t}(0))^2 \rangle \sim k_B T \int dq \frac{(1 - \cos(qz))}{\kappa q^2} \sim \frac{k_B T}{\kappa} z \quad (7)$$

The tangent correlations diverge as the distance between the points along the rod increases and for large z this invalidates the approximation of small fluctuations and inextensibility (equivalent to a unit tangent vector). However, one can find the value of z at which the tangent correlations first become of order unity; this defines the persistence length (Phillips *et al.*, 2008; Rubinstein and Colby, 2003), ζ of the chain and one finds $\zeta \sim \kappa / (k_B T)$. At scales smaller than the persistence length, the chain shows rigid-rod like behavior with relatively small bending fluctuations; at longer scales, the fluctuations are large and a random walk (or excluded volume random walk) picture is more appropriate.

D. Polymer gels

While single cytoskeletal proteins such as actin filaments or microtubules can be modeled as semi-flexible polymers, the CSK often contains crosslinked assemblies (gels) comprising these proteins, as in Fig. 1(c). The assemblies can be network-like (macroscopically isotropic) or ordered into bundle-like filaments. Here we review the response of semi-flexible polymers to applied, static forces that stretch the chains and determine the regimes in which the chains respond linearly or non-linearly to applied force.

For simplicity, we focus on a chain whose projected length is less than or of the order of its persistence length. In the context of a crosslinked gel, the projected length is determined by the distance between the crosslinks, assuming permanent crosslinks at whose positions the polymer is rigidly held fixed. The dissociation of the crosslinks disrupts the network and can lead to non-elastic (*e.g.*, viscous flow) response to stress; however, we focus on the early time (tens of seconds and possibly more in strongly adherent cells) behavior where the network response to force is elastic in nature (Wottawah *et al.*, 2005). We consider the elastic response of a single, semi-flexible polymer. Naively, one might think that this response will be typical of a polymer segment in the gel whose projected length is the *average* spacing between crosslinks; the distribution of crosslinks in the gel implies a distribution of polymer segment lengths between crosslinks. This would indeed be true for affine deformations, in which each chain is stretched in the same proportions as the macroscopically applied stress or strain. However, for large deformations, where the elastic response is highly non-linear, the distribution of stresses among the chains with varying segment lengths can be length dependent; the stresses will not be affine and it is harder to associate the gel with the response of one chain of *average* segment length (Head *et al.*, 2003a,b; Heussinger and Frey, 2006; Heussinger *et al.*, 2007; Wilhelm and Frey, 2003).

Before treating the case of semi-flexible polymers, we

briefly derive the elastic modulus that characterizes the response of flexible polymers to applied forces (so-called *rubber elasticity*). The modulus is completely determined by the changes in the chain entropy that are due to the applied strain, $\epsilon_i = \lambda_i - 1$ ($i = x, y, z$) that changes the macroscopic dimensions of the sample from (L_x, L_y, L_z) to $(\lambda_x L_x, \lambda_y L_y, \lambda_z L_z)$. Incompressibility of the chains and solvent implies that the volume must remain unchanged, so that the product $\lambda_x \lambda_y \lambda_z = 1$. The free energy per chain in the unstressed system is given by Eq. (5) and for affine strains where $\vec{R} = (X, Y, Z) \rightarrow (\lambda_x X, \lambda_y Y, \lambda_z Z)$, the free energy per chain becomes:

$$f = \frac{k_B T}{2} (\lambda_x^2 + \lambda_y^2 + \lambda_z^2 - 3) \quad (8)$$

We consider a uniaxial deformation in the x direction, $\lambda_x = \lambda$ and by incompressibility $\lambda_y = \lambda_z = 1/\sqrt{\lambda}$. The force applied to a single chain is $\partial f / \partial L_x$ and the stress in the entire system of chains, σ , is the total force applied per unit area: $\sigma = \rho k_B T (\lambda^2 - 1/\lambda)$, where ρ is the number of chain segments per unit volume. For small deformations, $\lambda \approx 1$, an expansion of the expression for σ shows that the stress is proportional to the product of the strain and $\rho k_B T$, similar to the pressure of an ideal gas. For large strains, the stress is non-linearly related to the strain but this arises from the incompressibility condition and not from any specific properties of the chains. Fluctuations of the crosslinks will further reduce the strain (Rubinstein and Colby, 2003).

Semi-flexible chains have a more complex response to applied forces and one can use the model described above to predict their stress-dependent elastic modulus. When semi-flexible chains are stretched near their limit, the additional force to stretch them further tends to diverge and this results in an elastic modulus that is intrinsically stress dependent. One considers a Hamiltonian that includes the bending energy as well as an energy that tends to equalize the projected length, L_p , and contour length, $L = \int_0^{L_p} dz \sqrt{1 + X'(z)^2 + Y'(z)^2}$. This arises from a tension (energy per unit length), τ that couples to the difference, $L - L_p$. In the approximation that the fluctuations are small, one can expand the square root to obtain:

$$H_\tau = \frac{\kappa}{2} \int_0^L dz (X''(z)^2 + Y''(z)^2)^2 + \frac{\tau}{2} \int_0^L dz (X'(z)^2 + Y'(z)^2)^2 \quad (9)$$

Using equipartition of the Fourier modes of the chain fluctuations (Landau and Lifshitz, 1970; Safran, 2003) one can calculate (Mackintosh, 2006) $\delta\ell$, which is the increase in the chain extension compared to its zero-tension, fluctuating value:

$$\delta\ell = \frac{L^2}{6\zeta} \left[1 + \frac{3}{\pi^2 \alpha} - \frac{3 \coth(\pi\sqrt{\alpha})}{\pi\sqrt{\alpha}} \right] \quad (10)$$

where $\alpha = \tau L^2 / \kappa \pi^2$ is a dimensionless measure of the applied force and ζ is the persistence length defined above.

For small forces, $\delta\ell \sim \tau L^4 / (\kappa \zeta)$; the excess strain, $\delta\ell/L$ is proportional to the force and the system is harmonic. For large forces, $\delta\ell$ approaches the value for full extension of $\delta\ell_0 = L^2 / (6\zeta)$ and the difference $\delta\ell_0 - \delta\ell \sim 1/\sqrt{\tau}$. This non-linear relationship between extension and applied force expresses the fact that as the chain approaches its maximum extension, a very large force must be applied. The measured elastic constant of the crosslinked, semi-flexible polymer gel is then stress dependent as discussed below in the context of actin gels.

E. Elements of elasticity

In the previous discussion, we have employed scalar definitions of the stress and strain developed in an elastic system that is subject to applied forces. While liquids and gases also resist compression, they do not show an elastic response to external forces that act only to change the shape of the system; such forces (per unit area) that do not induce any volume change, are called *shear stresses*. The elastic response (restoring force) to shear stresses are characteristic of solids. Crosslinked gels, while being disordered, are indeed classified as solids since they resist shape changes and can be described by elasticity theory. This is true when the crosslinks are permanent, or very long-lived; otherwise, one must deal with time (or frequency) dependent elastic constants (Boal, 2012; Fung, 1993). Biological gels are typically not permanently crosslinked (Lieleg *et al.*, 2008) and at long times one expects liquid-like flow instead of an elastic response to shear forces. This indeed is the time regime in which the CSK is modeled (Julicher *et al.*, 2007; Kruse *et al.*, 2004; Liverpool and Marchetti, 2003; Marchetti *et al.*, 2013) as an *active gel* that flows in response to internal forces generated by cell activity which is fueled by energy consumption. Here we restrict our focus to the early-time (tens of seconds) behavior of the CSK (Kollmannsberger and Fabry, 2011) where the crosslinkers still maintain the elastic response of the CSK to both internal and external forces. The elastic approach is also more appropriate for the ECM which remodels much less than the CSK.

In the presence of external or internal forces that are not part of the elastic network themselves (including thermal forces that change the positions of the particles), and in a continuum picture, the material particles that comprise an elastic system are assumed to be displaced from their equilibrium positions by a smooth displacement field $\vec{u}(\vec{r})$ where $\vec{r} = (r_1, r_2, r_3) = (x, y, z)$. The elastic energy arises from interparticle interactions and is thus a function not of $\vec{u}(\vec{r})$, but of its spatial gradients, that represent changes in the relative positions of the particles. This is true in the absence of any exter-

nal “pinning” forces for which translations of the system (where $\vec{u}(\vec{r})$ is constant), have no energy cost. The elastic energy is thus a function of the strain tensor u_{ij} defined (Landau and Lifshitz, 1970) as

$$u_{ij} = \frac{1}{2} \left(\frac{\partial u_i(\vec{r})}{\partial r_j} + \frac{\partial u_j(\vec{r})}{\partial r_i} + \frac{\partial u_l(\vec{r})}{\partial r_i} \frac{\partial u_l(\vec{r})}{\partial r_j} \right) \quad (11)$$

where summation over the repeated index l is implied. The non-linear term on the right can be neglected for small strains. The local change in a small length element dx is $dx(1 + u_{xx})$ so that the local volume change (given by the product $dxdydz$ minus the initial volume), is determined to first order in the strain by $tr(u_{ij}) = u_{ii} = u_{xx} + u_{yy} + u_{zz}$. These are coupled to isotropic compressions or expansions while shear forces that change the shape of the system couple to the off-diagonal strain components such as $\partial u_x / \partial y$ that represent changes in the interparticle spacing in the x direction that vary in the y direction.

Displacing the particles from their equilibrium positions creates strains that are resisted by internal restoring forces that originate in the intermolecular interactions (and in the case of polymeric gels, entropy) that provide shape memory and hence elasticity. The forces that arise from the elasticity are described by a stress tensor, $\sigma_{ij}(\vec{r})$. This is the force per unit area in the i direction that acts on the surfaces whose normal is in the j direction of an infinitesimal volume element. The pressure is the negative of one-third of the trace of the stress. In the absence of motion, the difference of the stresses on two surfaces separated by a distance $d\vec{r}$ is attributed to the presence of a local force density, $\vec{f}(\vec{r})$ within that volume element so that (Landau and Lifshitz, 1970) in equilibrium, $f_i(\vec{r}) = -\sum_j \partial \sigma_{ij} / \partial r_j$. It is important to note that the force per unit volume, f_i , is attributed to forces that are not included in the system’s elastic response and arise either from active internal elements or from macroscopic forces that act on the system boundaries. In the absence of such forces, mechanical equilibrium thus dictates that the divergence of the stress tensor vanishes.

For an isotropic body, rotational symmetry implies that there are two tensor components that must be considered for the strain and stress: (i) the trace that describes the local volume change, $u^0(\vec{r}) = u_{ij}(\vec{r})\delta_{ij}$ or the hydrostatic pressure, $-\sigma^0(\vec{r})/3 = -\sigma_{ij}(\vec{r})\delta_{ij}/3$ (where one sums over the repeated index) and (ii) the traceless shear, defined as $u_{ij}^s(\vec{r}) = u_{ij}(\vec{r}) - (1/3)u^0(\vec{r})\delta_{ij}$ with a similar expression for the shear stress. Since the internal forces that resist deformations can also include thermal effects at the intra-molecular level (such as changes in the conformations of polymers in gel networks), one considers the elastic free energy per unit volume (Landau and Lifshitz, 1970), f_e . The free energy associated with elastic deformations is a scalar and can be written from the following symmetry considerations. (i) The free energy depends only on the strains and not on the displace-

ments. (ii) There is no term linear in strain since the deformation free energy represents an expansion about equilibrium where the free energy is minimal. (iii) The free energy is a scalar and cannot depend on the coordinate system. Since $u_{ij}^0 u_{ij}^s = 0$, the free energy written up to quadratic order in the strains can only contain terms with $(u_{ij}^0)^2$ and $u_{ij}^s u_{ij}^s$:

$$f_e = \frac{K}{2} \left(\sum_i u_{ii} \right)^2 + \mu \sum_{ij} \left(u_{ij} - \frac{1}{3} \delta_{ij} \sum_l u_{ll} \right)^2 \quad (12)$$

where u_{ij} denotes the local strain, $u_{ij}(\vec{r})$. The first term accounts for the free energy associated with volume changes and is proportional to the bulk modulus, K , while the second term accounts for the shear response, proportional to the shear modulus μ . These two elastic constants that have the dimensions of energy per unit volume (the same as pressure, measured in Pa), are material dependent and can also be expressed (in three-dimensions) by the Young’s modulus $E = 9K\mu/(3K + \mu)$ and Poisson ratio $\nu = (3K - 2\mu)/(2(3K + \mu))$. As already mentioned above, the Young’s modulus is the elastic constant that appears naturally for a one-dimensional stretching experiment. Tensorial elasticity shows that even in the simplest case of linear isotropic elasticity, two elastic constants exist, with the Poisson ratio acting as a second elastic constant that accounts for how different dimensions are coupled to each other. The Young’s modulus can show tremendous variation depending on the strength of the interparticle interactions and the typical particle spacing: diamond or carbon sheets have $E \sim \text{TPa}$, metals have $E \sim 100\text{GPa}$, rubber has $E \sim \text{MPa}$, while tissue cells typically have $E \sim 10\text{kPa}$. The large differences between the rigidities of molecular and cellular systems are mostly determined by the very different length scales involved: the modulus (with dimensions of energy per unit volume) scales as the inverse of the cube of the characteristic length that determines the interactions. Materials whose cohesive energy is due to interatomic or intermolecular interactions on the nm scale can therefore have elastic moduli that are 6 orders of magnitude larger than the biopolymer gels that comprise the CSK or ECM where the crosslink distance can be 100 nm or more. For incompressible materials, $K/\mu \rightarrow \infty$ and $\nu \rightarrow 1/2$, while in the opposite limit of highly compressible materials, $\nu \rightarrow -1$. Most biological gels are fairly incompressible due to the presence of water that solubilizes the biopolymeric elastic elements, with ν in the range of 1/3 to 1/2.

The strains in an elastic material result in forces that tend to restore the equilibrium, unstrained state. These are most conveniently given by the stress tensor, σ_{ij} (force per unit area) that is derived from derivative of the free energy with respect to the strains (analogous to force given by the derivative of the energy with respect to

displacement): $\sigma_{ij} = \partial f_e / \partial u_{ij}$. This relationship implies that the elastic deformation energy per unit volume can also be written:

$$f_e = \frac{1}{2} \sum_{ij} \sigma_{ij} u_{ij} \quad (13)$$

Using the expression for the force balance in mechanical equilibrium, Eq. 13 for the free energy (for small strains), and the relationship between stress and strain, one finds:

$$\begin{aligned} f_i(\vec{r}) &= -\frac{\partial \sigma_{ij}(\vec{r})}{\partial r_j} = -\tilde{E} \left[\frac{\nu}{(1-2\nu)} \frac{\partial u_{\ell\ell}}{\partial r_i} + \frac{\partial u_{ij}}{\partial r_j} \right] \\ &= -\frac{\tilde{E}}{2} \left[\frac{\partial^2 u_i}{\partial r_j^2} + \frac{1}{(1-2\nu)} \frac{\partial^2 u_j}{\partial r_i \partial r_j} \right] \end{aligned} \quad (14)$$

where $\tilde{E} = E/(1+\nu)$ and a summation is implied by repeated indices. The second and third equalities in Eq. (14) are obtained from the definitions of the stress and strain tensors.

The solution of such linear differential equations with a source term (the internal force distribution, $\vec{f}(\vec{r})$) is given by the convolution of the source (the force at position \vec{r}') with the Green's function, $G_{ij}(\vec{r}, \vec{r}')$ of the system (Arfken and Weber, 1995). In our case this predicts the displacement:

$$u_i(\vec{r}) = \int d\vec{r}' G_{ij}(\vec{r}, \vec{r}') f_j(\vec{r}') \quad (15)$$

The Green's function itself is given by the solution of Eq. (14) for $u_i(\vec{r})$ for the case of a delta-function, point force located at \vec{r}' . For an infinite elastic domain, the Greens function depends only on $\vec{R} = \vec{r} - \vec{r}'$ and is written (Landau and Lifshitz, 1970):

$$G_{ij}(\vec{R}) = \frac{1}{8\pi\tilde{E}(1-\nu)R} \left[(3-4\nu)\delta_{ij} + \frac{R_i R_j}{R^2} \right] \quad (16)$$

While the angular dependence is complex and resembles that of an electric dipole, the distance dependence of $1/R$ is similar to the potential due to a point charge. Similar to electrostatics, elastic stresses and strains due to localized forces are long-ranged. As we shall see later, this allows cells to communicate with each other and with the boundaries of their physical environment over relatively large distances.

F. Adhesion of vesicles and capsules

Until now we have discussed bulk phases of soft matter and biomaterials. We next address finite-sized model systems that can account for some aspects (mainly passive responses) of cells, namely fluid droplets, elastic spheres, vesicles and capsules, as in Fig. 2. We consider the case

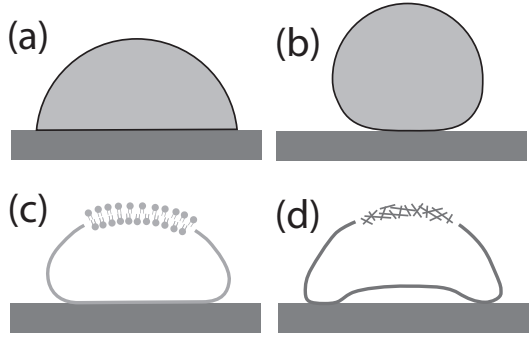


FIG. 2 Simple soft matter models relevant to the passive features of cell adhesion to a flat substrate. (a) A liquid droplet adhering to a surface is governed by surface tension. (b) A solid elastic sphere gains adhesion energy by forming a contact region whose size is determined by the balance of the adhesion and shear deformation energies. (c) A closed shell of a fluid, lipid bilayer (*vesicle*) is governed by bending energy. (d) A polymeric capsule has both bending and stretching energy; their interplay can lead to buckling in the contact area.

where these bodies are in contact with an attractive surface that favors adhesion. While fluid droplets and elastic spheres are both chemically homogeneous, with the same chemical species at both the surface and in the bulk, vesicles and capsules (also known as *polymerized vesicles*) are characterized by surfaces whose composition differs from that of the bulk. Vesicles typically consist of fluid, amphiphilic bilayers that enclose a spherical water core. Although the thermodynamic stable phase is usually the lamellar phase depicted in Fig. 1(d), vesicles are metastable over very long time scales and ubiquitous in biological systems. The bilayers respond to forces that couple to their curvature (bending response). The surface of capsules are typically thin polymer films with both bending and elastic response. Due to their membrane-like nature that is sensitive to bending and/or elastic forces, the adhesion of vesicles and capsules are interesting reference cases for the adhesion of cells.

The interface of a fluid droplet is defined as the region where two coexisting phases overlap (*e.g.*, fluid and vapour). The interfacial energy therefore scales to first order with the product of the geometrical area and the surface tension σ (Safran, 2003). The interfacial Hamiltonian is simply

$$U_i = \sigma \int dA \quad (17)$$

Variation of this surface functional with a Lagrange parameter Δp that enforces the conservation of volume (Δp simply corresponds to the pressure difference between the inside and outside of the sphere) yields the Laplace law $H = \Delta p/(2\sigma)$, where $H = (1/R_1 + 1/R_2)/2$ is the mean curvature of the surface and R_1 and R_2 are the two principal radii of curvature (Safran, 2003). For a free droplet, the solution will be simply a sphere, with the mean cur-

vature $H = 1/R$ everywhere. For an adherent droplet, the Laplace law is valid for the free part of the droplet, which therefore will be a spherical cap of radius R , as in Fig. 2(a). The exact dimensions of this spherical cap are determined by the overall volume and the contact angle θ , which in turn is determined by the interfacial energies according to Young's law:

$$\cos \theta = \frac{\sigma_{SG} - \sigma_{SL}}{\sigma} \quad (18)$$

where σ_{SG} is the interfacial energy between the substrate and the gas phase and σ_{SL} is the interfacial energy between the substrate and the liquid phase, respectively. The contact angle according to Young's law also determines the direction in which the interface is pulling as expressed by its surface tension. With a typical contact angle around 90 degrees, the pulling force is mainly normal to the substrate. The horizontal component of this pulling force is balanced by the surface energies associated with adhesion.

A filled elastic sphere of homogeneous composition and with radius R that adheres to a surface, forms a finite-sized contact region of radius a , as in Fig. 2(b). The size of the adhesion region is determined from the balance of the gain in adhesion energy per unit area W and the elastic energy penalty from the deformation that accumulates in the sphere due to the shape change upon adhesion. For a material that obeys linear elasticity, this depends on the Young's modulus E and the Poisson ratio ν . The balance of the adhesion and elastic forces is treated in contact mechanics and was first solved by Johnson, Kendall and Roberts (*JKR-theory*) (Johnson, 1985; Johnson *et al.*, 1971), who calculated

$$a^3 = \frac{9\pi(1-\nu^2)}{2E} R^2 W \quad (19)$$

Thus, the linear dimension of the adhesion area increases with adhesion energy (due to the gain in adhesion energy) and decreases with Young's modulus (since it tends to oppose the shape deformation induced by the attractive adhesion energy). Note that these calculations assume only normal forces. Contact mechanics predicts that in order to detach the elastic sphere in the normal direction, a critical force $F_c = 3W\pi R/2$ is required, which surprisingly depends only on the adhesion energy and is independent of the elastic constants. For an elastic sphere pushed onto the substrate by a normal force, one has the Hertzian stress profile $\sigma(r) = \sigma_0(1 - (r/a)^2)^{1/2}$, where r is the radial coordinate. In marked contrast to this, the JKR-solution, which applies to a self-adhered elastic sphere has an additional contribution $(1 - (r/a)^2)^{-1/2}$ that diverges at the boundary. The localization of the stress to the boundary make the contact prone to fracture from the periphery due to crack nucleation.

In contrast to droplets and elastic spheres, the interfacial energy of vesicles and capsules is determined by the

force response of the molecules on the surface. For thin, elastic shells (capsules) that obey linear, isotropic elasticity with bulk Young's modulus E and Poisson ratio ν , there are three main deformation modes: out of plane bending as well as in-plane shear and stretching. The bending energy reads

$$U_b = 2\kappa \int dA H^2 \quad (20)$$

where H is the mean curvature as above and κ is the bending rigidity which is related to the elastic properties of the material by $\kappa = Eh^3/12(1-\nu^2)$ (Landau and Lifshitz, 1970). A simple material law for the in-plane contributions is (Lim H. W. *et al.*, 2002)

$$U_p = \int dA \left\{ \mu \frac{(\lambda_1 - \lambda_2)^2}{2\lambda_1 \lambda_2} + \frac{K}{2} (\lambda_1 \lambda_2 - 1)^2 \right\} \quad (21)$$

where μ and K are two-dimensional shear and bulk moduli, respectively, which are related to the three-dimensional moduli by multiplication by the shell thickness h ; here $\lambda_i = 1+u_{ii}$ are the principal extension ratios.

For vesicles, comprising amphiphilic bilayers that are generally fluid, the in-plane deformations are not relevant for two reasons. Due to the fluid nature of the lipid bilayer, the shear modulus vanishes, and the bulk modulus is so large that the system is effectively incompressible. Therefore, only the bending energy is relevant; the form of the bending energy is the same as in Eq. (20), but the origin of the bending energy depends on the molecular characteristics; for systems with long chain molecules, the entropy which is a function of chain length, can play an important role (Safran, 1999). The typical bending rigidity of amphiphilic lipids that comprise biological membranes is $\kappa = 20 k_B T$. A detailed shape analysis of the bending Hamiltonian Eq. (20) and its extensions to account for each of the monolayers that comprise the bilayer has shown that free vesicles can adopt a large variety of often surprising shapes (Canham, 1970; Helfrich, 1973; Miao *et al.*, 1994; Seifert, 1997; Seifert *et al.*, 1991). In order to calculate vesicle shape upon adhesion, as in Fig. 2(c), one must consider the competition of the bending energy with the adhesion energy where W is the adhesion energy per unit area (Seifert, 1997; Seifert and Lipowsky, 1990). For weak adhesion or small radii of curvature, the bending energy dominates and the vesicle maintains its spherical shape without deforming to adhere to the surface. However, in the case of strong adhesion, $WR_0^2/\kappa \gg 1$ (where R_0 is the equivalent sphere radius defined by the vesicle volume $V = 4\pi R_0^3/3$), the vesicle shape effectively approaches a spherical cap with a well-defined contact radius. In this case, the adhesion forces will again be mostly normal and localized to the rim of the adhesion region.

As we will see later, an important aspect of cell adhesion is that adhesion molecules are mobile in the lipid

bilayers and can form local clusters. This has indeed been demonstrated experimentally in a vesicular systems by incorporating such adhesion molecules within the lipid bilayers (Albersdorfer *et al.*, 1997). Theoretical models have shown that membrane fluctuations lead to an effective attractive interaction between the adhesion molecules which can explain this clustering (Lipowsky, 1996; Menes and Safran, 1997; Smith and Seifert, 2005; Smith *et al.*, 2008; Weikl and Lipowsky, 2001; Zuckerman and Bruinsma, 1995) and there is experimental evidence that indeed this mechanism also operates in biological cells (Delano-Ayari *et al.*, 2004). However, despite the presence of this local clustering, the contact zone of vesicles that adhere to a surface through specific adhesion molecules tends to remain rather homogeneous.

In contrast to vesicle adhesion, capsule adhesion also involves in-plane elastic energies. It is well known that in particular the stretching energy cannot be neglected when dealing with the shape of capsules, because the ratio of stretching and bending energies for spherical shells scales as $(R/h)^2$ (where R is the radius of curvature and h is the shell thickness) and is therefore always large (Landau and Lifshitz, 1970). An important consequence of this fact is that thin elastic capsules buckle inwards when a critical pressure of $p_c \sim E(h/R)^2$ is exceeded (Landau and Lifshitz, 1970). In general, the interplay between stretching and bending (possibly complemented by sheet adhesion to itself) leads to a very rich phase diagram of possible shapes (Knoche and Kierfeld, 2011). A rich variety of phenomena also arises for forced crumpling of planar sheets such as paper or graphene (Lobkovsky *et al.*, 1995; Vliegenthart and Gompper, 2006a) or closed shells such as ping pong balls, fullerenes or virus capsids (Schwarz *et al.*, 2000; Vliegenthart and Gompper, 2006b). For red blood cells, one must combine the elasticity of thin shells with the bending energy; one then finds very good agreement between simulated and observed shapes, both for free cells (Lim H. W. *et al.*, 2002) and for cells in hydrodynamic shear flow (Noguchi and Gompper, 2005).

Because attraction to a flat substrate results in deformations that are similar to those induced by external pressure or forces, adhesion also can lead to the inward buckling of an adherent capsule, as in Fig. 2(d) (Fery and Weinkamer, 2007). A computer simulation for spherical shells adhering to a flat substrate has shown that as the adhesion energy increases, the shell first flattens like an elastic sphere, then buckles in a radially symmetric manner, and finally develops a polygonal adhesion region through the formation of elastic ridges running in parallel to the substrate (Komura *et al.*, 2005). This shows that capsules in adhesion can develop very inhomogeneous adhesion regions, and suggests that interfacial stresses will mainly be localized at the rim of the adhesion area.

Here we focused on the competition of adhesion and deformation energies in determining the shapes of adhering bodies as relevant background to understand the

specific features of cell adhesion. As we will see in the next section, however, cells adhesion is characterized by additional and mainly active features that do not exist in the passive systems discussed so far. Adherent cells tend to develop very inhomogeneous contact areas, with adhesion molecules strongly clustered along the periphery of the adhesion region. In particular, the inward buckling characteristic for homogeneously adhering capsules is not observed for cells. The stress localization expected for capsules is weakened by remodeling processes at the cell periphery, which are, in turn, closely coupled to the growth and stabilization of the adhesions. Most importantly, the adhesion structures of cells are extremely dynamic, with a constant flow of material from the cell periphery towards the cell center.

III. BIOLOGY BACKGROUND

A. Actin cytoskeleton and cell adhesion

Cells are the smallest units of life and widely vary in their shape, structure and function (Alberts *et al.*, 2007; Boal, 2012; Bray, 2001; Phillips *et al.*, 2008). For simplicity, we focus here on animal cells, thereby excluding *e.g.*, bacteria, protists and plant cells from our discussion. Typical cell sizes are of the order of tens of micrometers and there are roughly 10^{14} cells in humans. They can be classified into 200 major cell types ranging from connective tissue cells through epithelial and muscle cells to nerve cells (Alberts *et al.*, 2007). All cells in an organism carry the same genome, but as a result of differentiation, different cell types have different gene expression patterns, *i.e.*, different cell types produce different proteins. If viewed from the point of view of soft materials, however, all animal cells are similar, including a spatial organization determined by lipid bilayers and the polymer networks of the cytoskeleton.

Fig. 3 shows a schematic representation of the main structural elements of an animal tissue cell in suspension. The cell is separated from its surroundings by a *plasma membrane*, which is a bilayer that comprises different lipid molecules and is enriched by additional components such as cholesterol. The plasma membrane is fluid in nature (no fixed topological relations of neighboring molecules, flow under shear deformations) and acts as a carrier for a large variety of membrane-bound proteins and sugars. Underneath the plasma membrane is the actin cortex, a relatively thin (100 nm) dynamic layer of crosslinked actin filaments whose mechanical properties dominate the elastic response in reaction to deformations of the cell. The plasma membrane and the actin cortex are coupled through a variety of linker molecules that are separated by relatively large distances, so that the membrane between them can fluctuate relatively freely, leading to the phenomenon of *membrane flickering*. The

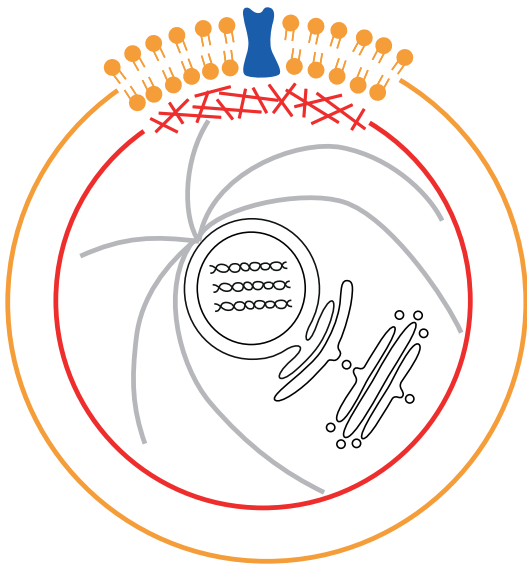


FIG. 3 (Color online) Schematic drawing of an animal cell in suspension. Such a cell is essentially round due to its effective surface tension. Important cellular organelles responsible for its internal structure and mechanical properties include (1) the plasma membrane (orange), a lipid bilayer that envelopes the entire cell and carries different proteins, including transmembrane receptors; (2) other membrane structures (thin black lines) such as the two membranes around the nucleus containing the genes, the endoplasmic reticulum, the Golgi apparatus and different kinds of vesicles; (3) the actin cortex (red), a thin shell comprising a polymer network underlying the plasma membrane; (4) the microtubule system (thick grey lines), a system of relatively stiff polymers that radiate outward from the microtubule organizing center that is attached to the nucleus.

cytoplasm of the cell refers to the cellular volume (excluding the nucleus containing the generic material in the form of DNA) delimited by the plasma membrane. It contains several organelles important for cell function, including a variety of additional membrane systems (such as the *endoplasmic reticulum* and the *Golgi apparatus*) and polymer networks. There are three important types of polymer networks, based on actin filaments, microtubules and intermediate filaments, respectively (Alberts *et al.*, 2007; Boal, 2012; Howard, 2001; Phillips *et al.*, 2008). Collectively, they are called the *cytoskeleton*. For a cell in solution, only the microtubule network is well developed in the cytoplasm.

Animal cells in suspension are usually round as depicted in Fig. 3, indicating an effective surface tension arising from the combined effect of plasma membrane and actin cortex. The round shape of a cell changes once it adheres to an external surface. If a cell encounters an external surface covered with specific ligand, it undergoes a multi-step process that determines whether or not it eventually will adhere (Bershadsky *et al.*, 2003; Cohen *et al.*, 2004). In general, cells use different mechanisms to avoid non-specific adhesion (*e.g.*, due to van der

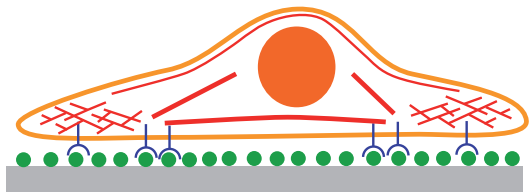


FIG. 4 (Color online) Schematic drawing of an adherent animal cell. Such a cell typically has the shape of a fried egg, with the nuclear region protruding in the middle while the rest of the cell remains relatively flat. As opposed to Fig. 3 for a freely suspended cell, here we do not depict the membrane or microtubule systems. In addition to the actin cortex (red) now forms several additional subsystems that extend throughout the cytoplasm. Here we depict a dendritic actin networks that pushes outwards against the plasma membrane (*lamellipodium*) and contractile actin filament bundles (*stress fibers*) that are anchored to the cellular environment through transmembrane receptors (blue) that bind extracellular ligands (green).

Waals forces), including a repulsive sugar layer anchored in the membrane (*glycocalyx*) as well as the steric (entropic) repulsion due to membrane fluctuations (Safran, 2003). Adhesion is only induced if it is promoted by specific molecular signals that are found on the substrate. The specificity of cell-matrix adhesion is implemented by transmembrane adhesion receptors (in humans, these are mainly the 24 variants of the integrin family), which bind to complementary ligands of the extracellular matrix (including collagen, fibronectin, vitronectin and laminin). Similar to passive vesicles or capsules, the early stages of cell adhesion and spreading can be strongly determined by viscoelastic processes, *e.g.*, the deformation of the rim of the developing contact region (Cuvelier *et al.*, 2007). Later stages are more strongly determined by remodeling of the cytoskeleton and the establishment of localized sites of specific adhesion. During the remodeling process, the actin system is organized into additional networks extending throughout the cytoplasm. Because these networks are crosslinked, the actin cytoskeleton provides the cell with elastic restoring forces that resist shear deformations and is thus essential in determining the shape, stability and mechanical response of cells. While the volume of a cell tends to stay constant during adhesion and spreading, the surface can increase by up to 50 percent, which occurs via the flattening of the undulated membrane as well as by the addition of new lipid material (Gauthier *et al.*, 2011).

Fig. 4 schematically depicts the actin structures that are typically developed during cell adhesion and spreading. In contrast to Fig. 3, we do not depict the microtubule system here, because it has only a supportive function in this context (its main function here is to coordinate processes involved in active transport and cell migration). The main mechanism that leads to outward expansion of the plasma membrane and thus to the devel-

Cite:

opment of a contact area with the substrate is the rapid polymerization of an actin network at the cell periphery (*lamellipodium*). Lamellipodia grow through the elementary processes of actin filament polymerization, branching, capping and crosslinking (Pollard and Borisy, 2003; Pollard and Cooper, 2009; Ridley, 2011), which have been extensively modeled (Mogilner, 2006; Pollard and Berro, 2009). The most common structure of the lamellipodium seems to be a tree-like (*dendritic*) network with a ± 35 degree orientation relative to the leading edge of the cell membrane due to the 70 degree angle in the protein complex Arp2/3 connecting branched-off daughter filaments to mother filaments (Svitkina and Borisy, 1999). The exact organization of the lamellipodium varies as a function of cell type, motility state and external signals (Urban *et al.*, 2010; Weichsel *et al.*, 2012). One of the most important aspects of lamellipodia growth is its force-velocity relation, for which conflicting experimental evidence exists (Marcy *et al.*, 2004; Parekh *et al.*, 2005; Prass *et al.*, 2006) and which has been treated by various modeling approaches (Camps *et al.*, 2012; Carlsson, 2003; Lee and Liu, 2009; Schreiber *et al.*, 2010; Weichsel and Schwarz, 2010; Zimmermann *et al.*, 2012).

Other types of actin structures that develop in cell adhesion are bundles and networks that are contractile due to the action of molecular motors that tend to slide actin filaments relative to each other. If the filaments are sufficiently anchored to their surroundings, they can no longer move; thus, instead of motion, tension is developed in the actin bundles or network by the forces exerted by the molecular motors. In adhesive cells, this is mainly achieved by the molecular motor protein myosin II. In contrast to muscle, where myosin assembles in groups of hundreds of motors, in the cytoskeleton of non-muscle cells, it organizes into myosin-minifilaments that typically contain only dozens of non-skeletal myosins II molecules (Verkhovsky and Borisy, 1993). The most prominent myosin-based contractile structures in adhesion-dependent cells are *stress fibers* (Burridge and Wittchen, 2013; Pellegrin and Mellor, 2007) shown schematically as thick red lines in Fig. 4. One can distinguish different types of stress fibers (Hotulainen and Lappalainen, 2006). Dorsal stress fibers connect to an adhesion site at one end and have their other end connected to other actin structures in the cell that are far from the substrate. Ventral stress fibers are connected to adhesion sites at both of their ends and thus run parallel to the substrate. In contrast to dorsal and ventral stress fibers, transverse arcs are usually not straight, are not connected to adhesion sites and typically extend parallel to the leading edge. Stress fibers are thought to serve as the main sources of cellular forces that are exerted on the substrate, since their endpoints are often found at large adhesion sites that correlate with large forces (Balaban *et al.*, 2001). Laser cutting experiments demonstrated that stress fibers are under large tension,

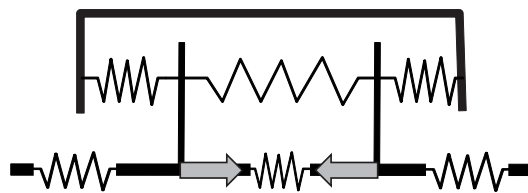


FIG. 5 Scheme for the overall force balance in an adherent cell. There are two actin-based processes that contribute to force generation at the cell-material interface. Contraction by myosin II motors in actin networks and bundles corresponds to a stretched spring pulling inwards in the cell center. Lamellipodium growth against the membrane corresponds to a compressed spring pushing outward at the cell periphery. The entire system is constrained by the cell envelope. Due to the position of the adhesion sites, a contractile force dipole emerges as the effective traction pattern on the substrate. This leads to deformation of the substrate (compression below the cell body, and elongation away from the cell).

since they retract over large distances when being cut (Colombelli *et al.*, 2009; Kumar *et al.*, 2006). Stress fibers are distinguished from *retraction fibers*, which are non-contractile actin bundles that specifically serve to anchor the cell to the ECM during cell division (Thery *et al.*, 2007).

The lamellipodium and stress fibers are actin assemblies that create pushing and pulling forces, respectively; hence, they are the two main force-generating mechanisms for cells that adhere to flat substrates. Although its effect is rather indirect, the plasma membrane plays a very important role in this context. Apart from acting as host for the transmembrane receptors from the integrin family, it also controls the polymerization of the lamellipodium and the contraction of the stress fibers by triggering biochemical signals that regulate these processes (Ridley, 2011). Equally important, the plasma membrane plays an important role in the overall force balance in the cell, since its tension and curvature elasticity provide the counterforces to actin-generated forces that tend to extend and deform the membrane. An imbalance in these forces is especially important in cell migration (Fletcher and Theriot, 2004; Lauffenburger and Horwitz, 1996).

In Fig. 5, we schematically show the overall force balance in the cell. To first order, the lamellipodium can be depicted as a compressed spring that pushes outward on the cell membrane and inward on the focal adhesion. The stress fibers appear as stretched springs that pull inward on the adhesion. In stationary or slowly migrating cells the sites of adhesion are typically located in between the polymerization-dominated lamellipodium and the myosin-dominated contractile structures that are located closer to the cell body (*lamella*); thus, both processes effectively lead to inward-directed forces on the substrate. For a strongly polarized, stationary cell, the traction force pattern therefore resembles a pair of oppo-

sitely directed forces (pointing from each side of the cell towards the cell body) of equal magnitude. As we will see later, this concept of a *contractile force dipole* (Schwarz *et al.*, 2002; Schwarz and Safran, 2002) is very powerful when describing cellular forces on a coarse-grained scale. The pulling of the force dipole on the substrate leads to compression below the cell body and elongation away from the cell, as schematically depicted by the springs in the substrate.

The counterforces exerted by the substrate on the cell originate in the substrate elasticity that resists deformation by the cellular forces (in physiological tissue, this is the elasticity of the ECM). The substrate resistance can reorganize the cellular cytoskeleton and change the size of the adhesive regions. The feedback between the cellular and substrate elastic forces means that cellular structure and function can be very sensitive to the elasticity and in particular to the rigidity of the substrate (Discher *et al.*, 2005; Schwarz and Bischofs, 2005). For example, cells tend to migrate from softer to more rigid substrates and to have larger adhesive regions and overall spread area on more rigid substrates (Engler *et al.*, 2004a; Lo *et al.*, 2000; Pelham and Wang, 1997; Trichet *et al.*, 2012). Moreover, the outside-in forces from the substrate that can modify the cytoskeletal organization, can also have genetic implications. In particular, it was found that skeletal muscle cells differentiate optimally on substrates with rigidities of 11 kPa (Engler *et al.*, 2004b) and that stem-cell fate strongly depends on substrate rigidity (Engler *et al.*, 2006).

The fluid nature of the plasma membrane means that it is only indirectly involved in force generation. Transmission of forces and in particular, the sensitivity to shear, requires a solid-like structure. In cells, the structural elements that give the cell its shape integrity and its ability to respond to and to transmit forces reside in the cytoskeleton. In addition to this role, the cytoskeleton is also important in anchoring organelles such as the Golgi apparatus in their place in the cell, in determining the organized changes that take place during cell division, in regulating the imbalance of internal forces that results in cell motion, and in providing a scaffold for signaling processes inside cells. Since in this review we focus on force generating processes during cell adhesion, we will be mainly concerned with the actin cytoskeleton. In cell adhesion most forces generated in the actin cytoskeleton are balanced over the sites of adhesion; thus, our second major focus area is the physics of adhesion sites.

B. Actin filaments and their assemblies

Most studies of cellular forces have focused on their origin in the actin cytoskeleton. This motivates our emphasis on the dynamics and larger-scale structural organization of this important cytoskeletal component. Actin

(in both monomeric and polymeric forms) comprises between 5%-10% of the protein in eukaryotic cells and is of great importance in cell structure and motility (Fletcher and Mullins, 2010; Stricker *et al.*, 2010). We begin with a discussion of the growth of actin polymers. In contrast to self-assembling, equilibrium polymerization, these are catalyzed by the binding of ATP to monomeric (globular) actin (*G-actin*). While many synthetic polymers are non-polar, actin polymers are chiral with each macromolecule comprising two helical, interlaced strands of monomeric subunits. The two-filament assembly is thus polar so that the two ends are therefore not equivalent; hence polymerization rates at one end are not necessarily equal to those at the other. Actin polymerization is therefore a polar, energy-consuming, non-equilibrium process (Phillips *et al.*, 2008).

A dynamical model for the growth of an actin filament takes into account that the polymer is polar and the dynamics of association of monomers at the two ends differ. That is, $k_{on}^{+,-}$ and $k_{off}^{+,-}$ are respectively the rates for monomers to associate with + (generally growing) or - (generally shrinking) ends and to dissociate from those ends. For equilibrium polymerization the association or dissociation energy itself must be the same at either end since although the monomers are asymmetric at the two ends, the molecular bonds that are formed are the same. Hence, by detailed balance, $k_{off}^+/k_{on}^+ = k_{off}^-/k_{on}^-$. Thus, for such equilibrium polymers one can show that (Phillips *et al.*, 2008) there is no state in which one end is growing and the other is shrinking; the polymer either grows or shrinks from both ends – albeit with different on and off rates for the two ends of polar chains. However, for the polymerization of actin in cells, detailed balance does not apply and a richer set of behaviors is found as we now discuss.

In living systems, polymerization is often a dynamic process that involves chemical changes that may differ at the two ends of a polar chain such as actin so that the polymerization and depolymerization rates differ. The chemical changes are catalyzed by an input of energy from the conversion of ATP (adenosine triphosphate with 3 phosphate bonds) to ADP (adenosine diphosphate with 2 phosphate bonds) (Alberts *et al.*, 2007; Phillips *et al.*, 2008). This conversion is known as hydrolysis since one phosphate group dissociates from ATP to remain solubilized in water; the breaking of one of the phosphate bonds releases about 10-20 $k_B T$ of energy since the hydration bonds between ADP and water and the released phosphate group and water are energetically more favorable than the bonds between the phosphate bonds in ATP. The energy released by hydrolysis of ATP can be used to modify the conformations of molecules, such as actin that is bound to ATP in its lowest energy state. The resulting conformational changes can result in increased or decreased bonding of the molecules to other molecules; in the case of actin, hydrolysis destabilizes polymerization

at its plus end.

The non-equilibrium nature of actin polymerization in cells is related to the conformational changes in the monomers that are catalyzed by ATP; G-actin monomers bound to ATP join the plus end of the actin polymer (Alberts *et al.*, 2007; Phillips *et al.*, 2008). Within a time of about 2 seconds, however, ATP is hydrolyzed to form ADP which reduces the binding strength of the monomers in the chain, thus destabilizing the polymer. There is therefore a non-equilibrium competition between growth and shrinkage of the polymer. Note that in solution, the G-actin monomers that have dissociated from the chain can dissociate from ADP and reassociate with ATP to rejoin the polymer; this turnover makes the process highly dynamic. Since the actin polymer is polar due to its double helical structure, the growth and shrinkage at the + and - ends is different, and in principle, one would need 4 rate constants to describe the on and off rates of the ATP and ADP bound monomers at each of the ends. Filaments elongate about 10 times faster at their + ends compared with their - ends and this leads to an apparent motion of the + end known as treadmilling (Phillips *et al.*, 2008). Typical values (Boal, 2012) are $k_{on}^+/k_{on}^- \approx 10$ for ATP-bound actin and about 70 for the predominant situation of ATP-bound actin at the + end and ADP-bound actin at the - end. The ratio $k_{off}^+/k_{off}^- \approx 5$ for ATP-bound actin at the + end and ADP-bound actin at the - end, with typical values of $k_{off} \sim 0.3 - 7.0 \text{ sec}^{-1}$ depending on which end is being considered and whether the actin is ATP or ADP bound. One can show (Phillips *et al.*, 2008) that there is a monomer concentration range for which the + ends are growing while the - ends are shrinking. Note that the treadmilling velocity can be finite while the total filament length remains the same. Whether the filament can move or not depends on its environment; for example, treadmilling actin filaments in the vicinity of the cell membrane have their motion impeded by the restoring forces (due to surface tension and curvature energy) of the membrane. This then leads to flow of the actin in the direction opposite to treadmilling, that is away from the cell membrane (*retrograde flow*), as can be measured with speckle fluorescence microscopy (Ponti *et al.*, 2004).

The larger-scale organization of actin can take several forms. *In vitro* studies have shown (Tempel *et al.*, 1996) that in some cases alpha-actinin crosslinkers can result in relatively thick actin bundles; in other cases, a crosslinked, isotropic gel is formed. The detailed phase diagram depends on both the actin and crosslinker concentration (Zilman and Safran, 2003). *In vivo*, many proteins can become involved in actin bundling which is utilized by the cell in maintaining relatively stable (Gov, 2006), finger-like protrusions called microvilli. These proteins also participate in more dynamical protrusions called filopodia (Mogilner and Rubinstein, 2005) that exert polymerization forces on the cell membrane and

play a role in cellular motion and shape changes. Actin bundling is also an important characteristic of stress fibers (Hotulainen and Lappalainen, 2006) that typically range over some fraction of the cell size and provide structural stability to the cell while transmitting contractile forces to its surroundings.

Due to the dynamics of the crosslinks and the treadmilling of actin, the cytoskeleton can be remodeled and is therefore not permanently crosslinked. However, experiments in which cells are subject to time varying strains that cause cytoskeleton reorganization, show that the overall time scale for reassembly and reorientation of stress fibers can be several hours (Brown *et al.*, 1998; Jungbauer *et al.*, 2008; Wang *et al.*, 2001). Entropic fluctuations occur on a time scale shorter than 0.01 s (Deng *et al.*, 2006), while on longer time scales the elastic response to time varying strain has been characterized as glassy. We first consider the elastic modulus of actin networks *in vitro* (Boal, 2012) on time scales shorter than those at which the shear modulus vanishes due to the crosslink disconnections (Lieleg *et al.*, 2008); on these time scales, the system in some average sense can be regarded as being permanently crosslinked.

The simplest model for the elastic constant of a permanently crosslinked polymeric network predicts a shear modulus $\mu \sim \rho k_B T$, where ρ is the number density of crosslinks (Rubinstein and Colby, 2003). The typical spacing between crosslinks with a 1:100 ratio of linker to actin monomers, is of the order of $0.1 \mu\text{m}$. This yields a shear modulus of about 1 J/m^3 at room temperature which is equivalent to 1 Pa. The measured value (Janmey *et al.*, 1990) in the presence of the crosslinker ABP (at a ratio of ABP:actin of the order of 1:100) is about one order of magnitude larger and is sensitive to the length of the actin segments; the observations also depend on the history of the sample, since shear can disrupt actin filaments and give misleadingly low values for the modulus. Higher values of the modulus than expected from simple considerations of crosslinked polymer networks can be due to the stiffening effects of the crosslinks themselves, the semi-flexible (as opposed to Gaussian) nature of biopolymers such as actin, and to non-linear shear-stiffening. On the other hand, the analogy with permanently crosslinked gels must be reconsidered in light of the finite lifetime of the crosslinks. Alpha-actinin has a dissociation rate of about 1 s^{-1} (Gardel *et al.*, 2008a; Xu *et al.*, 1998) which may explain why *in vitro* experiments using this crosslinker (Lieleg *et al.*, 2008) in actin gels yield a low frequency elastic modulus of about 1 Pa only at the very highest crosslinker concentrations (alpha-actinin:actin ratios of 1:15). The dissociation rate may be different in different geometries; in isotropically crosslinked gels, the crosslinkers can more effectively dissociate compared with their relatively tighter packing in actin bundles where neighboring filaments are nearby. The dissociation rate is also strongly temperature depen-

dent and of course very different for different crosslinkers (Xu *et al.*, 1998).

In addition to the finite residence time of the crosslinkers at the network junctions, another important difference between the elastic modulus of crosslinked biopolymers such as actin and synthetic polymer gels is the observation that the actin cytoskeleton shows a non-linear elastic response in a non-perturbative manner (Gardel *et al.*, 2004; Storm *et al.*, 2005). For small stresses, the elastic stress in actin gels is proportional to the strain, while for larger stresses, of the order of 0.2 Pa, the effective modulus varies as the 3/2 power of the applied stress due to the entropically dominated mechanical response of semi-flexible polymers of finite extensibility as described above (Storm *et al.*, 2005). This entropic nonlinearity is particularly interesting because the strains may still be relatively small (Gardel *et al.*, 2004; Storm *et al.*, 2005) even though the medium responds very non-linearly; this is quite different from analytical non-linearities (*e.g.*, due to additional quadratic terms in the stress-strain relationship or due to geometrical non-linearity) that arise when the strains become large in non-polymeric systems. Interestingly, cells can regulate the regime in which they function by changing their internal stress state through variation of the activity of molecular motors. Since the cell elastic modulus is of the order of 1-10 kPa (reflecting the types of stresses that cells can maintain), the cytoskeletal elastic response can easily operate in the non-linear regime. Finally, we note that many other important biopolymers (Klotzsch *et al.*, 2009; Storm *et al.*, 2005) also show similar non-linear response, including collagen which is an important part of the ECM.

C. Actomyosin contractility

In the preceding section, we have summarized the properties of crosslinked actin gels based on information obtained from *in vitro* experiments. However, one very important aspect regarding actin networks and bundles in cells is the fact that these networks are under tension due to the contractile activity of myosin motors (Howard, 2001) (pp. 265-273). Contractile actin networks (Koenderink *et al.*, 2009; Kohler *et al.*, 2011; Mizuno *et al.*, 2007; Murrell and Gardel, 2012; Silva *et al.*, 2011) and bundles (Thoresen *et al.*, 2011, 2013) have recently been reconstituted in biomimetic assays. In cells, the myosin motors generate internal forces in the actin network which are transmitted to its surroundings due to the “glue” the cell produces in the form of proteins that aggregate into focal contacts or focal complexes (Geiger *et al.*, 2009). The production of force is a non-equilibrium process that requires energy input via ATP hydrolysis that causes conformational changes in the myosin molecular motors (Howard, 2001) (pp. 229-238). The internal forces generated by molecular motors that act upon the

crosslinked actin assemblies in cells distinguishes them from “dead”, non-active gels and allows cells to pull on their environment and on each other. Motor activity also means that the cell can exert forces on itself and this, along with polymerization of actin, plays an important role in cell motility. Motors can also influence the conformations of the actin filaments in a manner that has to do with the motor and motor-actin dynamics. The stochastic nature of the motor-actin coupling in which the motor is associated with the actin for a finite time (Boal, 2012; Howard, 2001) after which it can detach and diffuse, affects the fluctuations of the filaments. These motor-driven fluctuations are distinct from the thermal fluctuations of the actin that are driven by Brownian motion of its aqueous environment (MacKintosh and Schmidt, 2010; Mizuno *et al.*, 2007). This leads to a breakdown of the fluctuation-dissipation theorem that relates the thermal fluctuations of an equilibrium system to its response to a deterministic force as discussed in the section on the physics background.

Because stress fibers are an important element of the force-generating apparatus of cells adhering to flat substrates, a large variety of models has been developed to describe their physical properties. Dynamical models show that actin filaments can be sorted by myosin II motors into a tensile state (Kruse and Julicher, 2000a, 2003; Stachowiak *et al.*, 2012; Yoshinaga *et al.*, 2010; Ziebert and Zimmermann, 2004). Models for mature fibers are often motivated by perturbation experiments on stress fibers, such as studies of contraction dynamics after activation (Peterson *et al.*, 2004) or relaxation dynamics after laser cutting (Colombelli *et al.*, 2009; Kumar *et al.*, 2006). They usually assume a sarcomeric organization of the stress fiber (Friedrich *et al.*, 2012) and couple elastic, viscous and contractile elements in a unit cell (Besser *et al.*, 2011; Besser and Schwarz, 2007; Luo *et al.*, 2008; Russell *et al.*, 2009; Stachowiak and O’Shaughnessy, 2008, 2009). Recently it has been demonstrated that such sarcomeric models predict some of the central physical properties of reconstituted contractile actin bundles (*e.g.* retraction velocity is proportional to length) (Thoresen *et al.*, 2013). On a very coarse-grained scale, such one-dimensional models can be regarded as more detailed versions of the force dipole model introduced in Fig. 5. In particular, they usually obey force balance on the substrate by construction. These types of one-dimensional models can also be used to predict the cellular response to substrate stiffness (Besser and Schwarz, 2010; Crow *et al.*, 2012; Marcq *et al.*, 2011; Mitrossilis *et al.*, 2009).

An important reference case for the physics of stress fibers is sarcomeric muscle, in which actin filaments, passive crosslinkers and myosin II motors are arranged in a very ordered fashion. The action of myosin II molecular motors can be modeled either with a generic two-state theory (Julicher and Prost, 1995; Placais *et al.*, 2009) or with more detailed cross-bridge models that go back to

the seminal work of Huxley (Duke, 1999; Erdmann and Schwarz, 2012; Huxley, 1957; Vilfan and Duke, 2003), where the cross-bridges refer to the acto-myosin coupling. This model accounts for the fact that a myosin II motor loaded with ATP goes through a cycle where it first binds weakly to the actin filament. Release of the inorganic phosphate (after hydrolysis of ATP to ADP) causes the myosin motor to make a powerstroke that creates force and motion. Finally, after the release of the ADP and binding of a new ATP-molecule, the myosin II motor unbinds from the filament and is ready for the next motor cycle. The effective force-velocity relation has been measured both in the context of muscle (Pate *et al.*, 1994) and in single molecule experiments (Veigel *et al.*, 2003). At vanishing force, the motors move with an ATP-dependent free velocity of about $1 \mu\text{m/s}$. As the external counter-force increases, the velocity of the motor along the filament drops in a hyperbolic manner, until it vanishes at a stall force of a few pN. This close coupling between force and sliding velocity was first noted by Hill in 1938, who described it using a phenomenological equation (called the *Hill equation*), which can be explained in detail by the cross-bridge models (Howard, 2001; McMahon, 1984). Alternatively, as we will see later, Hill-type relations can be used directly as an assumption in coarse-grained models. In particular, such a model has been used to argue that rigidity sensing is based on the same principles like muscle contraction (Mitrossilis *et al.*, 2009).

Contractility is also observed in biological systems with no apparent sarcomeric order. For example, the contractility of the actin ring during cell division may rely on depolymerization forces (Pinto *et al.*, 2012). It has been shown theoretically that in one-dimensional actin bundles containing myosin, contractility can occur even in the absence of spatial organization of the bundle, due to bundle shortening (Kruse and Julicher, 2000b; Kruse *et al.*, 2003). The existence of net contractility is related to the assumption that a myosin motor which binds to or arrives at the plus end (but not at the minus end) of a filament remains attached for some time. This model does not contain additional crosslinkers (similar to Z-bodies found in sarcomeres) that may tend to associate with only one end of the polar actin molecules. Another recent suggestion (Lenz *et al.*, 2012) for how contractility can arise in bundles without sarcomeric order is based on an the asymmetric response of the filaments to longitudinally applied stresses, *e.g.*, a tendency to yield under compression while resisting extension. Such buckling has been observed in *in vitro* experiments containing actin, smooth muscle myosin and ATP. We note that additional crosslinkers, such as those found in sarcomeres and possibly stress fibers, may break the symmetry were not included. Whether stress fibers, contractile rings, and smooth muscle fibers are ordered and function in a manner similar to sarcomeres should be investigated by future experiments. The sarcomeric order discussed be-

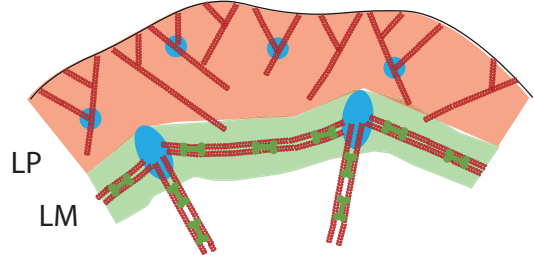


FIG. 6 (Color online) Spatial organization of focal adhesion growth and the actin cytoskeleton. The actin lamellipodium (LP) is assembled at the leading edge and flows from there towards the cell center. Small adhesions are formed along the way and mature into focal adhesions as they move with the actin flow. At the boundary with the myosin-dominated lamella (LM), only a few mature focal adhesions persist; those are stabilized by large contractile forces which are mainly due to the activity of myosin II minifilaments in stress fibers.

low in terms of smectic ordering of force dipoles is meant to apply to nascent muscle cells where striations have indeed been observed (Engler *et al.*, 2004b; Friedrich *et al.*, 2011). In a somewhat similar manner, striations have also been reported in studies of non-muscle stress fibers (Peterson *et al.*, 2004). Here the microscopic, anti-parallel arrangement of adjacent actin polymers was not directly observed, but the striations measured do suggest a sarcomeric analogy.

D. Focal adhesions

Understanding the mechanical response of stationary cells involves analysis of the internal elastic response of contractile cells as well as their mechanical coupling to their surroundings. While the response of cells to external forces or other mechanical perturbations can necessitate the disassembly and rebuilding of the actin cytoskeleton, the stable coupling of the cell to the surrounding elastic matrix is due to sites of adhesion called *focal adhesions* that connect the actin cytoskeleton to transmembrane adhesion receptors from the integrin family. These are then connected, on the extracellular side, to the substrate or extracellular matrix.

In contrast to the adhesion of passive vesicles or capsules, the spatial distribution of the adhesion structure of cells is very heterogeneous. It is mainly localized at the cell periphery, because it is strongly coupled to the growth processes of the lamellipodium. Fig. 6 depicts the spatial coordination between the growth of adhesions and the actin cytoskeleton. Nascent adhesions are initiated close to the leading edge and then move towards the cell center. This movement is mainly driven by the flow of actin away from the leading edge (*retrograde flow*) due to the counterforces exerted on the polymerizing actin by the membrane. As they move towards the cell center, the small adhesions either mature into micrometer-sized focal

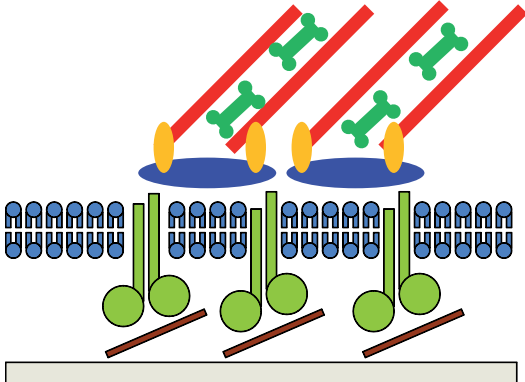


FIG. 7 (Color online) Schematic view of a focal adhesion. The transmembrane adhesion receptors from the integrin family (light green, a heterodimer with two subunits) bind to the extracellular matrix (brown, for example collagen) on the outside and are crosslinked by cytoplasmic proteins such as talin (blue) in the inside. Talin binds to actin (red) and this binding is further strengthened by proteins such as vinculin (orange). The contractility of the actin cytoskeleton is determined by the activity of myosin II minifilaments (dark green).

adhesions, or decay again. This switch typically occurs near the lamellipodium-lamella boundary, where a more condensed and myosin II-rich actin network replaces the dendritic network of the lamellipodium (Schwarz and Gardel, 2012; Shemesh *et al.*, 2012). Whether the adhesion grows and matures or whether it decays is strongly coupled to the mechanics of the system. The adhesions are stable only if sufficient force is exerted upon them and this is not possible on very soft substrates. This force is mainly applied by contractile stress fibers and networks connecting them to the focal adhesions in the lamella, although the force resulting from retrograde flow also might play an important role. Because focal adhesions are connected to the matrix, these forces are transmitted to the substrate and can be measured there with traction force microscopy on flat elastic substrates (Butler *et al.*, 2002; Dembo and Wang, 1999; Legant *et al.*, 2013; Plotnikov *et al.*, 2012; Sabass *et al.*, 2008; Schwarz *et al.*, 2002) or with fields of elastic pillars (Saez *et al.*, 2005; Tan *et al.*, 2003; Trichet *et al.*, 2012). These studies have shown that force and protein assembly are linearly coupled at focal adhesions, resulting in a constant stress for adhesions of about $5 \text{ nN/nm}^2 = 5 \text{ kPa}$ (Balaban *et al.*, 2001; Tan *et al.*, 2003). For elastic substrates, recently it has been suggested that this relation only holds for growing adhesions (Stricker *et al.*, 2011). For pillar assays, recently it has been reported that there exists a constant stress, but that it depends on extracellular stiffness due to global feedback (Trichet *et al.*, 2012). At any rate, the typical stress at single focal adhesions is close to the value of the physiological stiffness of matrix and cells; this suggests that these forces are used for mechanosensing in the physiological environment of the cell.

The detailed molecular organization of focal adhesions is a very active area of research that is very challenging due to the large number (more than 150) of different components that are involved (Kuo *et al.*, 2011; Zaidel-Bar *et al.*, 2007). Recent progress includes the use of electron tomography (Patla *et al.*, 2010) and superresolution microscopy (Shtengel *et al.*, 2009) to discern focal adhesion structure at scales smaller than the optical resolution, and the use of high throughput RNA-interference screens to dissect the regulatory hierarchy of focal adhesions (Prager-Khoutorsky *et al.*, 2011). Kinetic models have been used to describe the temporal and spatial coordination of the different components (Civelekoglu-Scholey *et al.*, 2005; Hoffmann and Schwarz, 2013; Macdonald *et al.*, 2008). Fig. 7 shows a schematic representation of a focal adhesion. In general, focal adhesions have a layered structure determined by the two-dimensional nature of the plasma membrane. The transmembrane adhesion receptors of the integrin family consists of two subunits, with relatively large headpieces that bind to the matrix and relatively small cytoplasmic tails. In the absence of special signals, the integrins have a low affinity for matrix binding. However, due to inside-out signaling (related to the cytoskeletal forces), the integrins can become activated and are then primed for matrix binding. This in turn leads to stabilization of the intracellular part of the adhesion complex that through the binding of a variety of cytoplasmic proteins, forms a two-dimensional plaque that reinforces the attachment of the cytoskeleton and the integrin layer. One of the main molecules responsible for cross-linking neighboring integrins is talin (Alberts *et al.*, 2007) (p. 842), which extends over 60 nm. Since talin also binds actin, it connects the integrins in the focal adhesion to the actin cytoskeleton. As the adhesion matures, this crosslinking is strengthened by additional proteins such as vinculin and paxillin, whose recruitment seems to be increased by force.

Focal adhesions act not only as mechanical linkers that anchor the cell to its substrate, but also as very prominent signaling centers that activate biochemical signaling molecules that diffuse into the cytoplasm and towards the nucleus (Vogel and Sheetz, 2009; Zaidel-Bar *et al.*, 2007). In our context, the most important signaling molecules are the small GTPases from the Rho-family (Rho, Rac and Cdc42), that regulate the assembly and activity of the actomyosin system. Each of these molecules acts like a molecular switch which is activated by exchanging GDP by GTP (analogous to ADP to ATP conversion); the active form then diffuses in the cytoplasma and activates downstream targets. For example, mature adhesions are known for Rho-signaling, which up-regulates both actin polymerization (through the formin mDia1) and contractility of non-muscle myosin II motors (through the Rho-associated kinase, ROCK). Moreover, many signaling molecules responsible for cell migration, differentiation and fate are localized to focal adhesions,

most prominently the focal adhesion kinase, FAK, which is known to be important in many types of cancer (Mitra *et al.*, 2005).

Adhesion proteins localized to focal adhesions coexist with the same proteins in relatively dilute solution in the cytoplasm or the membrane. The domains as a whole have relatively long lifetimes (tens of minutes) which suggests that the two coexisting phases might be at equilibrium. However, fluorescence studies (Wolfenson *et al.*, 2011) show that the adhesions continuously exchange proteins with the cytoplasm even though the large-scale composition and structure seem to remain unchanged. Thermodynamic equilibrium would dictate much larger domain sizes (or no domains at all) and why the adhesions are stable on the micrometer scale is not obvious (Lenne and Nicolas, 2009). This puzzle might be resolved by noting that in addition to diffusion, energy consuming, active processes may transport free proteins from the dilute phase in the cytoplasm or membrane to the adhesion sites. These active processes involve molecular motor proteins and are highly regulated by the cell (Kawakami *et al.*, 2001). This suggests that non-equilibrium effects may be important in stabilizing these finite-size domains, similar to the situation with treadmilling actin filaments.

Naively, one might try to understand cellular adhesions by analogy with physical adhesion (*e.g.*, of a synthetic vesicle coated with ligands that are attracted to an appropriate surface, see the preceding section). However, while physical adhesion is a passive process, cell adhesion involves molecular motors that generate internal stresses. Force generation consumes ATP and results in the fact that in addition to passive contacts that result in forces mainly directed in the normal direction, cells also exert contractile forces that act mainly in the lateral direction, *i.e.*, parallel to the substrate. These contractile forces have been observed in experiments that measure surface deformation (Butler *et al.*, 2002; Dembo and Wang, 1999; Sabass *et al.*, 2008; Saez *et al.*, 2005; Schwarz *et al.*, 2002; Tan *et al.*, 2003). Although recent experiments have also provided evidence for vertical forces (Delano-Ayari *et al.*, 2010; Hur *et al.*, 2009), most of these experiments were done with rather weakly adhering cells, which share some similarities with the passive reference cases discussed above (droplets, vesicles, capsules). Thus on a planar substrate it is the actively generated and often tangential forces that are used by the cell to regulate its response to the physical environment. This conclusion is supported by the fact that use of the myosin blocker blebbistatin not only leads to the disappearance of these forces, but also eliminates the cellular response to stiffness. Thus the main challenge is to understand how actively generated forces allow the cell to probe the physical properties of its environment.

IV. PHYSICS OF CELL-MATRIX ADHESIONS

A. Physical motivation

As explained in the previous section, cell adhesion does not occur homogeneously at the cell-material interface, but instead is characterized by the local assembly of specific adhesion molecules into supra-molecular adhesion sites, the so-called *focal adhesions*. For cell adhesion to a flat substrate, these focal adhesions are mainly situated at the cell periphery. During the last decade, it has been shown that the protein assembly that comprises the focal adhesion is strongly coupled to mechanical force. Experimental studies inducing changes in mechanical stress at adhesions have used shear flow (Davies *et al.*, 1994; Zaidel-Bar *et al.*, 2003), optical tweezers (Choquet *et al.*, 1997), micromanipulators (Heil and Spatz, 2010; Paul *et al.*, 2008; Riveline *et al.*, 2001), laser nano-surgery (Colombelli *et al.*, 2009; Kumar *et al.*, 2006; Lele *et al.*, 2006) or pharmacological drugs (Chrzanowska-Wodnicka and Burridge, 1996; Kuo *et al.*, 2011; Wolfenson *et al.*, 2011) to perturb and hence study the nature of these contacts. In all cases, it was observed that focal adhesions respond to changes in mechanical load by growth, as evidenced by changes in focal adhesion morphology and size. Quantitative correlation indicated a linear relation between force and adhesion size (Balaban *et al.*, 2001; Tan *et al.*, 2003), although the history of the adhesion and global determinants also play an important role (Stricker *et al.*, 2011; Trichet *et al.*, 2012).

From the physical viewpoint, it is interesting to note that tensile mechanical deformation, such as the shear induced by the tangential displacement of a pipette, leads to growth of focal adhesions in the direction of applied force (Riveline *et al.*, 2001). De-activation of actomyosin contractility reduces the adhesion size and eventually leads to its complete disruption (Balaban *et al.*, 2001). Other forces, such as hydrodynamic flow (Zaidel-Bar *et al.*, 2003) or stretching forces applied to the substrate (Kaunas *et al.*, 2005), also cause growth of focal adhesions in the direction of the force. The anisotropy of focal adhesion growth under force is characterized both by overall growth of the adhesion (in which the number of molecules involved increases) and by treadmilling (or sliding) of the center of mass of the adhesion towards the direction of the applied force. These anomalies cannot be explained with standard models of nucleation and growth of molecules adsorbed from solution onto surfaces. The role of force in stabilizing and promoting growth of FA has been discussed from several different points of view with a focus on predictions of the growth of focal adhesions in the direction of actomyosin or externally applied forces (Bershadsky *et al.*, 2006).

However, before discussing the growth response of focal adhesions under load, it is instructive to consider why this response has evolved in the first place. From

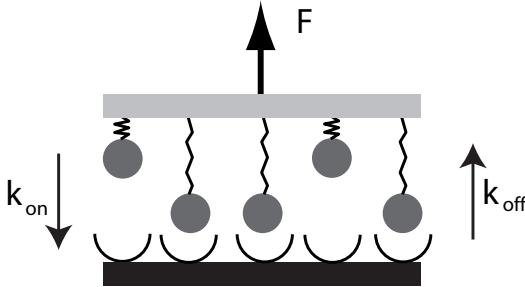


FIG. 8 Minimal model for an adhesion cluster under force: N_t adhesion receptors are arranged along the membrane. Due to this geometry, they share the load. At any time, $N(t)$ bonds are closed and $N_t - N(t)$ bonds are open. The applied force F is equally distributed over the closed bonds due to the parallel architecture, $F_{bond} = F/N(t)$. A bond dissociates with a force-dependent unbinding rate $k_{off}(F_{bond})$. The molecule can rebind with a constant rate k_{on} . Adapted from Erdmann and Schwarz (2004a).

the physical point of view, it seems obvious that in this way, the system avoids material failure. In general, failure under mechanical load is a phenomenon relevant to many systems of practical interest and on widely different scales, from muscle proteins (on the nanometer scale) through bone on a centimeter scale to bridges and buildings (on the meter scale) and earthquakes (on the kilometer scale) (Buehler and Keten, 2010). In contrast to the macroscopic systems considered in traditional fracture mechanics, biomolecular adhesions do not usually break at sharp, deterministic stability thresholds, but can unbind and rebind from the surface to which they adhere in a stochastic manner. This important observation is related to the weak interaction scales relevant to soft matter compared with hard matter. Thus, if one considers the stability of such assemblies (defined by either by their average lifetime or fracture strength), one must include stochastic effects, in contrast with traditional fracture mechanics of macroscopic systems where these effects are not relevant. Before we address the issue of growth, we therefore first consider the stability of adhesion clusters under load from the viewpoint of stochastic processes.

B. Stability of stationary adhesion clusters under force

We begin our discussion with physical considerations of the stability of stationary adhesion clusters of constant size. This crucial issue was first addressed in the seminal work of Bell (Bell, 1978). An adhesion cluster is modeled as a collection of N_t molecules near an adhesive surface, of which, at a given time t , a number $N(t)$ are bound and a number $N_t - N(t)$ are unbound, as shown in Fig. 8. Each of the bonds can break with a rupture rate k_{off} and each of the unbound molecules can bind with a rebinding rate k_{on} . Unbinding is assumed to

increase with force F as $k_{off} = k_0 e^{F/F_0}$, where F_0 denotes a molecular-scale force (typically of the order of pN). While Bell used this expression as a phenomenological ansatz, it was later motivated by Kramers theory (Hanggi *et al.*, 1990) for thermally assisted escape from a metastable state (Evans and Ritchie, 1997; Evans and Calderwood, 2007). Here the basic idea is that force lowers the height E_b of the transition state barrier. Because the escape rate scales as $\exp(-E_b/k_B T)$, adding a force term to the energy changes the escape rate by a factor $\exp(Fx_b/k_B T)$, where x_b is the position of a sharp transition state barrier. Indeed, this viewpoint has been impressively verified by dynamic force spectroscopy (Evans and Calderwood, 2007). For the rebinding rate, Bell assumed a value that is force independent. Note that this assumption does not reflect detailed balance (in which the ratio k_{on}/k_{off} is exactly equal to a Boltzmann factor related to the energy difference between the bound and unbound states). Thus, this model is one that is truly dynamic and can thus represent *e.g.*, different routes for binding and unbinding.

For the following, it is helpful to introduce the dimensionless time $\tau = k_0 t$, force $f = F/F_b$ and rebinding rate $\gamma = k_{on}/k_0$. Assuming a constant force f equally applied to all bound molecules, the following rate equation predicts the number of closed bonds:

$$\frac{dN}{d\tau} = -N e^{f/N} + \gamma(N_t - N) \quad (22)$$

While the second term representing rebinding is linear in the number of bonds, the first term representing forced-unbinding is highly non-linear and therefore leads to interesting feedback effects. As one bond opens, the remaining closed bonds must compensate to carry the additional load. Thus the coupling through force leads to a highly cooperative system. A bifurcation analysis of its steady state behaviour shows that the system is unstable (no steady state solution exists) when the force exceeds a critical value, f_c . This saddle-node bifurcation occurs when (Bell, 1978)

$$f_c = N_t \text{ pln}(\gamma/e) \quad (23)$$

where the product logarithm $\text{pln}(a)$ is defined as the solution of $xe^x = a$. Therefore an adhesion characterized by a finite number of bonded molecules is only stable up to a critical force f_c . For small rebinding rate γ , the critical force scales linearly with γ . Thus an adhesion cluster is completely unstable if the rebinding rate is zero; for finite rebinding the cluster stability (*i.e.*, the number of bonds formed) grows in proportion to the degree of rebinding. For large rebinding rates, the scaling becomes logarithmic; that is, once the rebinding rate exceeds the force-free unbinding rate, very large changes in γ are required to change the cluster stability in a significant manner.

The analysis of Bell immediately shows that due to the finite lifetime of single biomolecular bonds, adhesion

clusters can be stable under force only if rebinding takes place. However, Eq. (22) is a mean field description and does not include fluctuation effects, which are expected to be highly relevant in the biological context, both for the small precursors of focal adhesions and for possible subclusters that may exist within focal adhesions. Moreover, a description based on multiple bonds is required to treat more detailed situations of biological interest, as we discuss below. The natural extension of the mean field approach of Bell is a one-step master equation in the number i ($0 \leq i \leq N_t$) of bonded molecules (Erdmann and Schwarz, 2004a,b). Thus the probability $p_i(t)$ that i bonds are formed at time t evolves in time according to

$$\frac{dp_i}{dt} = r(i+1)p_{i+1} + g(i-1)p_{i-1} - [r(i) + g(i)]p_i . \quad (24)$$

The two positive terms represent the tendency for the number of bonds in state i to increase due to the dissociation of a formed bond in state $i+1$ and the formation of a new bond in state $i-1$, respectively. The two loss terms represent bond dissociation in state i (that contributes to state $i-1$) as well as the formation of a new bond (which changes the state from i to $i+1$), respectively. The rates corresponding to the Bell model Eq. (22) are

$$r(i) = ie^{f/i}, \quad g(i) = \gamma(N_t - i) . \quad (25)$$

As in Eq. (23), the first (rupture) term leads to strong cooperativity between the different bonds. The Bell equation Eq. (22) is recovered from the dynamic, stochastic model Eq. (24) if one calculates the average number of formed bonds, $N = \langle i \rangle$, in the limit of large system size (Kramers-Moyal expansion).

In contrast to the deterministic equation for the first moment, Eq. (22), which predicts infinitely long cluster lifetimes below the stability threshold, Eq. (23), the stochastic model Eq. (24) predicts finite lifetimes for any value of the force. The average lifetime of a cluster with $i = N_t$ bonds at time $t = 0$ can be identified with the mean time T for this cluster to stochastically evolve to the state $i = 0$ (no bound molecules). For a one-step master equation, this *mean first passage time* can be easily calculated (van Kampen, 1992):

$$T = \sum_{i=1}^{N_t} \frac{1}{r(i)} + \sum_{i=1}^{N_t-1} \sum_{j=i+1}^{N_t} \frac{\prod_{k=j-i}^{j-1} g(k)}{\prod_{k=j-i}^j r(k)} . \quad (26)$$

The first term in Eq. (26) is the result for vanishing rebinding, $\gamma = 0$. For small force, $f < 1$, it is analogous to the simple case of proportional (or radioactive) decay (for $\gamma = f = 0$, one basically deals with the stochastic version of $dN/dt = -N$). Using that approximation one finds that the cluster lifetime scales as $T \approx \ln N_t$; that is, the cluster size N_t has only a relatively weak effect

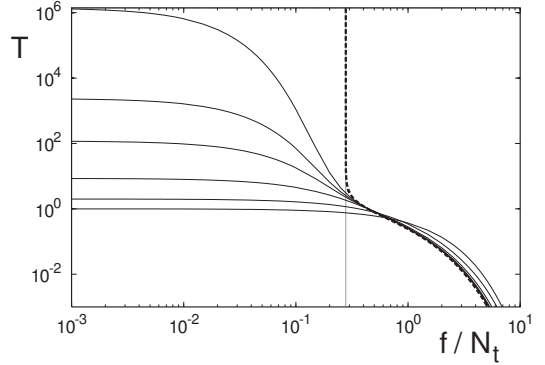


FIG. 9 Average cluster lifetime T for $N_t = 1, 2, 5, 10, 15$ and 25 (from bottom to top) as a function of $F/F_b N_t$ for $k_{on} = k_0$ as it follows from Eq. (26). The vertical line is the critical force predicted by Eq. (23) and the dashed line is the lifetime predicted by Eq. (22). Adapted from Erdmann and Schwarz (2004b).

on the stability of the cluster, because the bonds dissociate in parallel with no cooperativity. Finite force exponentially decreases the lifetime due to the Bell-equation. The second term in Eq. (26) increases the lifetime as a polynomial of order $N_t - 1$ in γ and approximately exponentially with increasing cluster size N_t . For $N_t = 2$, Eq. (26) reads

$$T = \frac{1}{2} \left(e^{-f/2} + 2e^{-f} + \gamma e^{-3f/2} \right) . \quad (27)$$

This simple but instructive formula shows how force f exponentially suppresses the cluster lifetime, while rebinding γ increases it in a polynomial fashion.

In order to study the cluster lifetime as a function of force, in Fig. 9 we plot T as calculated from Eq. (26) as a function of f/N_t for $\gamma = 1$ and different values of the cluster size N_t . For small force $f < N_t$, the mean lifetime increases exponentially with the cluster size N_t . For large force $f > N_t$, rebinding becomes irrelevant and all the curves for different values of N_t are very similar. One very interesting aspect here is the transition region, which is characterized by strong amplification (a small change in force f has a strong effect on the mean lifetime T). This transition region corresponds to the stability threshold from Eq. (23) (vertical line). Above this threshold, a deterministic lifetime can be defined by numerically solving Eq. (22) with $N(0) = N_t$ and solving for the time at which $N = 1$ (this replaces the criterion $i = 0$ from the stochastic case, which cannot be used in the deterministic case due to exponential approach of $N = 0$). The result (dashed line) corresponds well to the mean cluster lifetime from the stochastic model, but diverges at the threshold.

Eq. (26) can be used to make interesting estimates for experimental situations of interest. For example, in the case of zero rebinding rate ($\gamma = 0$) and zero applied force ($f = 0$), for a single bond lifetime of one second

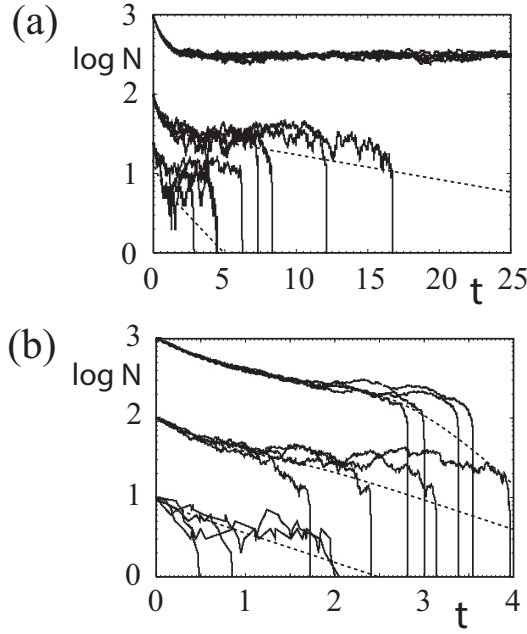


FIG. 10 Selected trajectories simulated with the stochastic master equation model. Rebinding rate $\gamma = 1$. (a) Force below threshold, $f/N_t = 0.25$. Small clusters ($N_t = 10$ and 100) are unstable due to fluctuations. (b) Force above threshold, $f/N_t = 0.3$. Now all cluster sizes are unstable. Lines are first moments. Adapted from Erdmann and Schwarz (2004a).

($k_0 = 1/s$), a cluster lifetime T of one minute could only be achieved with for the absurdly large number of 10^{26} bonds; this is because in this case, the cluster lifetime scales only logarithmically with cluster size. However, for a finite rebinding rate of $\gamma = 1$ ($k_{on} = k_0$, still at zero force), only $N_t = 10$ bonds are necessary, because the lifetime scales strongly with rebinding rate: $T \sim \gamma^{N_t-1}$. Increasing the dimensionless force to $f = 10$ (corresponding to 40 pN for $F_b = 4$ pN) would decrease the lifetime to $T = 0.05$ s, because T is an exponentially decreasing function of f . To reach a cluster lifetime of one minute in this case, the cluster size must be increased to 50 or the rebinding rate must be increased by a factor of 10.

One of the strongest advantages of the stochastic model is that it can be used to simulate single trajectories, which share many similarities with experimental realizations of individual experiments. In Fig. 10 we show selected simulated trajectories for forces below (a) and above (b) the critical force. We note that failure is rather abrupt due to cooperative effects: once sufficiently many bonds have broken, *e.g.*, due to a fluctuation that leads to a smaller number of bonds, the force on the remaining ones is so high that rebinding becomes very unlikely and the cluster fails in a cascade of dissociated bonds that leads to rupture of the adhesion cluster (*cascading failure*). Interestingly, this effect is not apparent if one calculates only the averages, which are shown as lines. We further note that even below the stability threshold

in (a), small clusters are likely to fail due to the finite probability for a devastating fluctuation that takes the system to a state with a small numbers of closed bonds. Above the threshold in (b), clusters of any size are unstable.

The conceptual framework introduced by Bell shows how an adhesion site can at the same time be highly dynamic and yet be stable up to some maximal force: while some bonds can dissociate and then rebind, the remaining adhesion bonds allow the transfer of force from the cell to the substrate. The simple model also shows that this mechanism leads to strong cooperativity, because each bond that forms or breaks leads to a fast redistribution of the force, thereby affecting all the other bonds. The same cooperative mechanism operates in many other biologically relevant situations, *e.g.*, during force generation in muscle (Duke, 1999; Huxley, 1957) or during cargo transport by multiple molecular motors (Gurin *et al.*, 2010; Klumpp and Lipowsky, 2005). The stochastic extension of the Bell model demonstrates that adhesions are not only unstable for large applied forces, but are also unstable at small sizes for which fluctuations to smaller numbers of closed bonds can be detrimental.

C. Adhesion between moving surfaces

Adhesion not only occurs via molecular binding of two stationary surfaces, but also frequently bridges two surfaces that move relative to each other. This is especially relevant for matrix adhesion underneath the cellular lamellipodium, where actin retrograde flow can transport individual binding molecules from the cell edge towards the cell body and where nascent adhesions form and mature in the region between the cell and the substrate. It has been found experimentally that in this case, a biphasic relation exists between the traction force on the substrate and the flow velocity in the cell: while the traction force and flow velocity are linear proportional in the case of mature adhesions, they are inversely related in the case of fast flow over nascent adhesions (Gardel *et al.*, 2008b). Experimentally, the threshold value of the velocity at which this change occurs has been found to be 10 nm/s and to be insensitive to various perturbations of the cellular system. Surprisingly, the simple conceptual framework introduced above for stationary adhesion sites can be extended to explain these experimental findings (Li *et al.*, 2010; Sabass and Schwarz, 2010; Srinivasan and Walcott, 2009).

Fig. 11 shows the minimal model for the situation of interest. The upper surface moves with a velocity v relative to the lower surface. Each bond is modeled as a spring with spring constant κ that immediately gets elongated with velocity v once it is formed. In contrast to the minimal model for a stationary adhesion cluster, see Fig. 8, there are two essential differences. First, the governing

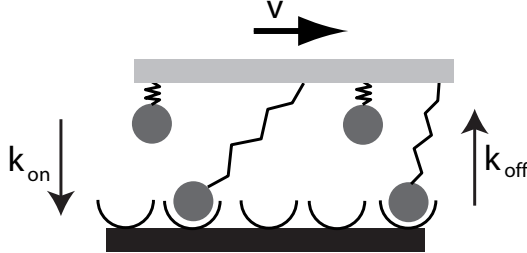


FIG. 11 Minimal model for an adhesion cluster that bridges two surfaces that move relative to each other with velocity v . Here we discuss this case in the limit of continuous ligand and receptor coverage. The situation described here is very similar to sliding friction as usually studied for macroscopic objects.

model parameter is the relative velocity v rather than the external force F . This also implies that different bonds are not coupled by force and a theoretical description can be constructed using a single bond model. Second, each bond is characterized by its dynamic length, namely its extension compared with the case of zero velocity, which we denote by x . This is in addition to the property of the bonds to dynamically form or dissociate. We therefore now introduce a probability that depends on both time and bond elongation, $p_b(x, t)$, that describes the likelihood that at time t a given bond is closed and has elongation x . The complementary probability that the molecule is dissociated is not related to the elongation x and we denote it by $p_u(t)$. From normalization we get

$$p_u(t) = 1 - \int_{-\infty}^{+\infty} dx p_b(x, t) = 1 - P_b(t) \quad (28)$$

where we have introduced the abbreviation $P_b(t)$ for the overall probability of a bond to be closed with some elongation x . When we assume harmonic springs with spring constants κ , the average traction on the substrate is determined by the first moment of $p_b(x, t)$:

$$F_T = N_t \kappa \int_{-\infty}^{+\infty} dx x p_b(x) . \quad (29)$$

We next consider the evolution equation for $p_b(x, t)$. In contrast to the equation for the fraction of bound bonds for the stationary adhesion cluster, Eq. (22), we now have a convective derivative that accounts for the change in extension due to the fact that the molecules (one end of which are fixed to the moving surface) are moving with velocity v :

$$\frac{\partial p_b}{\partial t} + v \frac{\partial p_b}{\partial x} = -p_b k_{off} + (1 - P_b) k_{on} \delta(x) . \quad (30)$$

Here p_u has been replaced by the right hand side of Eq. (28). The delta-function represents the assumption that a new bond forms with vanishing elongation x . For the

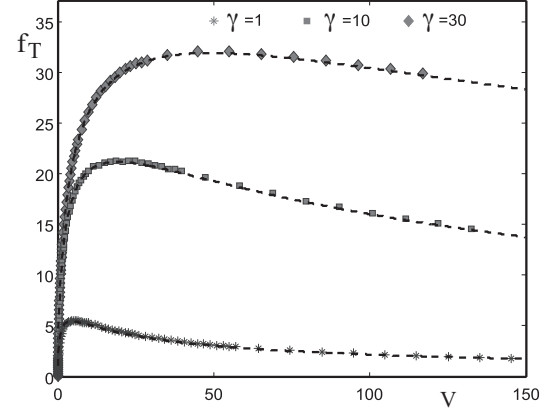


FIG. 12 Biphasic relation between dimensionless flow V and dimensionless traction force f_T predicted by the minimal model for cluster size $N_t = 25$ and for different values for the rebinding rate. Symbols are the results of stochastic simulations with N_t single bonds. Adapted from Sabass and Schwarz (2010).

single bond unbinding rate k_{off} and rebinding rate k_{on} , we make assumptions similar to those made for the bonds in a stationary cluster, namely a Bell model $k_{off} = k_0 e^{rx}$ for the unbinding rate and a constant rebinding rate, $k_{on} = const$. Here the reactive compliance $r = \kappa/F_b$ is a typical inverse length scale of the bond. With these simple form of the rates, the steady state with $\partial p_b / \partial t = 0$ can be calculated analytically (Sabass and Schwarz, 2010; Srinivasan and Walcott, 2009).

We first note that because bonds form with vanishing elongation and are then stretched by the motion of the upper surface (so that the elongation is positive), the probability of negative elongation vanishes, $p_b(x < 0) = 0$ (the time t does not appear because we consider steady state). From Eq. (30) we see that for $x = 0$ we have

$$p_b(0) = p_0 = (1 - P_b) \frac{k_{on}}{v} = (1 - P_b) \frac{\gamma r}{V} \quad (31)$$

where we have defined a dimensionless velocity $V = rv/k_0$ and $\gamma = k_{on}/k_0$ is the dimensionless rebinding rate defined above. For $x > 0$, Eq. (30) is solved by

$$p_b(x) = p_0 e^{\frac{1}{V}(1-e^{-rx})} \quad (32)$$

Therefore, the probability for a bond (with probability p_0 at $x = 0$) to be elongated by an amount x decays faster than exponentially as x increases. After calculating P_b from Eq. (32), one finds the traction force from Eq. (29) in dimensionless form:

$$f_T = \frac{r F_T}{\kappa} = N_t \frac{M(1/V)}{E_1(1/V) + (V/\gamma)e^{-1/V}} \quad (33)$$

where we have used two special functions, the exponential integral $E_1(x)$ and a Meijer G-function $M(x)$ defined by

$$E_1(x) = \int_0^\infty dy e^{-xe^y}, \quad M(x) = \int_0^\infty dy y e^{-xe^y} \quad (34)$$

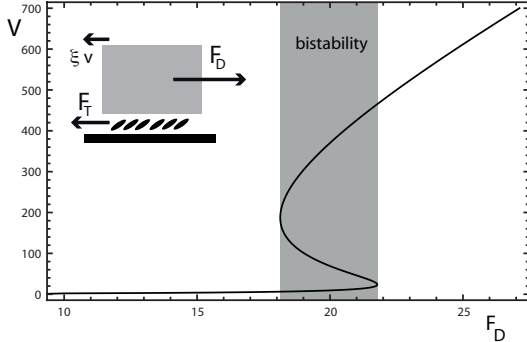


FIG. 13 The non-linear relation between the flow velocity v and the traction force F_T from Fig. 12 leads to a region of bistability for the flow velocity v as a function of the driving force F_D . Parameters $N_t = 25$, $\gamma = 10$, $\xi k_0/\kappa = 0.03$.

In Fig. 12, we plot this result for the traction force f_T as a function of the velocity V for three different values of the rebinding rate γ . One sees that the relation is biphasic: the traction force first increases linearly with velocity, but then decays again after going through a maximum value. The symbols in Fig. 12 are the results of computer simulations for stochastic models with the same number of bonds (Sabass and Schwarz, 2010). The analytical result from Eq. (33) agrees with the experimental observation of a biphasic relation in retrograde flow (Gardel *et al.*, 2008b). The fit of the model to the data can be improved by making more specific assumptions like catch bonding (Li *et al.*, 2010). For small flow, $V < 1$, the model predicts a linear relation between flow speed and traction force, as observed for flow over mature adhesions:

$$F_t = \frac{N_t k_{on}}{k_{on} + k_0} \kappa \frac{v}{k_0}. \quad (35)$$

Therefore, in this regime the traction force is simply the sum of the spring forces for the typical extension $x = v/k_0$ which is reached when a bond is elongated due to a velocity v applied for a time $1/k_0$. The prefactor represents the equilibrium number of bonds that were formed, that is the number of springs carrying force. For large force, $V > 1$, bond rupture predominates which does not allow transmission of appreciable levels of force. In that case, the velocity and traction force are inversely related, as observed for fast flow over nascent adhesions. The crossover between proportional and inverse regimes occurs when $V \approx 1$, that is $v = k_0/r$. With a typical unstressed unbinding rate of $k_0 = 1\text{Hz}$ and a typical reactive compliance of $r = \kappa/F_b = 0.5\text{nm}^{-1}$, this predicts $v = 2\text{ nm/s}$, on the order of the experimentally observed values of 10 nm/s .

The concept of friction has been discussed in the biological context before (Marcy *et al.*, 2007; Tawada and Sekimoto, 1991). Moreover, the biphasic relation between flow and traction has been noted before in a non-biological context for sliding friction mediated by discrete

microscopic bonds (Filippov *et al.*, 2004; Schallamach, 1963). The large velocity regime suggests the possibility of an instability: as the velocity increases, the traction force decreases, thus leading to an even larger velocity. In order to investigate this point in more detail, a dynamical model for flow over adhesion sites is required. A simple model motivated by the typical conditions at the lamellipodium is to assume that the actin cytoskeleton is driven by a constant driving force F_D (representing both the push of the polymerizing actin network away from the leading edge and the pull by the myosin motors towards the cell body). This force is balanced by the frictional force with the substrate and an intra-cellular viscous force representing dissipative processes in the lamellipodium. Thus the force balance reads

$$F_D = F_T(v) + \xi v \quad (36)$$

with $F_T(v)$ from Eq. (33). In Fig. 13, we numerically invert this equation to plot the velocity v as a function of the driving force, F_D . One sees that the non-linear relation from Eq. (33) leads to a region of bistability: there is an interval of intermediate driving force for which two values of the velocity are stable. In practice, this will lead to stochastic switching between periods of slow and fast flow, a phenomena which is known as *stick-slip motion* in sliding friction and which can be easily verified using stochastic simulations (Sabass and Schwarz, 2010). Indeed this irregular kind of motion has been observed for filopodia retraction and has been successfully simulated with a detailed stochastic model which also included the effect of stochastic force generation by myosin II motors (Chan and Odde, 2008).

D. Load localization and fracture in adhesions

The view of focal adhesions as bond clusters is a very flexible conceptual basis that can be applied to more specific situations of interest. As an instructive example, we now discuss its extension to include the role of elasticity of the anchoring bodies. This subject is very important because cells have been shown to respond very strongly to changes in cellular and environmental stiffness, mainly through changes in the stability of their adhesion sites. We consider the situation depicted in Fig. 14 as analyzed in Qian *et al.* (2008). A single adhesion site of size $2a$ is located between two elastic halfspaces, one representing the cell (C) and the other the substrate (S). The cell has Young's modulus E_C and Poisson's ratio ν_C , while the substrate is characterized by E_S and ν_S . The two half-spaces are pulled apart by a pair of equal and opposite forces (a force couple) of magnitude F , acting in the plus and minus z -directions. The density of ligands in the adhesion is $\rho = 1/b^2$. By considering cylindrical geometry and a section of thickness b in the y -direction, the model is reduced to one lateral dimension whose coordinate is

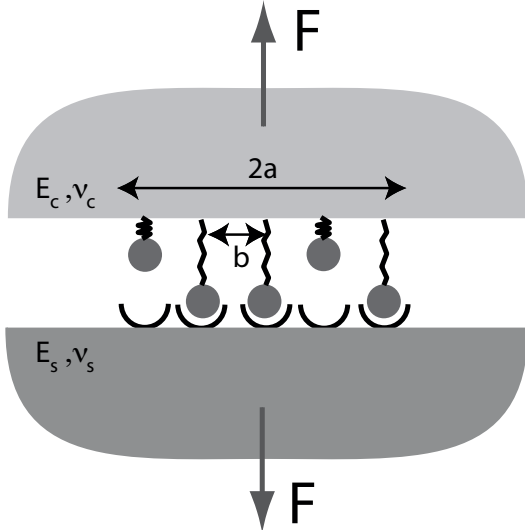


FIG. 14 Model of an adhesion cluster loaded by equal and opposite forces of magnitude F , each applied to an elastic halfspace. E_C and ν_C denote the Young's modulus and Poisson's ratio of the cell, and E_S and ν_S , those of the substrate. $2a$ and b are the linear dimension of the adhesion cluster and the distance between receptor-ligand bonds, respectively.

denoted by x . The number of bonds in the adhesion is $N_t = \rho 2ab = 2a/b$. As above, we ask how the cluster stability is affected by force, for example by calculating the mean cluster lifetime T or the critical force F_c as a function of the model parameters.

In order to treat the mechanical aspects of the model, we use continuum mechanics. As it is common in contact mechanics, we define an effective elastic modulus E^* that accounts for both the cell and substrate by

$$\frac{1}{E^*} = \frac{1 - \nu_C^2}{E_C} + \frac{1 - \nu_S^2}{E_S}. \quad (37)$$

The adhesion cluster is loaded by interfacial stress $\sigma(x)$ that acts in the normal direction; the force determining the rupture rate of a single bond located at x would then be $\sigma(x)b^2$. We first consider the case when all the molecules are bonded to the lower surface. Then $\sigma(x) = \rho\kappa u(x)$, where κ is the spring constant of a single bond as before and $u(x)$ is the bond extension. From continuum mechanics, which shows that stress and strain propagate with an elastic Green's function that decays in space as $1/r$ (Landau and Lifshitz, 1970), the following equation can be derived for $\sigma(x)$:

$$\frac{d\sigma(\hat{x})}{d\hat{x}} = \frac{2\alpha}{\pi} \int_{-1}^1 \frac{\sigma(\hat{s})}{\hat{x} - \hat{s}} d\hat{s}. \quad (38)$$

Here we have used dimensionless variables and have defined the *stress concentration index* α as

$$\alpha = \frac{a\rho\kappa}{E^*}. \quad (39)$$

Thus the stress concentration index is linearly proportional to the adhesion size, bond stiffness and bond density, and inversely proportional to the effective elastic modulus.

Eq. (38) can be solved in two limiting cases of immediate interest. For $\alpha \rightarrow 0$, we find that $\sigma(x)$ is a constant independent of x . Thus for rigid surfaces, the elastic model reduces to that of stationary adhesions introduced above; in that case, small clusters are the most unstable. For $\alpha \rightarrow \infty$, Eq. (38) is solved by

$$\sigma(x) = \frac{F}{\pi ab} \frac{1}{\sqrt{1 - (x/a)^2}}. \quad (40)$$

Thus, the stress distribution at the edge becomes singular, similar to that of a crack. A numerical solution shows that in general, the interfacial stress is distributed rather uniformly for α smaller than 0.1, and becomes localized to the adhesion rim for α larger than 1. Because the crack-like distribution will lead to cascading failure from the rim, large adhesions will be unstable since they give rise to a large stress concentration index according to Eq. (39). Thus, both very large and very small clusters are predicted to be unstable, suggesting that intermediate cluster sizes have the longest lifetimes.

E. Adsorption kinetics for growing adhesions

Up to now, our discussion has centered on the physical limits for the stability of adhesion clusters under conditions in which forces tend to destabilize the bonds that are formed. We have seen that force, adhesion cluster size, surface motion and elasticity define clear limits for the physical stability of adhesion sites. We now address the question of how biological focal adhesions (FA) can protect themselves against these limiting factors. The main mechanism which seems to have evolved in this regard is growth under force, which we will now discuss.

We begin with a generic treatment of adsorption kinetics that are governed by the chemical potential differences of molecules in the solution and those adsorbed to the adhesion on the substrate. If the FA is under conditions close to equilibrium and if the growth is reaction-limited as opposed to diffusion-limited, the growth dynamics of the adhesion depend on the dimensionless chemical potential difference (in units of $k_B T$) between molecules in solution and those adsorbed to the FA. The dimensionless, local (fractional) area coverage by these molecules is denoted by $\phi(\vec{r})$ which is also time dependent: $d\phi(\vec{r})/dt = (1/\tau)(\mu_b - \mu_a(\vec{r}))$ (Diamant and Andelman, 1996), where t is the time variable and τ is a characteristic time; since ϕ and μ are dimensionless each side of the equation scales as the inverse of a time. Here τ is the attempt time for molecules near the surface to adsorb, and μ_b and $\mu_a(\vec{r})$ are the dimensionless chemical potentials (in units of $k_B T$) of molecules in the bulk

cytoplasm and the FA, respectively. When $\mu_a < \mu_b$ adsorption is locally favored and the local concentration of adsorbed molecules grows in time. We classify the chemical potential of molecules in the FA by terms with different symmetries with respect to the external force and afterwards discuss the molecular origins of these terms in different models. We therefore write:

$$\frac{\partial\phi(\vec{r})}{\partial t} = \frac{1}{\tau} \left(\mu_b - \left(\mu_\ell(\vec{f}) + \mu_i(\phi(\vec{r})) + \mu_f(\vec{f}, \phi(\vec{r})) \right) \right) \quad (41)$$

The term $\mu_\ell(\vec{f})$ depends on the cytoskeletal (CSK) force, \vec{f} , but not on the local, dimensionless, local area fraction covered by adhesion molecules, $\phi(\vec{r})$. It originates in those terms derived from the derivative of the free energy with respect to $\phi(\vec{r})$ that are independent of ϕ and are thus not cooperative in nature. The next term depends on the local concentration (and hence reflects cooperativity of the adhesion molecules) but not on the force, while the last term depends on both.

The local, chemical interaction (ligand binding) of the adsorbing molecules with the surface, $\mu_i(\vec{f})$, includes the effects of force-induced changes in the single-molecule conformations. Since the chemical potential is a scalar quantity while the force \vec{f} is a vector, symmetry dictates that to quadratic order in the force (which is assumed to be small) it must have the form $\mu_i = \mu_0 + \alpha < \vec{f} \cdot \vec{d} > + \beta f^2$ where μ_0 is force independent and α and β are constants. The angle bracket $< \vec{f} \cdot \vec{d} >$ denotes an average over all the orientations of a vector that resides in the adsorbed molecule \vec{d} to which the force (possibly) couples; this coupling results in a conformational and hence in an energy change. If the adsorbing molecules are oriented at a fixed angle relative to the CSK force, this term will depend only on the magnitude of the CSK force.

The mutual, force independent, interactions of the molecules that assemble in the FA, are reflected in the term $\mu_f(\phi(\vec{r}))$ and is derived from the functional derivative of the interaction free energy with respect to $\phi(\vec{r})$ (Safran, 2003). For convenience, one can consider a Ginzburg-Landau expression for the free energy for interacting molecules that nucleate a condensed phase in equilibrium with a “gas” (low concentration) phase of adsorbates on the surface (Safran, 2003). In order to obtain an analytical solution it is convenient (but not necessary in general) to focus on values of ϕ that are close to the critical value, ϕ_c at which the condensation first occurs as the temperature is lowered (Safran, 2003) as the system parameters approach a critical value (which for simple systems can be the critical temperature but for more complex systems can depend on the interaction energies, effective temperature and other parameters). The chemical potential, $\mu_i = \delta F_0 / \delta \psi$ is derived from a free energy (in units of $k_B T$) of the form:

$$F_0 = \int dx dy \left[-\frac{1}{2} \epsilon \Psi^2 + \frac{1}{4} c \Psi^4 + \frac{1}{2} B (\nabla \Psi)^2 \right] \quad (42)$$

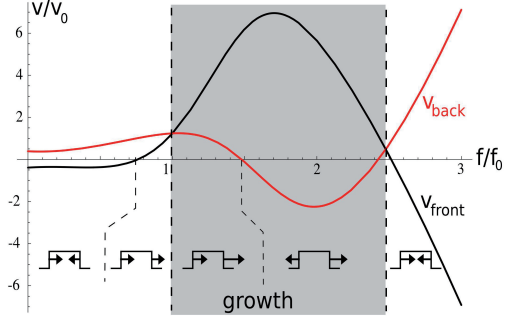


FIG. 15 (Color online) Calculated velocities of the front (closer to the direction of the pulling force in this figure, to the right) and back of the adhesion for a rigid matrix. Courtesy of A. Nicolas and adapted from Besser and Safran (2006) and Nicolas *et al.* (2008).

where $\Psi = \phi - \phi_c$, ϵ is the deviation from criticality (for simple systems $\epsilon \sim (T_c - T)/T_c$), c is a number of order unity, and B is proportional to the attractive interaction between the molecules (Safran, 2003).

We note that the scalar nature of the chemical potential means that the lowest order term in μ_f must be the dot product of two vectors: the local force and the gradient of the adhesion molecule density so that μ_f is proportional to $\vec{f} \cdot \nabla \phi(\vec{r})$. Such a term cannot be derived from the direct functional derivative of a free energy that is only a function of \vec{f} and $\psi(\vec{r})$ and its derivatives. However, as discussed in the context of the molecular models, the adsorption may be coupled to other degrees of freedom in the system such as its mechanical properties (*e.g.*, strain, anchoring to the substrate). These can give rise to terms in the free energy that are manifestly and linearly force dependent and that can equilibrate more quickly than the adsorption. The discussion below of the microscopic models demonstrates that this coupling can effectively yield the term $\vec{f} \cdot \nabla \psi(\vec{r})$, written here from symmetry considerations alone.

With these expressions for the various contributions to the chemical potential, one can analytically solve Eq. 41 in one dimension in terms of $\Psi = \phi - \phi_c$ where ϕ_c is the average concentration of the coexisting high and low density phases on the surface (*i.e.*, the adhesion and a low density “gas” of isolated, surface adsorbed molecules). The protein assembly grows (Besser and Safran, 2006) in the direction of the force with a profile given by: $\Psi(x, t) = \Psi(x - vt)$ with the growth velocities at front and back related to the characteristic velocity $v_0 = \xi/\tau$ where ξ is the correlation length that characterizes the interface width: $\xi^2 \sim B/\epsilon$. In the limit of small chemical potential differences between the molecules in solution and those in the FA, we can calculate the velocities of the front (closer to the pulling direction) and back of the

adhesions as shown pictorially at the bottom of Fig. 15:

$$\begin{aligned} v_{front} &= +v_0 \Delta\mu(f) + f\sigma \\ v_{back} &= -v_0 \Delta\mu(f) + f\sigma \\ v_{tot} &= v_{front} - v_{back} = v_0 \Delta\mu(f) \end{aligned} \quad (43)$$

where $\Delta\mu(f) = \mu_b - \mu_0 - \alpha < \vec{f} \cdot \vec{d} > -\beta f^2$. The term $f\sigma$ arises from the symmetry-breaking term in the chemical potential $\vec{f} \cdot \nabla\psi(\vec{r})$. One considers the case where $\mu_0 > \mu_b$, $\alpha < 0$ and $\beta > 0$ (so that $\Delta\mu(f) > 0$), favoring adsorption for some range of force, but not for forces that are too small or too large; the quadratic term in f inhibits growth when the force becomes too large. Note that the overall growth velocity of the adhesion depends on the homogeneous activation term but is independent of the symmetry breaking term $\vec{f} \cdot \nabla\psi(\vec{r})$. These findings indicate that both force-induced activation modes are required to explain the anisotropic growth of focal adhesions: the homogeneous activation term alone could not explain the anisotropy of the aggregation, whereas the symmetry breaking term alone could not account for overall adhesion growth.

The stress dependence of the velocity is shown in Fig. 15 for a rigid substrate. As expected, this model accounts for both the growth and sliding of the adhesion, based on a treadmilling mechanism. This treadmilling mechanism was recently observed experimentally (de Beer *et al.*, 2010). In addition, the theory also predicts a range of stress in which the adhesion indeed grows. Furthermore a regime where the front and back edges move apart is predicted; this was also recently reported (de Beer *et al.*, 2010; Heil and Spatz, 2010).

F. Force-induced growth of adhesions

We now discuss two classes of models that motivate the general treatment presented here from more molecular considerations to explain the stability and growth of focal adhesions under CSK force: (i) microscopic models that motivate the nucleation and growth picture described above and (ii) an analogy to force induced polymerization that takes into account the imbalance of CSK stresses and adhesion molecule anchors. These two approaches differ in several aspects, the most important of which is whether the symmetry breaking exists already at the genesis of the adhesion (model (ii)) or whether it is a spontaneous consequence of force applied to an adhesion (model (i)) with no intrinsic asymmetry in its internal structure. The first class of models that are based on nucleation and growth is supported by experiments that suggest that focal adhesion growth occurs primarily at the front and back of the plaque (de Beer *et al.*, 2010; Heil and Spatz, 2010). As explained below, the second class of models would allow for adhesion molecules to accrue all along the plaque. On the other hand, experiments also show that the focal adhesion is not symmetric;

the front is acted upon by the CSK stress fibers while the back is facing the lamellipodium. This provides support for the intrinsic asymmetry of binding and force that is the basis for the second class of models. All of these models focus on forces that are tangential to the substrate, appropriate to stress fibers near the basal cell surface. Adhesion growth induced by forces normal to the surface has been modeled in Walcott *et al.* (2011). Their results and related experiments show that for normal forces, adhesion nucleation and decay depends sensitively on the substrate stiffness; however, the growth and decay dynamics themselves are stiffness independent.

(i) *Symmetry breaking due to activation of mechanosensors (within the adhesion) by force:* The model introduced by Nicolas and coworkers (Besser and Safran, 2006; Nicolas *et al.*, 2008, 2004; Nicolas and Safran, 2006a) assumes that the dynamics of FA is governed by the activation of mechanosensitive units, that are part of the adhesion. Since the molecules in the FA are attached both to the matrix and to the CSK, they sense variations of mechanical stresses in the cell as well as the local, elastic properties of the extracellular matrix. The symmetry breaking occurs spontaneously, without introducing an adhesion geometry that desymmetrizes the front and back. Instead, the adhesion treads or slides in the direction of the force because the force itself is a vector that breaks symmetry via the term in the chemical potential $\vec{f} \cdot \nabla\psi(\vec{r})$ where it couples to the concentration gradients in an asymmetric manner at the front and back of the adhesion.

The model includes two modes of deformation (Nicolas and Safran, 2004). (a) The stretching of the individual molecules of FA assembly by the CSK force, which corresponds to a shear deformation of the FA and (b) the effect of compression induced by lateral compressions (due to forces tangential to the substrate); this is a cooperative effect involving the displacements of neighboring molecular units (Ali *et al.*, 2011). The compressive mode is asymmetric in its response to a local, tangential stress since the back edge of the FA is expanded while the front edge is compressed. Assuming that compression induces adhesion growth (*i.e.*, lowers the adsorption free energy of molecules in solution that contact the substrate) and that expansion induces desorption, the front of the adhesion may grow, while the back may shrink. This results in a treadmilling of the adhesion and an apparent motion in the direction of the force. In contrast to this, the stretching mode is symmetrical in response to the tangential stress; both the back and the front edges are activated with identical probabilities. If the stretching results in conformations that stabilize adsorbed molecules, this will result in growth of the front of the adhesion in the direction of the force and in the growth of the back of the adhesion in the opposite direction; the net result will be an overall growth of the size of the adhesion. It should be noted that activation of the adhesion molecules is ex-

pected to require tensile forces. In a picture in which the mechanosensor is a single molecule, it is not obvious how these forces can arise from compression at the front edge of the adhesion. However, if one associates the mechanosensor with a complex assembly of molecules that include the integrins and the protein plaque, reorientation and interactions may indeed give rise to molecular extensions in the direction perpendicular to the compression *e.g.*, by the tendency for a molecular assembly to conserve its volume. These effects may activate adsorption even in the absence of externally generated tensile forces. FA growth as a function of substrate rigidity can be predicted if one assumes that the adsorption is partially controlled by the energy invested by the CSK in deforming the substrate; this of course depends on the size and nature of the adhesion. For soft substrates, the substrate is deformed over a thickness related to the adhesion size. This limits the maximal size of the adhesion due to the stresses and strains that the CSK forces induce in the underlying matrix via the coupling by the FA (Nicolas *et al.*, 2008).

A related point of view was recently presented by Garikipati and collaborators (Olberding *et al.*, 2010) who used a general thermodynamic argument to motivate the symmetry breaking term in μ_f . Instead of assuming that the adhesion molecules are activated to adsorb near regions of compression and desorb near regions of expansion as in Nicolas *et al.* (2008) and Nicolas and Safran (2006a), the “negative work” done by the CSK pulling forces is included in the energetics at the outset. The resulting energy is decreased when the adhesion moves in the direction of the force (towards the nucleus); this apparent sliding occurs by the adsorption of molecules at the edge of the adhesion that is closest to the nucleus (or direction of applied force) and desorption at the other end. We note that this mechanism can lead to growth all along the adhesion surface and not just at the edges, as discussed below in relation to the work of Shemesh *et al.* (2005).

Another model that focuses on the integrin binding with the adhesion has been suggested by Deshpande and coworkers (Deshpande *et al.*, 2006, 2007; McGarry *et al.*, 2009; Pathak *et al.*, 2008) who have developed a thermodynamically motivated computational approach that has three essential features: (i) coexistence of both low and high affinity integrins in thermodynamic equilibrium, (ii) mobility of the low affinity integrins within the plasma membrane, and (iii) mechanical equilibrium of the contractile forces generated by the stress fibers – these forces affect the free energies of the integrins and give rise to a coupled thermo-mechanical response. An initial prediction based on this is the correlation of the distributions of the normalized focal adhesion densities (as parameterized by the high affinity integrin concentration) and contours of the stress fiber density. However, this model does not contain spontaneous symmetry breaking and the growth

of adhesions in the direction of the applied force requires the ad-hoc inclusion of anisotropic activation signals.

Another recent model of focal adhesion growth focuses on the bond attachment-reattachment dynamics discussed above and combines this with considerations related to clustering. The stochastic elastic model combines theory and Monte Carlo simulations (Gao *et al.*, 2011) and suggests that FA growth is self-limiting since growth eventually leads to crack-like delamination failure near the adhesion edges. Very soft substrates tend to diminish the adaptive capability of cells by suppressing bond rebinding irrespective of the cytoskeleton stiffness, which may prevent short-lived, small focal contacts from maturing into stable FA.

(ii) *Symmetry breaking due to the geometrical structure of the adhesion:* The model introduced by Kozlov and coworkers (Shemesh *et al.*, 2005) uses a general thermodynamic argument to write $\mu_f = -\vec{f} \cdot \vec{d}$ where \vec{f} is the force applied by the CSK to one adhesion molecule and \vec{d} is a particular bond in the molecule that is stretched by that force. In the one-dimensional version of the model described in Shemesh *et al.* (2005), the force and bond are in the same directions. This energy represents the “negative work” done by the CSK against the adhesion when an additional protein is allowed to adsorb. In the absence of this additional protein, the adhesion would be stretched and deformed by the CSK force; the presence of an additional protein adsorbed from solution relaxes this deformation to some extent and thus lowers the free energy of the adhesion; hence the negative sign in the expression for μ_f .

To predict the growth of the adhesion in the direction of the applied force, several assumptions are made. First, the FA is assumed to be capable of adsorbing and releasing adhesion molecules at every point along its surface; this differs from models of polymerization where the monomer exchange occurs only at the ends of a linear polymer. For the FA plaque, plausibility of this unusual property has some experimental support (von Wichert *et al.*, 2003). However, other studies have shown that the growth primarily occurs at the two ends of the adhesion and not uniformly along its surface (de Beer *et al.*, 2010; Heil and Spatz, 2010). Second, the pulling forces \vec{f} are assumed to be applied to the FA surface at discrete points that are distributed along the FA length with a particular density. Finally, the FA plaque is taken to be anchored to a rigid external substrate by discrete linkers spread over the adhesion length with a density that differs from the density of the pulling forces. This intrinsic asymmetry in the geometry of the adhesion leads to its asymmetric growth.

The interplay between the distribution of the pulling forces and the anchors leads to an inhomogeneous stretching stress within the FA and, consequently, to an uneven distribution of the chemical potential μ_f along

the adhesion. Hence, the tendency to assemble or disassemble can vary along the FA resulting in different regimes of the overall molecular exchange between the FA and the adhesion molecules in solution.

The model predicts different modes of the FA assembly that are largely consistent with the experimentally observed FA behavior. As a function of the chemical potential difference, the FA can exhibit unlimited growth, complete disintegration, or reach a stable force-dependent steady state dimension. The sliding of the adhesion in the direction of the force is explained by an explicit symmetry-breaking introduced in this model due to an imbalance of local forces and anchors; this would require additional specific modifications of the generic model and may be due to the presence of the lamellipodium on the far side (close to the cell membrane) of the adhesion and the stress fibers on its near side (closer to the nucleus). In contrast to other models of FA mechanosensing, the thermodynamic model does not require any special conformational changes of proteins upon force application. At the same time, the model assumes that the FA plaque is an elastic body able to accumulate mechanical stresses. Moreover, the plaque must possess a mechanism to accommodate new FA proteins without undergoing stretch-induced rupture. This may require the presence of delicate molecular mechanisms having properties similar to those of the members of the formin protein family (Kovar, 2006), which are able to maintain a stable connection to an associated protein complex (the growing ends of actin filaments) and at the same time, enable insertion of the new protein monomers into the complex and stabilization of the growing structure.

V. CELL SHAPE AND FORCES

A. Physical motivation

We now move from the level of cellular adhesions to the level of whole cells and address the question how the forces in an adherent cell are balanced over the entire cell. From the preceding section, we have learned that cells adhere through relatively few but stable sites of focal adhesion. At the same time, they tend to be very contractile provided that the environment is sufficiently rigid to balance these forces. The interplay between contractility and spatially localized adhesions leads to interesting phenomena which can be understood best by first considering the shape of cells.

Depending on cell type and environment, cells adopt a large variety of different shapes (Bray, 2001; Kollmannsberger *et al.*, 2011; Mogilner and Keren, 2009). For cells in the human body, for example, we observe such diverse shapes as the biconcave disc of the red blood cell, the invaginated shapes of single fibroblasts in connective tissue, the polygonal shapes of cells in densely packed epithelial

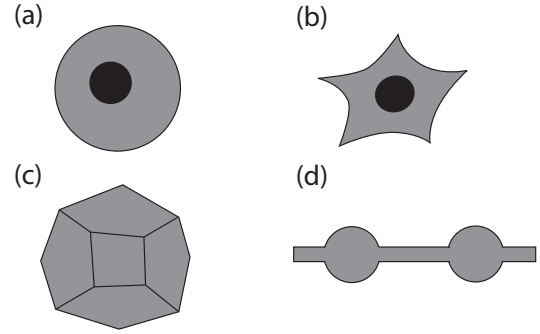


FIG. 16 Cell shapes are often dominated by tension. (a) Single cells in solution are usually round. (b) Isolated tissue cells like fibroblasts commonly show an invaginated shape between distinct sites of adhesion. (c) Epithelial cells in closely-packed tissue are usually polygonal, both in two and three dimensions (here a polyhedron is schematically depicted for the 3d case). (d) Cylindrical cell extensions such as axons tend to pearl when the tension is increased.

tissue, and the highly branched networks formed by neurons in the brain. In fact the term *cell* was coined by Robert Hooke who in his 1665 book *Micrographia* was the first to report on the many shapes visible under the microscope. He chose this term *cell* because of the near rectangular shapes of the building block of cork reminded him of monk cells in a monastery. Due to the evolutionary process, the shape of cells is closely related to their function. For example, red blood cells are optimized to squeeze through narrow capillaries, fibroblasts are sufficiently contractile to deform and remodel extracellular matrix, epithelial cells pack tightly to seal certain regions, and neurons form a highly connected communication network.

In 1917 D'Arcy Thompson suggested in his book *On Growth and Form*, that the shapes of cells and organisms must be closely related to physical forces (Thompson, 1992). The interest in shape somehow declined in the wake of the molecular revolution in biology, but has recently been re-invigorated by the finding that cell shape strongly effects cellular function. By using micro-contact printing of adhesive patterns to constrain cells into pre-defined shapes, it has been shown that it is not the total amount of adhesive ligand available to the cell, but rather its spatial distribution that determines cell fate (Chen *et al.*, 1997). In fact, relatively little ligand is sufficient to ensure cell survival if it is arranged in such a way as to allow the cell to spread over a large area on the substrate. In contrast, a cell constrained to occupy a small area or volume goes into programmed cell death even if many ligands are available in that small space. More recently, it has also been shown that stem cell differentiation depends on cell shape (Kilian *et al.*, 2010).

During the last decade, the use of micropatterned substrates has developed into a standard technique employed to investigate many details of the spatial organization

of cells. For example, it has been shown that the spatial coordination of lamellipodia (Parker *et al.*, 2002), stress fibers (Thery *et al.*, 2006), spindle formation (Fink *et al.*, 2011; Thery *et al.*, 2007) and cell-cell adhesions (Tseng *et al.*, 2012) strongly depends on the geometry of the extracellular environment. Moreover, micropatterned substrates can also be used to quantitatively analyze cell shape. It has long been noticed that on flat substrates, most tissue cell types adopt shapes that are indicative of cell contraction, often characterized by invaginations between pinning sites (Zand and Albrecht-Buehler, 1989). The tendency to invaginate becomes even more pronounced when the actin cytoskeleton is disrupted, which leads to a ray-like morphology of adhering cells (Bar-Ziv *et al.*, 1999). Recently micropatterning and image processing have been combined to quantitatively study the relation between cell shape and adhesive geometry (Bischofs *et al.*, 2008).

In general, many of the observed cell shapes can be understood with concepts borrowed from soft matter physics. The round shape of cells in solution, the invaginated shapes of single tissue cells on flat substrates and the foam-like packing of cells in epithelial tissue point to a strong role of cellular tension, compare Fig. 16(a)-(c). Tension also plays an important role in many dynamical situations, such as the pearlizing of cell extensions after changes in pressure (Pullarkat *et al.*, 2006) or cell elasticity (Bar-Ziv *et al.*, 1999), as in Fig. 16(d). Tensions that contract cell-cell junctions have emerged as a key factor that determines the dynamics of tissues (Aliee *et al.*, 2012; Farhadifar *et al.*, 2007; Lecuit and Lenne, 2007; Paluch and Heisenberg, 2009). However, in order to quantitatively explain the experimental data for single cells, tension arguments must be combined with elements of elasticity (Bar-Ziv *et al.*, 1999; Bischofs *et al.*, 2008). During recent years, different modeling approaches have been suggested to describe the interplay between myosin II contractility which is balanced by elastic forces exerted by the cytoskeleton and the adhesions (that couple to the substrate). In the following we discuss and compare some of the suggested approaches. This then forms a basis that allows us to consider even more coarse-grained models of cells (cellular force dipoles) in the next section.

B. Contour-models for cell shape

Because adhering cells on flat substrates spread to become very thin compared with their lateral extensions, it is appropriate to describe them as approximately two-dimensional objects, see Fig. 17(a). The simplest approach is to focus only on cell shape and to consider only the two-dimensional contour $\vec{r}(s)$ describing the cell boundary, with s (which has units of length) defined as the distance coordinate along the contour. At any point s along the boundary, we define the tangent vector

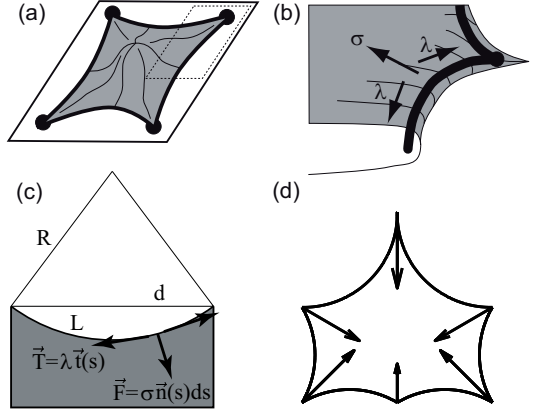


FIG. 17 Simple tension model for cell shape on a flat substrate. (a) The cell is very flat and therefore effectively two-dimensional. The outlined region is shown in (b) with more details. (b) Along the contour between two neighboring adhesion sites, surface tension σ pulls inward, while line tension λ pulls tangentially. (c) Along the contour, surface tension and line tension pull in normal and tangential directions, respectively. For a circular arc, radius R , contour length L and spanning distance d are geometrically related to each other. (d) For a house-shaped cell, all arcs have the same radius, although the spanning distance is larger on the diagonals. Also shown are the traction forces derived from the shape model. Adapted from Bischofs *et al.* (2009) and Guthardt Torres *et al.* (2012).

$\vec{t}(s) = (d\vec{r}(s)/ds)/|d\vec{r}(s)/ds|$ and the normal vector $\vec{n}(s)$ perpendicular to it. These two unit vectors are connected by the geometrical relation $d\vec{t}(s)/ds = \vec{n}(s)/R(s)$, where $R(s)$ is the local radius of curvature. We first consider the simplest model geometry possible, namely, a contour which is pulled in towards the cell in the region between two adhesion points, as shown in Fig. 17(b). We shall relate this to the forces that arise from acto-myosin contractility in cells.

We begin with the most elementary example, the *simple tension model*, in which these forces arise from the energies associated with changes in the contour length and surface area. In the simple tension model, a constant surface tension σ pulls in the contour (thereby reducing the surface area) and is balanced by the effects of a constant line tension λ which tends to straighten the contour (thereby reducing the line length), see Fig. 17(b). The surface tension acts on a line element and points in the normal direction, leading to a force $\vec{F} = \sigma \vec{n}(s)ds$, while the line tension acts on every point of the contour and in the tangential direction with a force $\vec{T} = \lambda \vec{t}(s)$. This situation is depicted in Fig. 17(c). The force balance on a contour element ds then leads to a Laplace law:

$$\vec{F} = \vec{T}(s + ds) - \vec{T}(s) \Rightarrow \sigma \vec{n} = \lambda \frac{d\vec{t}}{ds} = \frac{\lambda}{R} \vec{n} \Rightarrow R = \frac{\lambda}{\sigma} \quad (44)$$

Note that this result is expected from dimensional analysis. The simple tension model thus predicts that the

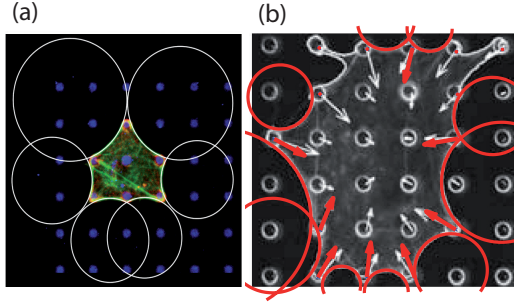


FIG. 18 (Color online) (a) House-shaped cell on an adhesive micropattern created by microcontact printing. Note the circular arcs with radii that are larger at the two diagonals. From (Bischofs *et al.*, 2008). (b) Cell on a pillar array that allows a simple read-out of local forces from measurements of the deflection of each pillar. Circular arcs describe most of the cell contour, but not for example at the upper left corner, where an internal fiber distorts the contour. From Bischofs *et al.* (2009).

contour forms perfect circular arcs, which indeed is often observed in cell experiments. In Fig. 18(a) and (b), this is demonstrated for cells on a dot micropattern and on a pillar array, respectively. Note that due to its local nature, the simple tension model does not obey total momentum conservation that is expected for a closed system like a single cell.

The last equality in Eq. (44) resembles the Laplace law $R = (2\sigma)/\Delta p$ for a sphere (*e.g.*, a soap bubble) whose surface is contracted by a surface tension σ and stabilized by a pressure difference Δp (compare section IIF). We note that in three dimensions, λ and σ (related to line and surface) are replaced by σ and Δp (related to surface and volume), respectively, and that a factor 2 appears (compare section IIF). These two effects obviously result from the different dimensionalities. However, a more fundamental difference is the fact that while the sphere stabilizes itself without any need for attachment, the simple tension model for the invaginated contour only makes sense in the presence of the two adhesion sites. Without the adhesions, both tensions would work in the same direction and the contour would simply contract to a point.

In single cells adhered to a flat substrate, the two tensions have contributions from different processes. The surface tension σ mainly results from the pull of the myosin motors in the actin cytoskeleton (including the actin cortex), but can also have a contribution from the tension in the plasma membrane. The line tension λ is expected to primarily arise from the elastic pull of the thick and contractile actin bundles lining the cell periphery. If cells are treated with pharmacological drugs that disrupt the actin cytoskeleton, they tend to invaginate more strongly, indicating that effectively the line tension λ is reduced more than the surface tension σ (Bar-Ziv *et al.*, 1999; Bischofs *et al.*, 2008).

Interestingly, very strong invaginations necessarily lead to tube-like extensions connecting the retracted cell body to the sites of adhesions (here we assume a three-dimensional viewpoint again). A cylindrical tube in which the surface tension is the only relevant force undergoes a Rayleigh-Plateau instability (Safran, 2003). Thus one also expects pearling of the cellular tubes. Indeed this is exactly what has been observed experimentally (Bar-Ziv *et al.*, 1999) once the elasticity of the tube is suppressed, similar to the pearling which can be induced, for example in axons, by changing the osmotic pressure (Pullarkat *et al.*, 2006).

For contractile cells, the force due to the surface tension σ is mainly balanced by the elasticity of the actin cortex underlying the plasma membrane. Experimentally, it was found that thinner tubes are unstable whereas thicker ones are not. This can be explained as follows. One considers a cylindrical tube with undulations by defining a local radius that varies along the tube axis in the z direction: $R(z) = R_0 + \Delta R \cos(2\pi z/\lambda)$. There are two energy contributions, the change in surface energy and an elastic energy that includes bending and stretching energies. Using the constraint of volume conservation the sum of these two energies reads (Bar-Ziv *et al.*, 1999)

$$E_t = \sigma \frac{1}{4} u^2 (k^2 - 1) + \frac{1}{4} \frac{3ER_0}{1+\nu} u^2. \quad (45)$$

Here $k = 2\pi R_0/\lambda$ and $u = \Delta R/R_0$ are the dimensionless wavenumber and amplitude of a perturbation of wavevector k , respectively, while E and ν are the Young's modulus and Poisson's ratio of the cortex, respectively. Because both terms have the same scaling with u , these terms cannot determine the amplitude. However, the wavelength at which the system is unstable is determined by this expression. The first term can become negative for large wavelengths, $k < 1$. In this case, the energy is negative if the tension exceeds a critical threshold of

$$\sigma_c = \frac{3ER_0}{1+\nu} \quad (46)$$

which increases with R_0 . This makes thicker tubes more stable than thinner ones, as observed experimentally.

The pearling study indicates that in cellular systems, tension and elasticity are strongly coupled. A similar result was obtained by a quantitative study of cell shape on micropatterned substrates (Bischofs *et al.*, 2008). Although this analysis revealed that invaginations of the cell contour are usually close to circular as predicted by the Laplace law from Eq. (44), it also showed that the arc radius R varies with the spanning distance d (defined in Fig. (17)) between the two neighboring adhesion sites, while the Laplace law would predict a constant radius independent of spanning distance. Again, this can be explained by an elastic analysis, the *tension-elasticity model* (Bischofs *et al.*, 2008). The circular nature of the arcs

suggests that a modified Laplace law must hold. While the surface tension σ is expected to be determined mainly by myosin motor activity in the bulk cytoskeleton and therefore should be the same and constant for all arcs, the line tension λ might be determined locally by the mechanics of the peripheral bundles. The simplest possible model is to take into account the fact that the actin cortex, localized near the line, can behave elastically. The line tension then has a contribution from the stretching of this cortex relative to its relaxed state:

$$\lambda = EA \frac{L - L_0}{L_0} \quad (47)$$

where the product of three-dimensional modulus E and cross-sectional area A is the effective one-dimensional modulus of the bundle, and L and L_0 are its actual stretched length and relaxed length, respectively. Together with the geometrical relation

$$\sin\left(\frac{L}{2R}\right) = \frac{d}{2R} \quad (48)$$

between the contour length L , radius R and spanning distance d (compare Fig. 17(c)), one obtains a self-consistent equation for the arc radius R :

$$R = \frac{EA}{\sigma} \left(\frac{2R}{L_0} \arcsin\left(\frac{d}{2R}\right) - 1 \right). \quad (49)$$

The simplest model assumption for the resting length is $L_0 = d$. A numerical solution of Eq. (49) shows that R is a monotonically increasing function of d , as observed experimentally. For small invaginations, $d/R \ll 1$ and one can expand Eq. (49) to obtain

$$R = (EA/24\sigma)^{\frac{1}{3}} d^{\frac{2}{3}}. \quad (50)$$

Thus R increases with the contour rigidity EA and spanning distance d , but decreases with increasing surface tension σ . Note that compared with the Laplace law from Eq. (44), one still has an inverse relation between radius and surface tension, but now with a different exponent.

C. Whole-cell models

As shown in Fig. 18, contour models can also be used to analyze the shape of whole cells that are characterized by geometrically prominent features like circular arcs. One model class that addresses whole cells by construction are cellular Potts models, which have been successfully used to evaluate and predict cell shape on dot-like micropatterns (Vianay *et al.*, 2010), with an example shown in Fig. 18(a). In essence, the cellular Potts model is very similar to the simple tension model, because its main ingredient is tension at the interface. There are many situations of

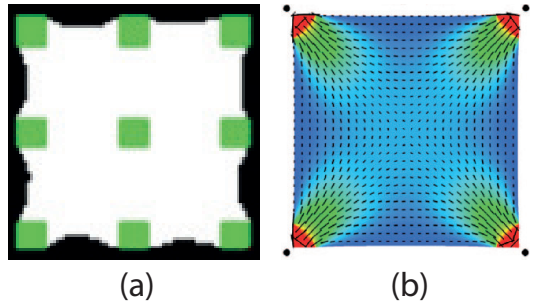


FIG. 19 (Color online) Two model approaches for whole cells. (a) Cellular Potts models use spins on a lattice to simulate the contour between the cell and its surroundings. From (Vianay *et al.*, 2010). (b) Finite element methods (FEM) can be used to implement any material law of interest. Contractility is implemented by thermoelasticity. The vector field represents the direction and activation level of stress fibers. From Deshpande *et al.* (2006).

interest, however, for which such a simple approach is not sufficient to account for cell behavior; one example is the case where the actin cytoskeleton locally reorganizes into contractile bundles (in addition to those that line the cell periphery). However, a theory based only on structural elements visible with standard microscopy procedures might not be sufficient as many observations in single cell experiments point to the existence of a much finer-scale network of additional fibers that coexist with the stress fibers. The natural theoretical framework for studying this situation is continuum mechanics. Although traditionally used mainly to address the mechanics of macroscopic objects like growing tissue (Ambrosi *et al.*, 2011), different continuum mechanics approaches have recently been developed to describe the shapes and forces of adherent cells (Kollmannsberger *et al.*, 2011). In particular, the powerful framework of the finite element method (FEM) has been adopted for this purpose. A detailed FEM-model integrating mechanical and biochemical aspects has been developed that is able to explain many details of cell adhesion (Deshpande *et al.*, 2006, 2007; McGarry *et al.*, 2009; Pathak *et al.*, 2008). Here, we discuss this model as one representative example that demonstrates how a detailed whole-cell model can be constructed. Note that this kind of model ensures total momentum conservation by construction.

As before, the nearly flat adherent cell is treated as an effectively two-dimensional object. In continuum elasticity theory, this corresponds to a plane stress approximation for thin elastic films in which the stress is approximately constant throughout the film in z-direction (Landau and Lifshitz, 1970). The stress in the cell is assumed to have both active and passive contributions that are additive :

$$\Sigma_{ij} = \sigma_{ij} + \left(\frac{E\nu}{(1-2\nu)(1+\nu)} \epsilon_{kk} \delta_{ij} + \frac{E}{(1+\nu)} \epsilon_{ij} \right) \quad (51)$$

The first term represents active, contractile stresses σ_{ij} . The second term represents the passive elasticity of the cell, which here is assumed to have a linear elastic response. E and ν are the Young's modulus and Poisson's ratio of the cell, respectively, and ϵ_{ij} is the strain tensor. If required, this constitutive law can be easily replaced by a more complicated one, *e.g.*, the Neo-Hookean model for non-linear materials.

We now outline how the active stress, σ_{ij} , can be related to the kinetics of contractile, acto-myosin stress fibers (Deshpande *et al.*, 2006, 2007; McGarry *et al.*, 2009; Pathak *et al.*, 2008). Because stress fibers are essentially one-dimensional objects, the corresponding theory is a scalar one. At any position of the two-dimensional cellular domain, one assumes a distribution of stress fibers to exist, which point in the direction parametrized by the angle ϕ . Next, one defines a direction-dependent activation level $\eta(\phi)$ for stress fibers ($0 \leq \eta \leq 1$) where the time derivative of the activation level is determined by the following first-order kinetics:

$$\dot{\eta}(\phi) = [1 - \eta(\phi)] \exp(-t/\theta) \frac{\bar{k}_f}{\theta} - \left[1 - \frac{\sigma(\phi)}{\sigma_0(\phi)} \right] \eta(\phi) \frac{\bar{k}_b}{\theta} \quad (52)$$

The first term describes stress fiber formation with a dimensionless rate \bar{k}_f . In addition, the model assumes a temporal decay that accounts for the finite time scale θ over which a biochemical signal activates the formation of stress fibers (for example the influx of Calcium-ions or the effect of a contractile agent like LPA). The second term describes stress fiber dissociation with a dimensionless rate \bar{k}_b . Because the formation term decays in time, the system will, in principle, eventually relax to vanishing activation. However, if the system is able to reach maximal stress σ_0 , then the decay does not take place. Because one typically starts with the initial conditions $\eta = 0$ and $\sigma = 0$, the system will develop an appreciable level of stress fiber activation only if it is able to build up sufficient levels of stress in a certain direction on the time scale of the decaying activation signal. In the framework of the FEM, this will depend strongly on the mechanical boundary conditions, thus making the cell model very sensitive to external mechanical cues. Motivated by models for muscle, the tension $\sigma(\phi)$ in the stress fiber and the rate of strain $\dot{\epsilon}(\phi)$ in the fiber are assumed to obey a Hill-like relation (compare section IIIC). For a fiber of constant length, $\dot{\epsilon} = 0$, a constant stall tension is assumed. As the velocity of fiber shortening increases, $\dot{\epsilon} < 0$, the tension drops towards zero. For fiber lengthening, $\dot{\epsilon} > 0$, the tension remains constant, at the level of the stall tension.

In order to connect the tensorial model for passive elasticity and the scalar model for stress fibers, homogenization techniques are used to construct the active stress tensor σ_{ij} from the scalar stress $\sigma(\phi)$ and the scalar rate of strain $\dot{\epsilon}(\phi)$ from the strain tensor ϵ_{ij} . In Fig. 19(b) a

typical outcome is shown for the simulations of a square cell which adheres at its four corners. One clearly sees that stress fibers develop in the diagonal directions and along the boundaries, in agreement with experimental observations. However, the model does not allow for the crossing of stress fibers in the cell center due to the averaging procedure for the order parameter field. Moreover there are clear differences between these simulations and the contour models discussed above: the cell shape is much less invaginated and the free boundaries are relatively flat, mainly because the passive cell elasticity resists compression.

The active stress σ_{ij} introduced in Eq. (51) can be implemented in FEM-software by using established routines for thermal cooling. In general, the analogy between cellular contractility and thermoelasticity is very instructive and has also been used to evaluate stresses in cell monolayers. For example, it has been shown that the proliferation pattern in cell monolayers on patterned substrates correlates with the stress distribution in the thin contractile layers (Nelson *et al.*, 2005). An analytically solvable thermoelastic model has been used to explain why stress and strain are localized at the periphery of such monolayers (Edwards and Schwarz, 2011). Combining such calculations and experiments, it has been shown that for larger cell colonies, the traction pattern of the monolayer is increasingly dominated by the tensional elements (Mertz *et al.*, 2012a), and that these collective effects disappear if cell-cell adhesion is disrupted in the monolayer (Mertz *et al.*, 2012b).

The FEM-model for single cells shows that tension in contractile cells must be balanced by structural elements that can carry compressive load, such as microtubules. Indeed buckling of microtubules has been observed in many different contexts within cells (Brangwynne *et al.*, 2006) and has been shown to occur for pico-Newton forces in *in vitro* assays (Dogterom and Yurke, 1997). This proves that microtubules are indeed load-carrying elements in the cell. It has been suggested early on that the balance between contraction in the actomyosin system and compression of the microtubules is essential for the mechanical stability of cells and implements an architectural principle known as *tensegrity* (Ingber, 1993; Stamenovic and Ingber, 2009). As cells adhere to substrates, the contractile forces are then increasingly balanced by sites of adhesion (Stamenovic *et al.*, 2002). Because microtubules alone would not be able to carry the large load developed by adherent cells, the establishment of large adhesions seems to be a necessary condition for the development of contractility in adherent cells. In contrast to FEM-models that couple continuum elasticity to discrete, actively contractile stress fibers, the tensegrity models consider discrete structural elements such as compression struts connected by tensed cables, as a model of single stress fibers (Luo *et al.*, 2008). Because they model discrete elements and do not require homogeniza-

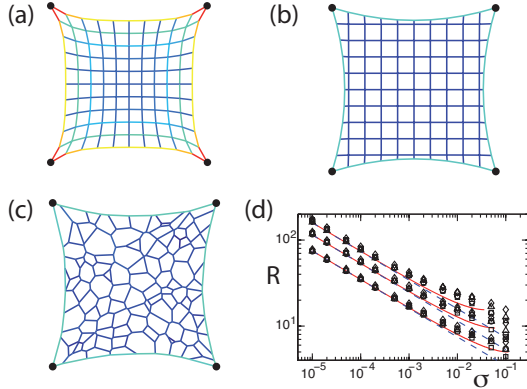


FIG. 20 (Color online) (a) A spring network which is constrained to be located at the four adhesion points indicated (and in which the equilibrium spring length is smaller than the distance between neighboring adhesion points divided by the number of springs along that line), relaxes to a shape similar to the FEM-model – that is, one with relatively flat free edges. Note also the variation in force along the boundary indicated by the colors. (b) An actively contracting cable network results in circular arcs and shows hardly no variation in force along the boundary. (c) The results do not depend on network topology, as shown here for a disordered network. (d) Arc radius R depends on network tension σ as predicted by the tension-elasticity model. Adapted from Guthardt Torres *et al.* (2012).

tion, tensegrity models can be compared more directly with experiments, for example when cutting discrete elements with lasers (Kumar *et al.*, 2006; Luo *et al.*, 2008).

Given the success of the contour models in explaining the appearance of circular arcs of adherent cells, it is interesting to ask if whole-cell models can predict the same shapes. Recently it has been suggested that this can indeed be achieved by modelling cells as actively contracting cable networks (Bischofs *et al.*, 2008; Guthardt Torres *et al.*, 2012). This approach combines elements from FEM and tensegrity models. It considers the extreme case in which contractile forces are balanced by the stretch response of the cytoskeletal polymers and by forces from the elastic environment that couple to the cell at the adhesion sites. The model does not include any compressive response from within the cell or any area conservation because it is assumed that cytoplasm is not constrained to the 2d plane; the rest of the 3d cell therefore acts as a reservoir for adhesion area. A 2d mechanical network is constructed which consists of a set of nodes locally connected by mechanical links. If the links are taken to be linear springs, the network propagates compression similar to the FEM-model. However, if the links are taken to be cables, only tension and not compression is propagated. This representation is appropriate to the polymeric nature of the cytoskeleton, whose filaments tend to buckle or depolymerize under compressive strain (Coughlin and Stamenovic, 2003). In

principle, contraction can be modeled by reducing the relaxed length of the springs or cables. However, this does not represent the properties of actin bundles contracted by myosin II minifilaments, which do not have a well-defined reference state, but contract in a Hill-type fashion until a certain stall force is reached. A simple way to achieve this feature is to add a pair of constant forces (force dipole) to each network link, thus creating permanent contraction between two connected nodes. With these very simple prescriptions, actively contracting cable networks can be simulated. In Fig. 20(a), we demonstrate that contracting spring networks do not result in the circular arc morphology, but rather show a flat contour as does the FEM-model. Circular arcs appear for actively contracting cable networks, independent of network topology, compare Fig. 20(b) and (c). In the second case of a disordered network, a constant tension per length has been assumed. Depending on the link density at the boundary, this translates directly into an effective tension σ that acts within the network. Fig. 20(c) demonstrates that the arc radius R scales with network tension σ as predicted by the tension-elasticity model (TEM), see Eq. (50). Here different symbols correspond to different network topologies and the three sets of curves correspond to three different spanning distances d . Solid lines correspond to the numerical solution of Eq. (49) while dashed lines are the analytical results from Eq. (50). Deviations between computer simulations and TEM occur only at very large tensions.

The continuum mechanics approaches described here are especially suited to investigate static situations relevant mature cell adhesion; however, to treat cell migration, one must consider a dynamically changing cell shape. A natural framework for this is hydrodynamics in the overdamped limit, since cellular flows are characterized by very small Reynolds numbers. For example, the shape of migrating keratocytes has been investigated by a hydrodynamic model representing the flux of newly polymerized actin networks (Barnhart *et al.*, 2011). Here, the shear and compressive forces in the viscoelastic fluid are balanced by forces arising from myosin contractility and flow over adhesion sites. Membrane tension enters as a boundary condition. A similar approach is taken by active gel theory, which can be considered as a hydrodynamic theory for polarized active gels (Julicher *et al.*, 2007) that is based only on the symmetries and conservation laws of the system and is independent of any particular molecular model. Alternative approaches are level set (or phase field) models (Shao *et al.*, 2010; Ziebert *et al.*, 2012) or models incorporating discrete elements such as single focal adhesions and stress fibers (Loosli *et al.*, 2010; Shemesh *et al.*, 2012, 2009).

D. Force from shape

The various elastic forces predicted from the shape models can be verified with experimental measurements, *e.g.*, for cells on soft elastic substrates or on pillar arrays. The simplest possible evaluation can be obtained by comparing measurements with the simple tension model (Bischofs *et al.*, 2009). We now discuss the forces one might expect for different adhesion geometries. Typical micropatterns can be circular islands, rectangular islands, islands with concave parts (such as U-, Y- and X-shapes) or dot patterns. For a circular island of radius R , both tensions pull in the same direction and the boundary force per length is simply $\sigma + \lambda/R$ (compare the force balance given in Eq. (44)). For a rectangular island, the inward force per unit length is simply σ along the flat parts of the perimeter, because here contributions from the curvature and hence from the line tension λ vanish. At the corners, however, the situation is reversed. We can calculate the corresponding force by approximating the corner by an arc with radius ϵ and then taking the limit of a sharp corner:

$$\vec{F} = \lim_{\epsilon \rightarrow 0} \int_{-\frac{\varphi}{2}}^{\frac{\varphi}{2}} (\sigma + \frac{\lambda}{\epsilon}) \vec{n}(\theta) \epsilon d\theta = 2\lambda \cos\left(\frac{\phi}{2}\right) \vec{n}_b \quad (53)$$

where ϕ is the opening angle, $\varphi = \pi - \phi$ and \vec{n}_b points in the direction of the bisecting line. We thus see that the surface tension does not contribute because it is associated with a line element. The interpretation of Eq. (53) is very simple: the force at the corner is simply the vectorial sum of two forces of magnitude λ pulling along the two incoming contour lines. For very small opening angle ϕ , these two forces pull in the same direction and one obtains the maximal value 2λ .

The same line of reasoning can now also be used to predict forces for free contours, as they appear on concave and dot patterns. Again the forces at the adhesion sites directly depend only on the line tension λ . However, now the surface tension σ enters indirectly as it determines the arc shape and therefore the effective angle of the arc that pulls on the contact. We consider three neighboring adhesion sites where the two spanning distances d are identical and with an opening angle ϕ . The force can then be calculated to be:

$$\vec{F} = 2\lambda \left[\beta \sin\left(\frac{\phi}{2}\right) + \sqrt{1 - \beta^2} \cos\left(\frac{\phi}{2}\right) \right] \vec{n}_b \quad (54)$$

where $\beta = \sigma d / 2\lambda$ can be interpreted as a dimensionless measure of the strength of the inward pull or of the dimensionless spanning distance d . In the limit $\beta = 0$, the contour becomes straight and we recover the result from Eq. (53) for pinned straight edges. For finite values of β , however, the edge is curved and the spanning distance d and surface tension σ enter through the arc shape. The larger the spanning distance d , the larger the

surface tension σ or the more acute the opening angle ϕ , the steeper the inward pull and the closer the force comes to its maximal value 2λ . At the critical parameter value $\beta_c = \sin(\phi/2)$, the two arcs actually touch each other and pearling is expected to occur as explained above.

These results suggest a simple procedure to estimate forces from shape, see Fig. 18(b). Using pillar assays or micropatterned elastic substrates, one could look for images of cells in which two circular arcs meet at the same adhesion point. In this case, the traction force at this adhesion point is the vectorial sum of the two arc forces. The direction of each of these forces follows from fitting a circle to the arc; the force magnitude is simply the line tension λ_i . Because the same surface tension acts on both arcs, from the Laplace law Eq. (44) we have $R_1/R_2 = \lambda_1/\lambda_2$. Therefore, one only needs to calibrate the force at one adhesion to obtain the force of the others from geometrical considerations. Applying this procedure to an experiment with a pillar array (Fig. 18(b)) resulted in a value of $\sigma = 2 \text{ nN}/\mu\text{m}$. This tension value is higher than the lysis tension of lipid membranes and presumably corresponds to the actin cortical tension generated by myosin motors. Interestingly, a very similar value has been reported for the effective tension in a cell monolayer (Mertz *et al.*, 2012a). The procedure outlined here also shows that forces measured on the substrate might be substantially smaller than the forces that act within cells, because it is only the vectorial sum of the internal force which is transmitted to the substrate, as in the example treated here of the sum of two forces from two adjacent arcs.

VI. ACTIVE RESPONSE OF CELLS

A. Mechanical response of force dipoles

In this section we focus on active cell mechanics due to the presence of acto-myosin force dipoles; since cellular contractility is due to ATP-dependent conformational changes of myosin, these non-equilibrium processes are denoted as active. The concept of force dipoles is useful at multiple scales. At the level of the entire cell, the overall force balance in the cell suggests a coarse grained picture in which a contractile cell is modeled as a pair of equal and opposite forces (*contraction force dipole*), as shown in Fig. 5 and suggested experimentally (Schwarz *et al.*, 2002). Indeed each of the whole-cell models discussed in section V suggest such an approach. The same argument also applies within a cell to individual molecular force generators in the actin cytoskeleton (CSK) of tissue cells, namely myosin II minifilaments, see Fig. 7. In either of these two scenarios, all internally generated stresses must balance due to momentum conservation and thus the force monopole term in a force dipolar expansion is expected to vanish, leaving the force dipole

term as the leading contribution. The overall force exerted by the cell depends on the arrangement of its internal force dipoles which in turn is a function of cell shape as discussed in section V. Transmission of these internal forces to the cellular environment occurs via the adhesions discussed in section IV.

The stress generated by cellular force dipoles is balanced by the elastic restoring force of the medium (the CSK in the case of acto-myosin minifilaments together with the matrix/substrate or the matrix/substrate alone in the case of a coarse-grained force dipole that represents the entire cell). This is illustrated by the cartoon in Fig. 21 for the case of a cell in an elastic medium (in Fig. 5, we presented a more detailed cartoon that included representations of the internal structure of the cell; we now focus on the effective force dipole arising from this configuration of forces). The situation depicted in Fig. 21 has been analyzed with calculations carried out at varying levels of detail *e.g.*, in Marcq *et al.* (2011); Mitrossilis *et al.* (2009); Schwarz (2007); Schwarz *et al.* (2006); Walcott and Sun (2010); and Zemel *et al.* (2010b).

In general, these studies have validated the following simple physical picture (Schwarz *et al.*, 2006). By measuring how much force or work it requires to achieve a certain deformation, the cell can sense the stiffness of its environment. Because cells themselves are soft objects, the cartoon also shows that the cell tends to deform not only the environment, but also itself. For two springs in series, the inverse of the effective spring constant is the sum of the inverse spring constants. Therefore, if the environment is very stiff, the cell only deforms itself and cannot sense its surroundings. On the other hand, if the environment is very soft, the cell can easily deform it, but does not build up much force and therefore does not gain much information; in particular, any positive feedback triggered by mechanosensors will not work well. Therefore the best working or set point for a cell seems to be a situation in which the two stiffnesses of cell and environment are nearly matched. Indeed it was found experimentally that cells tend to match their stiffness to that of the environment (Solon *et al.*, 2007).

In this section, we discuss how active force generators such as myosin II minifilaments in the actin cytoskeleton or entire contractile cells in an elastic matrix interact with their mechanical environment. The deformations induced in the matrix by cell activity allow us to deduce effective interactions between the force dipoles themselves via their mutual effects on the elastic environment. In the case of individual acto-myosin minifilaments modeled as force dipoles, the elastic environment includes the CSK of the cell itself (in addition to its surroundings), while in the case of entire, contractile cells modeled as force dipoles, the elastic environment is the matrix or substrate. The elastic properties of the environment can be easily controlled in experiments so that predictions and measurements of their role in modulating cellular force

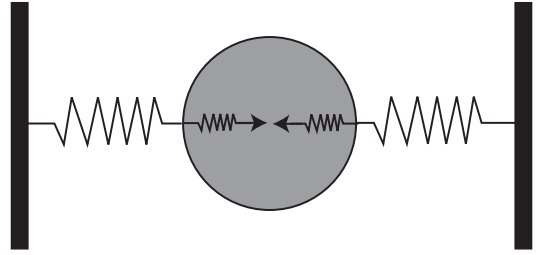


FIG. 21 Two-spring model for cell-substrate interactions. In addition to springs that characterize the cellular and substrate deformations, the cell exerts active, contractile forces shown by the double arrows. This simple cartoon shows that cells can measure the stiffness of their environment, which is, however, convoluted with their own stiffness. In contrast to Fig. 5, here we do not consider compression of the substrate, because we consider only the far field.

dipole assemblies provide insight into these fundamental processes.

In order to obtain analytical insight, linear elasticity theory is applied to an isotropic medium (or substrate) to model the mechanical properties of cells and their environment (Landau and Lifshitz, 1970), although later on, we briefly comment on possible extensions to more detailed models for the elasticity of biomaterials, including non-linear elasticity. Alternatively one could also employ more microscopic models for the propagation of stress and strain in polymer networks (Head *et al.*, 2003a,b; Heussinger and Frey, 2006; Heussinger *et al.*, 2007; Wilhelm and Frey, 2003), but this may preclude the insight gained by the use of elastic theory generalized to include force dipoles. In the framework employed here, cytoskeletal force generators (*e.g.*, acto-myosin minifilaments or entire cells) are viewed as active, elastic inclusions in (or on) a homogeneous and isotropic medium. This suggests the use of Eshelby's theory of elastic inclusions, that was originally developed in the context of materials science (Eshelby, 1957, 1959). In the limit that the inclusions are much smaller than the length scales of interest, one can use the theory of elastic point defects, which also originated in materials science, and has been used extensively to model the elastic interactions of hydrogen in metal (Siems, 1968; Wagner and Horner, 1974).

There are a few important assumptions made in the following treatment of force dipoles and cellular/matrix elasticity: (i) The build-up of force occurs on short enough time scales (10s of seconds) for which the CSK responds elastically to internal forces and does not flow. This was discussed previously in a comparison of elastic versus flowing gel models of the CSK. Even if the matrix flows on larger time scales, the cell will react on a shorter time scale by building up new forces via a remodeled CSK. Elastic relaxation after pharmacological inhibition of actomyosin contractility, laser cutting or disruption of adhesion (*e.g.* by trypsinization) proves that adherent cells

and matrix are continuously under elastic stress. (ii) The matrix-induced forces that act to organize the cytoskeleton arise from the potential energy that accounts for the deformation of the matrix by the dipoles. In this sense, matrix can refer either to those parts of the CSK not included in the acto-myosin dipoles themselves and/or to the surrounding matrix or substrate. However, these forces are taken to determine only the organization of the dipoles (*e.g.*, nematic or smectic order) but not their existence or magnitude which depends in a more complex manner on non-equilibrium cellular activity. These same forces would be present and act on artificial force dipoles were they present in the CSK or matrix/substrate. (iii) The time scale on which elastic signals are propagated in the CSK or matrix/substrate is faster than internal relaxation times due to dissipation arising from internal viscosity or fluid flow; for experimental measurements of these time scales see Fig. 3 of Kollmannsberger and Fabry (2011). This allows us to predict force dipole organization by elastic forces from energetic or force balance arguments. We recognize that this is a crude approximation that must be tested under various circumstances; a dynamical theory of elastic signal propagation in the CSK or matrix/substrate is a topic of current research. (iv) The theories below focus on cytoskeletal force generation and predict dipole arrangements for a fixed cell shape. Experiments that measure the response of cells to time varying stresses show (Faust *et al.*, 2011) that cell shape *follows* cytoskeletal reorientation by several hours.

B. Force dipoles and their interactions

A simplified model of a contractile actomyosin unit (or in a coarse gained picture, an entire, polarized cell) is that of a source of two equal and opposite forces, \vec{F} , separated by a nanoscale (or, for cells, micrometer scale) distance, \vec{d} . By analogy with electrostatics, these are termed *force dipoles*. The dyadic product of the force and the distance defines a local elastic dipole: $P_{ij} = d_i F_j$. In contrast to electric dipoles that are vectors given by product of the scalar charge and the distance, the elastic dipole is a tensor. In a continuum representation, valid for scales much larger than $|d|$, one therefore considers a coarse-grained force density $f(\vec{r})$ (which is not the same as the local force \vec{F}) whose average in some small volume vanishes (since the forces are equal and opposite) but whose first moment with \vec{r} is finite. The force density is written as the sum of two, localized force distributions with opposite signs whose centers are separated by a distance \vec{d} . One expands these distributions for small values of \vec{d} relative to the distance \vec{r} at which the strains and stresses are measured and finds that the net force is related to derivatives of the localized force distributions. Using this approximation for the local force density and defining the local dipole tensor density, p_{ij} (local force dipole tensor

per unit volume), one can show that:

$$\partial p_{ij}(\vec{r}) / \partial r_j = -f_i(\vec{r}) \quad (55)$$

Using this relationship between the force density and the divergence of the dipole density in Eq. 15 and performing an integration by parts (with the assumption that the surface terms vanish or are accounted for explicitly), shows that the strain is related to the dipole density by:

$$u_{ij}(\vec{r}) = \int d\vec{r}' G_{il,k'j}(\vec{r}, \vec{r}') p_{kl}(\vec{r}') \quad (56)$$

where the two indices in G after the comma indicate derivatives with respect to r'_k and r_j respectively. Eqs. 13, 55 and 56 and further partial integrations demonstrate that the deformation energy of the medium acted upon by localized elastic dipoles can be written as an effective interaction of those dipoles. This is important since if the dipoles are free to arrange themselves to minimize the deformation energy (*e.g.*, if the cell activity tends to minimize the energy expended in deforming the CSK or the matrix), their spatial arrangement can be deduced from their interactions, perhaps also accounting for noise which can in some cases be modeled as an effective temperature as discussed in the section on physics background.

For translationally invariant systems where the Green's function depends on the difference $\vec{r} - \vec{r}'$, the total deformation energy of the medium is:

$$F_e = \frac{1}{2} \int d\vec{r} d\vec{r}' p_{ij}(\vec{r}) G_{il,k'j}(\vec{r} - \vec{r}') p_{kl}(\vec{r}') \quad (57)$$

In this case, one can also write the interaction energy in terms of the Fourier transforms of the dipole density and the Greens' function:

$$F_e = \frac{1}{2} \int d\vec{q} p_{ij}(\vec{q}) G_{il,kj}(\vec{q}) p_{kl}(-\vec{q}) \quad (58)$$

where $G_{il,kj}(\vec{q}) = G_0(q_k q_j / q^2) (\delta_{il} + q_i q_l / (2q^2(1-\nu)))$ follows from the exact (*Kelvin*) solution for a full elastic space and G_0 is a constant proportional to $1/E$. In the presence of an externally imposed strain, $u_{ij}^e(\vec{r})$ (in addition to the strains induced by the internal force dipoles), one can use Eq. 12 to show (Bischofs *et al.*, 2004) that the interaction energy of the dipoles with the external strain is:

$$F_e = \int d\vec{r} p_{ij}(\vec{r}) u_{ij}^e(\vec{r}) \quad (59)$$

The theory described here is relatively simple to use for the case of dipoles in an infinite medium. It can be applied to an entire contractile cell that is placed in one region of a much larger elastic environment (as a model of an infinite medium). However, when the force dipole concept is used to account for the interactions of

acto-myosin minifilaments within one cell which itself is an elastic medium, the situation is more complex. The cell itself can be situated in (or on) an elastic matrix (substrate) whose rigidity can be different from that of the cell. The resulting Green's function will then depend on the cell shape and both the cell and matrix elastic constants. The same complications can also arise in the case of entire contractile cells modeled as effective force dipoles (Bischofs *et al.*, 2004; Bischofs and Schwarz, 2003; Schwarz and Safran, 2002; Zemel *et al.*, 2006) that are placed in an elastic matrix which itself is surrounded by another material with different elastic properties. This may be applicable to models of cells in tissues that are contained within the extracellular matrix that itself is coupled to another elastic medium in which the tissue resides. In this case as well, it is necessary to consider the shape and elastic boundary conditions in order to predict the interactions among the cells that lead to their self-assembled structures (Zemel and Safran, 2007).

The real-space solution of the elastic deformation of such a composite medium was considered by Eshelby (Eshelby, 1957, 1959) who calculated the strain inside of an ellipsoidal inclusion embedded in a three-dimensional elastic matrix. Although these inclusions do not actively produce forces, they can exert stresses on their surroundings as the temperature is changed and the inclusion thermally expands or contracts in a manner that is larger or smaller than that of the matrix. The Eshelby results can be mapped to the strain experienced either by an entire contractile cell modeled in a coarse grained manner or by individual acto-myosin force dipoles (Zemel *et al.*, 2010b; Zemel and Safran, 2007) within a cell embedded in a three-dimensional matrix. Once the local strain due to a given dipole distribution is known, the dipole interactions are given by the product of the local dipole density and the local strain. Later in this review, we consider specific predictions for the orientational and spatial organization of force dipoles in cellular systems and summarize the results obtained from Eshelby theory. However, this theory with its focus on the real-space boundary conditions is complex (Eshelby, 1957, 1959; Mura, 1991) and is also specific to systems of ellipsoidal inclusions whose dimensionality is the same as that of the surrounding matrix. This is not quite the case studied experimentally where well-spread (nearly two-dimensional) cells are plated on semi-infinite, elastic substrates, although recent experiments (Rehfeldt *et al.*, 2012) show that the behavior of thick substrates and of 3d surroundings are very similar. Thus, to provide a simpler and more intuitive theory of deformation induced interactions of elastic dipoles that are relevant to cells on semi-infinite substrates we review here a simplified model (Friedrich and Safran, 2012) that can be solved using Fourier methods.

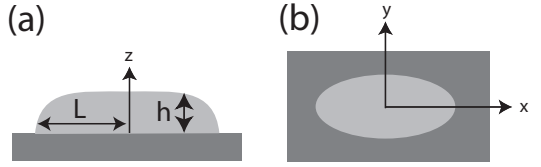


FIG. 22 Simple model of a contractile and widely spread cell on an semi-infinite elastic substrate.

C. Elastic model for cells on a substrate

The particular scenario that we focus upon here is that of acto-myosin minifibrils modeled as force dipoles within a cell that is spread and adhered to an elastic substrate. The theory predicts the conditions under which the elastic interactions of these dipoles with both the cellular CSK and the substrate mediate dipole-dipole interactions that tend to orient the minifilaments. In this simplified model, the spread cell adheres to the upper free surface of the substrate, which is taken to lie in the $z = 0$ plane, of a semi-infinite ($z < 0$) substrate, as in Fig. 22 (Friedrich and Safran, 2012). The thickness of the cell may vary as a function of position and is denoted by $hS(x, y)$. Here, h denotes the height of the contractile region of the cell, while the function $S(x, y)$ specifies variations of cell thickness within the cell, and is zero outside the cell. Thus, the dimensionless function $S(x, y)$ characterizes the shape of the cell. The integral $\int dx dy S(x, y) = A$ defines a weighted cell area A (which is related to the volume of the cell by $A = V/h$) and a characteristic length-scale $L = A^{1/2}$ of the spread cell. For simplicity, the discussion is restricted to cell shapes that are symmetric with respect to each of the x - and the y -axis. In this case, the Fourier transform $S(\vec{q}) = (2\pi)^{-1} \int dx dy S(x, y) \exp(-iq_x x - iq_y y)$ of the shape function is real and has typical dimensions A or L^2 . There are three important moments of the cell shape function defined by:

$$\mathcal{J}_n = \frac{1}{L} \int d^2\vec{q} q |S(\vec{q})|^2 \exp(2inw(\vec{q})) \quad (60)$$

where $w(\vec{q}) = \tan^{-1}(q_y/q_x)$ and $n = 0, 1, 2$. These moments are dimensionless and depend only on the shape of the cell. They play a role similar to that of the shape-dependent depolarization factors in electrostatics (Beleggia *et al.*, 2006) or the Eshelby tensor in Eshelby's theory of elastic inclusions (Beleggia *et al.*, 2006; Eshelby, 1957; Mura, 1991). For cells with mirror-symmetry (considered here for simplicity), the moments \mathcal{J}_n are real. \mathcal{J}_1 characterizes cell shape anisotropy and is zero for radially symmetric cells.

The discrete actomyosin contractile elements are characterized, in a coarse-grained description, by a bulk force dipole density $p_{ij}(\vec{r})$ with units of energy per unit volume. A mean-field approximation regards these dipoles as being uniformly distributed within the cell with a mean

force-dipole density \bar{p}_{ij} . The upper surface of the cell is stress-free, and for a cell whose thickness is much smaller than its lateral extent, the stresses and force dipoles with components in the z -direction can be neglected (for details see Friedrich and Safran (2012)). To highlight the symmetries of the problem, one can decompose the mean dipole density tensor \bar{p}_{ij} into an isotropic part that is analogous to a hydrostatic pressure, $\bar{P}_0 = \bar{p}_{xx} + \bar{p}_{yy}$, and two invariants that characterize pure shear stresses, $\bar{P}_1 = \bar{p}_{xx} - \bar{p}_{yy}$ and $\bar{P}_2 = \bar{p}_{xy}$. In matrix notation, $\bar{p}_{ij} = \bar{P}_0 E_0 + \bar{P}_1 E_1 + \bar{P}_2 E_2$ with respect to a convenient basis of the space of symmetric rank-2 tensors,

$$E_0 = \frac{1}{2} \begin{pmatrix} 1 & 0 \\ 0 & 1 \end{pmatrix}, \quad E_1 = \frac{1}{2} \begin{pmatrix} 1 & 0 \\ 0 & -1 \end{pmatrix}, \quad E_2 = \begin{pmatrix} 0 & 1 \\ 1 & 0 \end{pmatrix} \quad (61)$$

By virtue of the Stokes theorem, each force dipole density $\bar{P}_k E_k$ is equivalent to a set of surface forces $f_k = \bar{P}_k E_k \cdot \vec{n}$ that act at the boundaries of a cellular volume element.

Cellular strain for soft substrates: The active dipolar stresses contract and elastically deform the cytoskeleton. For a spread cell whose thickness is much smaller than its extent, $h \ll L$, the local displacement, $\vec{u}(x, y)$ has only x and y components. The corresponding strain matrix $u_{ij} = (\partial_i u_j + \partial_j u_i)/2$ can be written as the superposition of a homogeneous dilation $U_0 E_0$ where $U_0 = u_{xx} + u_{yy}$ is the trace of the strain matrix, and the traceless strain matrix $u_{ij} - U_0 E_0 = U_1 E_1 + U_2 E_2$, which characterizes pure shear strain without area change with two measures of shear strain $U_1 = u_{xx} - u_{yy}$ and $U_2 = u_{xy}$. The geometry of the problem implies that $U_1 E_1$ and $U_2 E_2$ are symmetric and anti-symmetric with respect to a reflection about a coordinate axis, respectively. The elastic deformation energy of the cellular domain is thus written:

$$F_c = h \int dx dy S(x, y) \left[\frac{K_c}{2} U_0^2 + \frac{\mu_c}{2} (U_1^2 + 4U_2^2) \right] \quad (62)$$

If the cell were not coupled to the substrate (or if the substrate had vanishing rigidity), the cell would not be subject to restoring forces from the substrate and the cell boundary would be stress-free. In this case, the only source of cellular elastic stress $\sigma_{ij}^{(c)}$ would be the forces exerted by the dipoles and thus $\sigma_{ij}^{(c)} = p_{ij}$. Alternatively, one can solve for the resulting minimal strain by minimizing a Legendre transform that includes the work done by the dipole (so that one now can minimize the transformed free energy with respect to the strains for a given? but arbitrary – dipole arrangement), $G = F_c + F_d$ of the free energy where

$$F_d = -h \int dx dy S(x, y) (U_0 \bar{P}_0 + U_1 \bar{P}_1 + 4U_2 \bar{P}_2) / 2. \quad (63)$$

The convexity of the free energy dictates that cellular strain is constant throughout the cellular domain

and moreover is independent of cell shape since the cell boundaries are stress-free so that $U_i \equiv \bar{U}_i = \bar{P}_i/(2B_i)$ where $i = 1, 2, 3$ and $\vec{B}_i = (K_c, \mu_c, \mu_c)$. Note that, irrespective of any anisotropy of cell shape, the strain components depend only on force dipole components of the same symmetry type. Actomyosin production that controls the strength of microscopic, contractile force dipoles, but not their orientation, induces only an isotropic (negative) “hydrostatic pressure” $\bar{P}_0 E_0$ and thus a homogenous dilation $\bar{U}_0 E_0$, but no shear. Thus, in the absence of other factors that break the system symmetry, a “floating cell”, decoupled from its substrate, does not feel anisotropic mechanical guidance cues, which could drive nematic ordering of force dipoles (*e.g.*, alignment along one of the cellular axes). The conclusion is that in the limit of a substrate with zero stiffness, the actomyosin network will remain symmetric, notwithstanding the fact that the cell shape may be asymmetric. This situation changes fundamentally, once the elastic deformations of the cell and the substrate are coupled.

Due to the coupling of the CSK forces to the focal adhesions, active cell contractility induces substrate deformations, $\vec{v}(x, y, z)$. The substrate surface strain at $z = 0$ is decomposed into its symmetry components $v_{ij}(x, y, z = 0) = V_0 E_0 + V_1 E_1 + V_2 E_2$. For simplicity (Friedrich and Safran, 2012) one can take the average strain inside the cell to be equal to the average substrate strain underneath the cell: $\bar{V}_k = \bar{U}_k$.

Substrate elastic energy: The substrate deformations induced by its coupling to the cell can now be included. The elastic energy of the substrate is written in terms of the Fourier transforms of the substrate displacements $\vec{v}(x, y, z)$ derived in Nicolas and Safran (2006a). This energy is proportional to μ_m , the shear modulus of the substrate, which is for simplicity taken to be incompressible. One next expresses the coupling condition in Fourier space and determines the strains by minimizing (Friedrich and Safran, 2012) the Legendre transform $G = F_c + F_m + F_d$ of the free energy of both the cell and substrate subject to the coupling condition $\bar{V}_k = \bar{U}_k$. The cellular strain components, U_i are then found as a function of the dipole components P_i : $U_i = A_{ij} P_j$. The coupling coefficients A_{ij} are functions of the cell-shape moments (Eq. 60) and of the cell and substrate elastic moduli (Friedrich and Safran, 2012).

Of particular interest is the fact that there are off-diagonal terms in this relationship. This means, for example, that a homogeneous and isotropic dipole distribution characterized by a non-zero value of P_0 can induce a shear strain such as U_1 . The coefficient that quantifies this symmetry breaking, \mathcal{A}_{01} depends on both the cell shape and matrix rigidity. In particular, it is proportional to \mathcal{J}_1 (which vanishes for cells with circular cross sections) and vanishes when the substrate modulus is either very small or very large.

The elastic energy is the product of the local strain and

local force dipole density and can be written in terms of effective interactions of the force dipoles:

$$F_i = (L^2 h / 4) (\mathcal{A}_{00} \bar{P}_0^2 + 2\mathcal{A}_{01} \bar{P}_0 \bar{P}_1 + \mathcal{A}_{11} \bar{P}_1^2 + 4\mathcal{A}_{22} \bar{P}_2^2). \quad (64)$$

The terms proportional to \bar{P}_0^2 and \bar{P}_1^2 are the “self-energies” of the isotropic and nematic components of the force dipole respectively; they represent the energy to deform the cell itself together with the elastic substrate (Fernandez and Bausch, 2009). In addition, the shear stress induced by the isotropic dipole component couples the \bar{P}_1 nematic dipole component to the isotropic contractility, \bar{P}_0 , for cell shapes that are anisotropic for which \mathcal{J}_1 is non-zero. This implies that the effects of cell shape on elastic interactions can induce nematic order of the cellular force dipoles even if local cell activity results only in isotropic contractility.

The coupling of the isotropic component of the dipole tensor to the cellular shear allows the cytoskeletal shear to present mechanical guidance cues for the polarization and alignment of cytoskeletal structures and eventually of cellular traction forces. Initially isotropic cytoskeletal contractility can result from a local regulation of myosin activity within the cell, that may tune \bar{P}_0 to a set value \bar{P}_0^* . Considering \bar{P}_1 as an effective degree of freedom, the total elastic energy of cell and substrate, Eq. 64, is minimized when \bar{P}_1 is non-zero, which corresponds to anisotropic cellular contractility.

Physical insight into the coupling of symmetry modes can be obtained considering the limiting cases of very soft and very stiff substrates. Since the strain propagates (Banerjee and Marchetti, 2012; Friedrich and Safran, 2012) into the substrate a distance of order of the cell extent, L , (but only a distance of order h – the cell thickness – within the cell) the effective Young’s modulus of the substrate is given by the product of its Young’s modulus E_m and a factor of L/h where h is the cell thickness: $\tilde{\mu}_m = E_m L/h$. This predicts that both the stiffness ratio as well as the cell geometry (height and lateral extent) will determine cytoskeletal organization and ordering, which can be tested by changing both substrate rigidity and cell volume (Guo and Weitz, 2012).

In the limit of a very soft substrate, $\tilde{\mu}_m \ll E_c$, the situation is that of an isolated cell; cellular strain components couple only to force dipole components of the same symmetry type. Cell activity that results in locally isotropic contractile dipoles cannot give rise to nematic order. In the limit of a very stiff substrate, the cellular strain scales as $1/\tilde{\mu}_m$. For isotropic, cellular contractility with only $\bar{P}_0 \neq 0$: $\bar{U}_0 = \mathcal{J}_0 \bar{P}_0 / 8\tilde{\mu}_m$, $\bar{U}_1 = \mathcal{J}_1 \bar{P}_0 / 8\tilde{\mu}_m$, and $\bar{U}_2 = 0$. Thus, while the symmetric part of the cell contractility, P_0 , does induce shear strain due to the shape anisotropy, this shear strain attenuates as $\tilde{\mu}_m \rightarrow \infty$. Similar conclusions are reached for the induction of nematic order (non-zero values of \bar{P}_1) by locally isotropic contractility. If, however, substrate stiffness and cellular stiffness match,

$\tilde{\mu}_m \sim K_c, \mu_c$, the symmetric shear component \bar{U}_1 is induced by the symmetric dipole component: $\bar{U}_1 \sim \mathcal{J}_1 \bar{P}_0$. This shear is a result of anisotropic, cell-shape dependent, elastic restoring forces from the substrate. For an asymmetric cell shape that is elongated in the direction of the x -axis, $\mathcal{J}_1 < 0$ and isotropic contractility with $\bar{P}_0 < 0$ induces cellular shear strain $\bar{U}_1 > 0$, which is expansive in the x -direction (and compressive along the y -direction). This causes nematic ordering of the dipoles themselves along the x -axis, characterized by negative values of \bar{P}_1 .

D. Cell polarization guided by substrate rigidity

These intuitive results were used in a more formal theoretical model to predict that cells with anisotropic shapes on substrates of intermediate rigidity will spontaneously show CSK nematic order (Friedrich and Safran, 2011; Zemel *et al.*, 2010b). A phenomenological model couched in terms of active gel theory was presented in Banerjee and Marchetti (2011). The case of stem cells is particularly applicable since at early times, the CSK is not yet well formed and oriented and one can study the genesis of CSK formation and orientation starting with relatively short actomyosin minifilaments that can indeed be modeled as force dipoles contained within the cell. The paper by (Zemel *et al.*, 2010b) uses the real-space Eshelby formalism (Eshelby, 1957, 1959) for an ellipsoidal inclusion to calculate the real space strains inside a cell contained in an elastic medium of the same dimensionality (either 2d or 3d). The shear strains induced by the medium are non-zero for cells that are not circular (2d) or spherical (3d) and are predicted to give rise to orientational order of the internal force dipoles (short actomyosin minifilaments). The nematic order, as expressed by \bar{P}_1 is related to the shear strain by a susceptibility whose form in the limit of large noise (expressed as an effective temperature) was discussed in Zemel *et al.* (2006). The work of Friedrich and Safran (2011) provided a more general statistical mechanical basis for the nematic ordering. An energy similar to Eq. 64 was obtained using Eshelby theory; this was used as a Hamiltonian in a Maier-Saupe (Maier and Saupe, 1959) theory as described above in Eq. 2. This self-consistently predicts the nematic order parameter, \bar{P}_1 as a function of the cell and matrix elastic constants, cell shape, and the noise (modeled as an effective temperature). In both models, if the noise is moderately large, the nematic order of the CSK is maximal in some optimal range of substrate rigidity and is small for very small or very large rigidities.

The dependence on the boundary conditions (*i.e.*, the global cell shape and substrate rigidity) highlights the importance of the long-range elastic interactions, in contrast to the general situation for nematic ordering in molecular systems where the interactions are short range. The Mair-Saupe theory predicts that for small noise (or

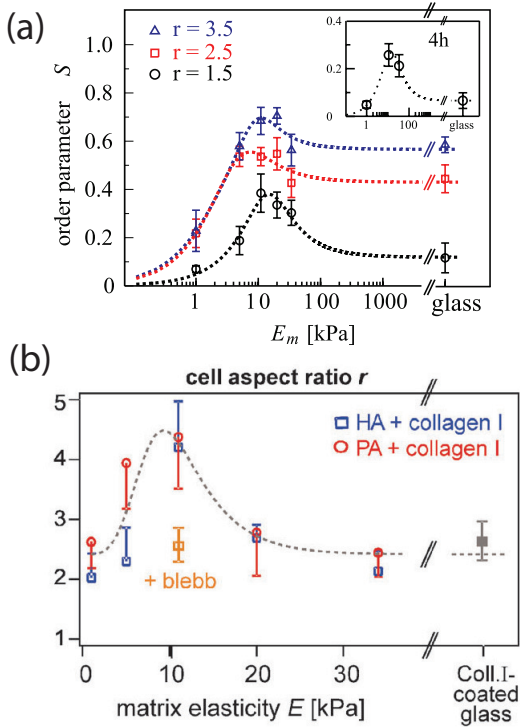


FIG. 23 (Color online) (a) The experimental values of the stress-fiber order parameter, $S \sim \bar{P}_1$ (which indicates the extent to which the nascent stress fibers are aligned along the long axis of the cell) for three groups of stem cells (of aspect ratios 1.5, 2.5, 3.5) as a function of the Young's modulus of the matrix, E_m . For the smallest aspect ratio, the order is clearly maximal for $E_m \sim 11\text{kPa}$; for the other aspect ratios this trend may also be obeyed although it is less clear. The fit is motivated by the theory described in the text, see Zemel *et al.* (2010b). From Zemel *et al.* (2010b). (b) Aspect ratio of stem cells as a function of substrate elasticity. The point marked blebb refers to cells where myosin activity has been suppressed by treatment with the drug blebbistatin; this shows that the peak observed for untreated cells is related to cell contractility. From Rehfeldt *et al.* (2012).

large values of \bar{P}_0), the nematic order may increase monotonically as a function of substrate rigidity due to the increasing importance of short-range interactions such as the excluded volume of the dipoles themselves.

Experiments were carried out (Zemel *et al.*, 2010b) to systematically analyse the alignment of stress fibers in human mesenchymal stem cells as a function of the cell shape and the rigidity of the environment. Cells were cultured on substrates of varying stiffness and sorted by their aspect ratio. A quantitative analysis of stress-fiber polarization in cells was obtained by staining for both actin and non-muscle myosin IIa and applying a segmentation algorithm to map their spatial organization in the cell. Both the magnitude of the dipoles, as measured by the number of actomyosin minifilaments (Zemel *et al.*, 2010a) and their orientation were measured. The results are shown in Fig. 23. They suggest a generic

mechanical coupling between the cell shape, the rigidity of the surroundings and the organization of stress fiber in the cytoskeleton of stem cells, again pointing to the role of long-range interactions. This identifies a mechanical property of cells – stress-fiber polarization – that is maximized at an optimal substrate rigidity, analogous to the optimal rigidity found in stem-cell differentiation (for example, to muscle cells) (Engler *et al.*, 2006). The fact that the CSK is maximally polarized for substrate rigidities of about 10 kPa may help explain why stem-cell differentiation into muscle cells occurs optimally in this same rigidity range. Stem cells on such substrates are muscle-like in their CSK structure and the resulting contractile forces; the latter may play a role in nuclear deformations resulting in gene expression that is muscle-like for precisely such contractile cells. We note that the time scales observed for stress fiber development (Zemel *et al.*, 2010b) and orientation (1–24 hours) and for the genetic changes in the cell (Engler *et al.*, 2006) (about a week) are quite different. In addition, recent experiments have shown that differentiation may also depend on the mechanics of the ligand molecule and not only on the bulk rigidity of the substrate (Trappmann *et al.*, 2012).

The ordering of the cytoskeleton on substrates of different rigidities eventually affects the overall mechanical response of the cell. Recent studies (Janmey and Miller, 2011) have shown that cell cortical stiffness increases as a function of both substrate stiffness and spread area. For soft substrates, the influence of substrate stiffness on cell cortical stiffness is more prominent than that of cell shape, since increasing adherent area does not lead to cell stiffening. On the other hand, for cells constrained to a small area, cell shape effects are more dominant than substrate stiffness, since increasing substrate stiffness no longer affects cell stiffness.

E. Single cell response to rigidity gradients

The previous section looked “inside the cell” and considered the elastic interactions and orientational ordering of short actomyosin minifilaments modeled as force dipoles that are internal to the cell. This is relevant to stem cell development at relatively early times (1–24 hours in which the stress fibers do not yet span the entire cell). Mature cells such as fibroblasts or muscle cells have long and well-ordered stress fibers (Hotulainen and Lappalainen, 2006; Thery *et al.*, 2006) and in some cases, the cell can be represented by a single, anisotropic force dipole (Bischofs *et al.*, 2004; Bischofs and Schwarz, 2003; Pompe *et al.*, 2009; Schwarz and Safran, 2002). In the following we discuss the response of an entire, polarized cell (modeled in a coarse-grained approximation as a single, anisotropic force dipole) to rigidity gradients and in the next section, its response to dynamically applied stress.

Cell spreading, alignment and locomotion are con-

trolled by both biochemical activity within the cell as well as by the rigidity of the substrate on which the cell is plated (Discher *et al.*, 2005; Isenberg *et al.*, 2009; Lo *et al.*, 2000; Pelham and Wang, 1997; Saez *et al.*, 2007; Solon *et al.*, 2007). In general, these activities are enhanced on more rigid substrates. In addition, the forces that even static cells exert on substrates have been shown to increase with substrate rigidity (Choquet *et al.*, 1997; Saez *et al.*, 2005; Yeung *et al.*, 2005; Zemel *et al.*, 2010a). Moreover, very recent studies indicate that substrate viscoelasticity also plays a role in stem cell morphology and proliferation (Cameron *et al.*, 2011). Active gel theory has been used to model isotropic rigidity sensing in Marcq *et al.* (2011). Here we review how models of contractility based on force dipoles (Bischofs *et al.*, 2004; Nicolas and Safran, 2006b; Zemel *et al.*, 2010a) can provide insight into these observations.

Contractile cells are pre-programmed to exert force on their surroundings. It has been argued that the experimental observation that most cells types prefer stiff over soft substrates can be described by the assumption that cells effectively minimize the elastic energy invested in deforming the matrix (Bischofs *et al.*, 2004; Bischofs and Schwarz, 2003; Nicolas and Safran, 2006b). Neural cells, that prefer soft over stiff substrates, are exceptions to this rule of thumb (Janmey *et al.*, 2009). This minimization can be the result of evolution in producing optimized biological systems (Savir *et al.*, 2010), since the energy that the cell invests in deforming its surrounding is not directly useful to the cell. Alternatively, one can think of this approach as a convenient framework for analytical progress. Considering the cell as a uniform distribution of dipoles (that can either be ordered or random in their orientation), one can use Eq. 64. The dipole densities P_0 and P_1 are proportional to the number of dipoles and the cell volume while for fairly rigid substrates \mathcal{A}_{00} and \mathcal{A}_{11} scale inversely with $\bar{\mu}_m = \mu_m L/h$. Assuming that the cell optimizes its activity to avoid investing energy in substrate deformations, this predicts that cells will favor and spread optimally on rigid substrates.

This tendency of the cell to prefer rigid substrates is particularly important for cells on substrates with rigidity gradients or boundary regions (Allioux-Guerin *et al.*, 2009; Isenberg *et al.*, 2009; Ladoux and Nicolas, 2012; Lo *et al.*, 2000). The limiting cases of a cell on a substrate with a given rigidity near a boundary of a substrate with a much larger or smaller rigidity, can be understood by optimizing the deformation energy of a single force dipole in a medium with either clamped or free boundaries respectively. The corresponding elastic problem takes into account these boundary conditions using the technique of “image dipoles” (Bischofs *et al.*, 2004). As shown there, the preferred cell orientation close to the surface, as predicted by the configurations of minimal deformation energy, are parallel and perpendicular to the boundary line for free and clamped boundaries, respectively.

This leads to the prediction that cells preferentially locomote towards a clamped boundary, but tend to migrate away from a free boundary. One may think of a clamped (free) surface as the interface between the substrate on which the cell is placed and an imaginary medium of infinite (vanishing) rigidity, which effectively rigidifies (softens) the boundary region. Thus for clamped (free) boundary conditions, the cell senses maximal stiffness in the direction normal to (parallel to) the boundary line. The cell exerts force on the more rigid medium. For free boundaries, the substrate is more rigid and the cell orients parallel to the boundary to maximize the deformation of the substrate. Near a clamped boundary, there is less deformation if the cell orients perpendicular to the boundary line. Indeed such behavior has been observed experimentally, *e.g.*, for cells close to the boundary between soft and rigid regions of a soft substrate (Lo *et al.*, 2000). The tendency to migrate towards stiffer regions has been termed *durotaxis*. On a more microscopic level, this can be understood from the preferred growth of focal adhesions on more rigid substrates (see section IV).

F. Dynamical response of cells to mechanical stress

Cells in tissues respond to a variety of mechanical forces that influence their behavior and alignment such as gravity, muscle tension, blood pressure as well as from local active tractions of nearby cells (Chen, 2008; Ingber, 2003). The forces that act on cells can be static as well as time varying, *e.g.*, continuous loading occurs during development of long bone growth while cyclic loading occurs due to periodic blood pressure variations. These mechanical signals typically induce an active reorganization of the cell cytoskeleton and readjustment of the contractile forces exerted by the cells (Deng *et al.*, 2006; Stamenovic *et al.*, 2007). The active nature of this mechanotransduction is demonstrated by the fact that it often vanishes when actin-myosin contractility is inhibited (Zhao *et al.*, 2007).

The response to mechanical stress is demonstrated by cells that actively reorient and align themselves in preferred directions. It is interesting to note that, while in some studies cells were shown to align parallel to the direction of a static or quasi-static stress field (Brown *et al.*, 1998; Collinsworth *et al.*, 2000; Eastwood *et al.*, 1998; Samuel and Vandeburgh, 1990), other experiments find that cells remain randomly oriented (Jungbauer *et al.*, 2008). On the other hand, when subject to dynamically oscillating stress and strain fields (designed originally to study the effects of heart beat and blood pressure), cells tend to orient away (nearly, but not exactly perpendicularly) from the stress direction (Faust *et al.*, 2011; Hayakawa *et al.*, 2001; Jungbauer *et al.*, 2008; Kurpinski *et al.*, 2006; Shirinsky *et al.*, 1989; Wang *et al.*, 2001; Wang and Grood, 2000). As discussed below, this reori-

entation does not occur as a rigid body motion of the cell, but rather involves the disassembly and then re-assembly of the CSK in directions determined by the applied stress; it may also involve rotations of the stress fibers (Deibler *et al.*, 2011). In some of the experiments on static stress (Brown *et al.*, 1998), cells were placed in 3d collagen matrices and it is not clear whether remodeling of the matrix (Fernandez and Bausch, 2009; Takakuda and Miyairi, 1996) by the stress contributes to cellular orientation or if the orientation is solely a result of CSK reorganization within the cell in response to stretch. The experiments in Fig. 5 of Eastwood *et al.* (1998) do indicate random collagen alignment even under tension. In general, the roles of passive (CSK elasticity) and active (actomyosin contractility) forces in determining cell response to applied stress have yet to be fully elucidated (Nekouzadeh *et al.*, 2008). In the following, we first review some recent mechanobiological measurements that provide new insights for understanding the response of cells to applied stress. We then summarize several theoretical approaches that quantify these ideas.

CSK disassembly and reassembly: Recent experimental studies have shown that cell stretch induces CSK fluidization (Bursac *et al.*, 2005; Chen *et al.*, 2010a; Deng *et al.*, 2006; Krishnan *et al.*, 2009; Trepaut *et al.*, 2007) which occurs through direct physical effects of physical forces upon weak cytoskeletal crosslinks. CSK fluidization is typified by marked decreases of CSK stiffness, CSK tension, and cellular traction forces, and marked increases in the rate of CSK remodeling dynamics (Krishnan *et al.*, 2009; Trepaut *et al.*, 2007) and is accompanied by extremely rapid disassembly of actin bundles. These effects depend (Krishnan *et al.*, 2009; Trepaut *et al.*, 2007) on the load, loading frequency and on the magnitude of the pre-stretch actomyosin contractility.

To restore homeostasis in the cell (*i.e.*, a fixed level of contractility), CSK fluidization is immediately succeeded by CSK reassembly, a signaling driven response that restores molecular interactions that were disrupted by fluidization (Trepaut *et al.*, 2007). CSK reassembly results in gradual increases of CSK stiffness, CSK tension, and cellular traction forces, and gradual decreases in the rate of CSK remodeling dynamics. These are driven by slow reassembly that acts predominantly on those spatial sites where traction forces were markedly reduced by CSK fluidization (Krishnan *et al.*, 2009; Trepaut *et al.*, 2007). These processes govern the response of cells to applied stress in which the reorientation is a result of the CSK fluidization and reassembly.

CSK stiffness changes in response to applied stress: While it is clear that the CSK reorganizes in response to applied stretch, it is also important to know whether cell contractility and stiffness is increased or decreased during stress application. Experiments on fibroblasts in three-dimensional, collagen gels showed that overall, cells reduce their contractility during the stretch-relax

cycles (Brown *et al.*, 1998). This led those authors to suggest that cells have a homeostatic (or set-point) contractility that is reduced when the surrounding medium is stretched. The dynamics of this process were investigated in more detail in Nekouzadeh *et al.* (2008) who showed that when stretched for several minutes, contractile fibroblasts initially diminished the mechanical tractions they exert on their environment through depolymerization of actin filaments. The cells then restored tissue tension and rebuilt actin stress fibers through staged Ca dependent processes that consisted of a rapid phase that ended less than a minute after stretching, a plateau of inactivity, and a final gradual phase that required several minutes to complete. Active contractile forces during recovery scaled with the degree of rebuilding of the actin cytoskeleton. The final cell stress following a stretch exceeds the pre-stretch value; this is in contrast to the results reported by Brown *et al.* (1998). However, the observations of cellular ensembles might not be indicative of a “typical” cell; the highly repeatable ensemble behaviors may represent a diversity of responses at the level of individual cells

Trepaut and coworkers (Trepaut *et al.*, 2004) developed an experimental system to subject adherent cells to a global stretch while simultaneously measuring the local complex shear modulus ($G^* = G + iG''$) of the cells. They used this system to study the viscoelasticity of alveolar epithelial cells in response to stepwise stretch and found that with increasing levels of stepwise stress, both G' (elastic response) and G'' (viscous response) increased. These findings indicate that the cytoskeletal response shows a non-linear elastic response characteristic of strain-stiffening and that intracellular dissipation also increases with increasing cytoskeletal tension. In addition, they found that the ratio G''/G' decreased with stretch, consistent with an increase in the elastic rigidity of the CSK, corresponding to reassembly. In a later study, these authors observed that when the cytoskeleton was contracted with thrombin before application of a stepwise stretch, the strain-stiffening response was abrogated (Trepaut *et al.*, 2006), which suggests that the strain-stiffening regime is restricted to a range of cytoskeletal tension. The same experimental setup was used to test the viscoelastic response of a broad variety of cell types that were subject to a transient application of stretch-unstretch (Trepaut *et al.*, 2007). Contrary to the case of a stepwise stretch, a transient stretch that returns to zero strain caused a sharp drop in both G' and G'' and a sudden increase in the ratio G''/G' . Thus, while a stepwise stretch induces CSK rigidification, a transient stretch induces cell softening and fluidization. To test whether stretch-induced cell stiffening and softening were associated with changes in cytoskeletal tension, Gavara and coworkers developed a system to map traction forces at the cell-substrate interface during application of stretch (Gavara *et al.*, 2008). They observed

that cytoskeletal tension increased with application of a stepwise stretch, but decreased below baseline levels upon stretch removal. Analysis of traction maps before, during, and after stretch indicated that the regions of higher traction force application were those that exhibited a larger relative drop of traction after stress cessation, suggesting that those cellular structures subjected to a higher tension are disrupted by stretch. Taken together, these findings point to the existence of two different mechanisms by which cells respond to stretch. Strain-stiffening during a stepwise stretch is likely to arise from non-linear stretching of single cytoskeletal filaments. On the other hand, strain-softening after a transient stretch is probably caused by inelastic unbinding or unfolding of cytoskeletal crosslinks and actomyosin crossbridges. In response to a constant stepwise stretch, filament stretching appears to dominate over inelastic unbinding and unfolding of crosslinks and crossbridges. After stretch cessation, however, the contribution of filament stretching becomes negligible and the effect of inelastic unbinding and unfolding dominates.

CSK and cellular reorientation in response to cyclic stretch: In the introduction to this section, we mentioned several studies that showed that the cells orient away from the stress direction of cyclically applied stress. Recent experiments have provided quantitative measures of these effects. Experiments described in Deibler *et al.* (2011) and Jungbauer *et al.* (2008) investigated the dynamic reorientation of rat embryonic and human fibroblast cells over a range of stretching frequencies from 0.0001 to 20 s⁻¹ and strain amplitudes from 1% to 15%. Their measurements show that the mean cell orientation changes exponentially in time with a frequency-dependent characteristic time from 1 h to 5 h. At subconfluent cell densities (at which the cells are not yet close packed), this characteristic time for reorientation shows two characteristic regimes as a function of frequency. For frequencies below 1 s⁻¹, the characteristic time decreases with a power law as the frequency increases. For frequencies above 1 s⁻¹, it saturates at a constant value. In addition, a minimum threshold frequency was found below which no significant cell reorientation occurs. The results suggest a saturation of molecular mechanisms of the mechanotransduction response machinery for subconfluent cells within the frequency regime studied. One possible interpretation of these two time scales is given in the theoretical model described in the next section. Interestingly, recent work (Zahn *et al.*, 2011) by these researchers showed that the time scale is correlated with the amount of actin in the cell; aged cells, with less actin show faster reorganization in response to uniaxial tensile stress compared with younger cells which contain more actin and are elastically more rigid. In addition, other biochemical changes can modify the response time of the cytoskeleton and thereby control its orientation in response to cyclically varying stress (Hoffman *et al.*, 2011).

To control the strains both parallel and perpendicular to the stress directions, the researchers in Faust *et al.* (2011) used elastomeric chambers that were specifically designed and characterized to distinguish between zero strain and minimal stress directions and to allow accurate theoretical modeling. Reorientation was only induced when the applied stretch exceeded a specific amplitude, suggesting a non-linear response. However, on very soft substrates no mechanoresponse occurs even for high strain. This suggests an explanation for the necessity of rather stiff environmental conditions to induce cellular reorientation in mammalian tissues. For all stretch amplitudes, the angular distributions of reoriented cells could be modeled as discussed in the next section. Cyclic stretch increases the number of stress fibers and the coupling to adhesions. Changes in the cell shape follow the cytoskeletal reorientation with a significant temporal delay; this indicates that cell reorientation and shape is induced by CSK reassembly in response to stretch. In the frequency range studied of 10-50 mHz, the stress induces cell reorientation (after about 16 hours) in the direction of zero strain. A recent study by Livne and Geiger (unpublished) analyzed the reorientation dynamics of cyclically stretched cells, over a wide range stretch configurations, and observed a systematic deviation between the measured cell and stress fiber orientation and the zero strain prediction (up to 10 degrees). To address this discrepancy, a novel model which shifts the focus of the reorientation process to the FAs was developed.

Theory of cell response to applied stress: Models of cell response to applied stress are motivated by the questions of why stress fibers or cells orient nearly (but not always exactly) perpendicular to the direction of the applied stress. Macromolecular or biochemical models of cellular orientation and stress-fiber rearrangement in response to applied forces have been discussed in Hsu *et al.* (2009); Mogilner and Rubinstein (2005); Pirentis and LaZopoulos (2009); Pirentis *et al.* (2011); and Wei *et al.* (2008) while a more generic theoretical approach is given by De and Safran (2008); De *et al.* (2007, 2008); and Safran and De (2009). We first review more molecularly-based models that focus on the role of the stress fibers and then present a more phenomenological and general approach that in principle coarse grains over both stress fiber and focal adhesion response..

Molecularly-based models: The work of Wei *et al.* (2008) predicts the orientation of stress fibers in response to cyclic stretch based on a biochemical-mechanical model that relates the contraction and extension rate sensitivity of the stress fibers to the magnitude and frequency of the applied stress. These kinetics depend on a biochemical activation signal – the tension-dependent fiber dissociation rate – and the rate of force generation by myosin II motors. This assumes that the stress fibers are intact throughout the application of dynamically varying strain. Experiments (Bursac *et al.*, 2005;

Deng *et al.*, 2006; Trepat *et al.*, 2007) show that cells respond to mechanical stress via an initial, fast (sec timescale) fluidization of the stress fibers that then reassemble and reorganize. Motivated by this, Pirentis and Lazopoulos (2009) and Pirentis *et al.* (2011) focus on a mathematical model that simulates the effects of fluidization and reassembly driven rigidification (Chen *et al.*, 2010a; Krishnan *et al.*, 2009) on cytoskeletal contractile stress. They show how these phenomena affect cytoskeletal realignment in response to pure uniaxial stretching of the substrate. The model comprises individual elastic stress fibers anchored at the endpoints to an elastic substrate and predicts that in response to repeated stretch/unstretch cycles, stress fibers tend to realign in the direction perpendicular to stretching. The authors conclude that relaxation of cytoskeletal contractile stress by means of fluidization and subsequent stress recovery by means of CSK reassembly may play a key role in reorganization of cytoskeletal stress fibers in response to uniaxial stretching of the substrate.

A somewhat more general approach to the mechanical response of stress fibers that was taken by Kaunas and colleagues (Hsu *et al.*, 2009; Kaunas *et al.*, 2011) who developed a model that tracks the fate of individual, stretched stress fibers based on the hypothesis that stress fibers have an optimal prestrain due to actomyosin contractility (Lu *et al.*, 2008); perturbing the strain from that optimal value promotes stress fiber disassembly. Motivated by experimental evidence of stress fiber viscoelastic properties, stress fibers are assumed to relax at a rate proportional to the perturbation in fiber stretch away from this optimum. The dynamic turnover of stress fibers was described using a stochastic approach with the probability per unit time of stress fiber disassembly expressed as a constant plus a term quadratic in the deviation of the strain from its optimal value. The disassembly of a stress fiber is assumed to be immediately followed by the assembly of a new stress fiber at its optimal stretch and oriented in a randomly chosen direction. Model parameters were determined by fitting experimentally measured time courses of stress fiber alignment performed at different rates of strain (*i.e.*, 0.01 to 1 Hz). The model predicts that reorganization of the stress fibers is determined by the competition between the rates of stress fiber assembly and load-dependent disassembly. The stress fibers preferentially disassemble in the direction of stretch, while stress fibers reassembling in stochastically chosen directions gradually accumulate about the direction of least perturbation in fiber tension. At low strain rates, the stress fibers are predicted to align with random orientations with respect to the applied stress direction. While this has been reported in some cases for very slow cyclic stress, other experiments report alignment in the stress direction as discussed above. Recent studies (Tondon *et al.*, 2012) using non-sinusoidal waveforms show that the stress fiber reorientation is most sen-

sitive to the rate of lengthening; this provides support for the role of stretch of the actin filaments in cell reorientation under stress.

Coarse-grained models based on force dipoles: One goal of this more phenomenological approach (De and Safran, 2008; De *et al.*, 2007, 2008; Safran and De, 2009) is to explain the observed frequency dependence of cell orientation mentioned above. Another, is to understand why the characteristic time for the cell to reach its steady-state orientation, $\tau_c \sim 10^3 - 10^4$ seconds, is strongly frequency dependent for stretch frequencies smaller than about 1 Hz while at higher frequencies, τ_c is frequency independent. The experiments were conducted on anisotropic cells such as fibroblasts so the theory focuses on needle-like cells in which the entire cell is modeled in a coarse grained approximation as a single force dipole; for needle-like cells, the dipole component $P_2 = 0$. The dipoles can then be characterized by their magnitude $P_0 \equiv P < 0$ (to signify contraction) and direction, $\theta = \arctan [(P_0 - P_1)/(P_0 + P_1)] = \arctan [p_{yy}/p_{xx}]$, relative to the external stress.

It has been suggested (Brown *et al.*, 1998) that cells actively adjust their contractility by reorganizing the FA and stress fibers to maintain an optimal (or set-point) value of the stress or strain U^* in the adjacent matrix (De and Safran, 2008; De *et al.*, 2007, 2008; Safran and De, 2009). This translates via elastic theory, into an optimal value of the cellular dipole $P^* > 0$. The stresses are converted to energy units by multiplying by the cell volume and the externally applied stretch is denoted as $P_a(t) > 0$. In the presence of such time-dependent stretch that acts at an angle θ relative to the cell axis, it is assumed that the homeostatic, set-point *total* local stress in the matrix is achieved when the cellular force dipole obeys (Safran and De, 2009):

$$P = -P^* + \alpha_0 P_a(t) (\phi - \phi_1) \quad (65)$$

where $\phi = \cos^2 \theta$. Two limiting cases are where: (i) the cellular dipole is controlled by the matrix stress where $\phi_1 = 0$ (ii) the dipole is controlled by the matrix strain and $\phi_1 = \cos^2 \theta_0 \equiv \phi_0$, where θ_0 is the zero strain direction given by $\cos^2 \theta_0 = \nu/(1 + \nu)$. In general, α_0 can be either positive or negative corresponding to matrix stretch that causes either a decrease or an increase in the cytoskeletal forces respectively.

Deviations from the set-point result in internal forces within the cell that reestablish the optimal stress condition. These forces can be derived from derivatives of an effective, harmonic “free energy” (more precisely, a cost function whose minimum represents the optimization of the cellular activity) due to cell activity, F_a , that includes the active processes within the cell that establish cellular response to its *local* environment.

$$F_a = \frac{1}{2} \chi (-P + \alpha_0 P_a(t) (\phi - \phi_1) - P^*)^2 \quad (66)$$

where χP^{*2} (with units of energy) is a measure of cell activity that establishes the set-point.

In addition to the cell activity, the model also includes the effect of mechanical matrix forces, Eq. 59 that yields an energy, F_e proportional to the product of $P_a(t)$ and P . The goal is to solve for the dipole magnitude and direction in the presence of a time-varying stress: $P_a(t) = P_a(1 - \cos \omega_a t)$, where $P_a > 0$ for stretch. In general, the dynamics of the cytoskeleton are governed by complex, viscoelastic processes that also involve liquification and reassembly of the stress fibers (Deng *et al.*, 2006). In a coarse grained picture, one can write relaxational equations for the dipole magnitude and direction, that are governed by the derivatives of $F = F_a + F_e$:

$$\frac{dp(t)}{dt} = -\frac{1}{\tau_p} f_p \quad \frac{d\theta(t)}{dt} = -\frac{1}{\tau_\theta} f_\theta \quad (67)$$

where $p = P/P^*$, the dimensionless, effective free energy $f = F/(\chi P^{*2})$, and $f_p = \partial f / \partial p$ and $f_\theta = \partial f / \partial \theta$. Noise terms modeled as a dimensionless, effective temperature, T_s , can also be included in this formalism (Safran and De, 2009); note the caveats on the use of effective temperature and Boltzmann distributions discussed in the section on the physics background.

Based on experiments (Deng *et al.*, 2006; Gavara *et al.*, 2008; Nekouzadeh *et al.*, 2008), it has been suggested that the liquification and repolymerization of the actin stress fibers after stretch is applied, occurs on a short time scale on the order of several seconds, while the correlated re-orientation occurs on much longer time scales (on the order of many minutes) (Brown *et al.*, 1998; Eastwood *et al.*, 1998; Jungbauer *et al.*, 2008). It is thus assumed that $\tau_p \ll \tau_\theta$: the time scale associated with changes in the magnitude of the dipole is much faster than that associated with the dynamics of its highly correlated re-orientation. In this approximation, the dipole magnitude reaches a steady-state value in a short time; this value may be time dependent and oscillatory due to the cyclic nature of the applied, time dependent stress.

One therefore first solves for the dipole magnitude, $p(t)$, treating the slowly-varying dipole orientation, $\phi(t)$, as a constant; for details, see Safran and De (2009). The average value of $\phi = \cos^2 \theta$ is calculated as a function of the frequency depends on the effective temperatures for the cases of both stress and strain as set-points. At high frequencies and low effective temperatures, the average angle is nearly perpendicular (or in the zero-strain direction, θ_0 , for cells whose set-point is determined by matrix strain), due to the dynamical frustration of the cell which is unable to adjust its force dipole to the time-dependent matrix stresses. At very low frequencies, the average angle is nearly parallel and for both the case of stress and strain as set-points, consistent with some of the experiments (Brown *et al.*, 1998). At higher effective temperatures, the orientation distribution is random and the average value of ϕ (in two-dimensions) is 1/2

for all frequencies. At intermediate temperatures, one finds the interesting possibility of nearly perpendicular orientation for high frequencies, but nearly random orientation for low frequencies (for details, see Safran and De (2009)). Biochemical changes can modify the response time of the cytoskeleton and thereby change cell orientation from nearly perpendicular – when the CSK cannot follow the applied, cyclic stress – to parallel – when CSK remodeling time scales are short enough (Hoffman *et al.*, 2011). In addition, experiments on 3d matrices (Riehl *et al.*, 2012) indicate parallel orientation of stress fibers even at relatively high frequencies. The systematic understanding of when cells respond by orienting parallel compared to the relatively well-studied response of cells on relatively stiff substrates to cyclic stretch is a challenge that has yet to be met.

The dynamical theory is also used to calculate (Safran and De, 2009) the characteristic time, τ_c , for a cell to attain its steady-state orientation. At high frequencies, τ_c is frequency independent, while at low frequencies, $\tau_c \sim 1/\omega^2$; in both regimes τ_c depends on the amplitude of the applied stress and this is related to the fact that the zero-strain or zero-stress direction orientation occurs only when the applied stress exceeds a threshold value (De and Safran, 2008; De *et al.*, 2007; Safran and De, 2009). Both the predicted frequency and amplitude dependence are in qualitative agreement with experiments (Jungbauer *et al.*, 2008).

VII. CELL ASSEMBLIES

A. Matrix-mediated cell interactions

After treating the response of isolated cells to changes in their elastic environment, we now discuss the elastic responses of and interactions in ensembles of cells. We restrict the analysis to the effects of elastic interactions on the relative positions and orientations of cells. Moreover, we focus on the case in which cells are well separated and interact with each other only via the matrix and not through direct cell-cell interactions. This is fundamentally different when modeling growing epithelial tissue or tumors, when cell-cell interactions dominate. A popular model system for epithelial tissue formation is the Drosophila wing disc, which often is treated using vertex models (Aegerter-Wilmsen *et al.*, 2010; Aliee *et al.*, 2012; Canelas-Xandri *et al.*, 2011; Farhadifar *et al.*, 2007; Hufnagel *et al.*, 2007; Landsberg *et al.*, 2009; Rauzi *et al.*, 2008). In our focus here on matrix mediated interactions, we do not discuss the effect of cell proliferation and cell death, that also leads to interesting features in cell assembly (Basan *et al.*, 2009; Ranft *et al.*, 2010; Shraiman, 2005).

An early study that highlighted the effect of elastic substrate deformations in modulating the relative posi-

tions of cells placed far apart was presented in Korff and Augustin (1999). They observed that capillary-like structures formed by two, initially separated groups of cells were associated with tensional remodeling of the collagen matrix and directional sprouting of the outgrowing capillaries towards each other. These experiments presented evidence that tensional forces on a fibrillar, extracellular matrix such as type I collagen, but not fibrin, are sufficient to guide the directional outgrowth of endothelial cells. More recently Califano and Reinhart-King (2010) and Reinhart-King *et al.* (2008) used matrices of varying stiffness and measurements of endothelial cell migration and traction stresses, to show how cells can detect and respond to substrate strains created by the traction stresses of a neighboring cell; they demonstrated that this response is dependent on matrix stiffness. Other studies suggest that on some matrices, cells can sense each other (most probably via elastic deformations) at distances on the order of $400\mu\text{m}$ (Winer *et al.*, 2009). Recently it was also reported that cardiac cells can synchronize their beating through substrate deformations (Tang *et al.*, 2011). The various experiments imply that matrix mechanics can foster tissue formation by correlating the relative motions or even internal dynamics of cells, thereby promoting the formation of cell-cell contacts. The theoretical studies below model an entire cell as a single, usually anisotropic, force dipole. Interactions among cells are taken into account for several simple geometries. A simple analogy to dielectric media with predictions of the elastic susceptibilities and “dielectric constants” of force dipole assemblies was presented in Zemel *et al.* (2006) where the effective elastic constants of materials containing force dipoles are calculated as a function of the dipole density. The results, valid in the relatively dilute limit, indicate an effective stiffening of the material due to the alignment of the contractile dipoles parallel to the applied stretch. It remains to be seen how to take this analogy further to include dynamical, tensorial and non-local spatial effects as well as the development of a theory that is valid for both high and low force dipole concentrations. In addition, one must decide whether the dipoles are translationally mobile (as is the case for counterion screening in electrostatics) or only orientationally mobile (as assumed in Zemel *et al.* (2006)).

B. Elastic interactions of force dipoles

The anisotropic and long-range nature of the interactions of cell dipoles leads to a rich variety of self-assembled structures (Bischofs *et al.*, 2004; Bischofs and Schwarz, 2003, 2005, 2006). Monte Carlo simulations of these dipolar interactions in the presence of noise, modeled as an effective temperature, predicted cellular structure formation on elastic substrates as a function of the

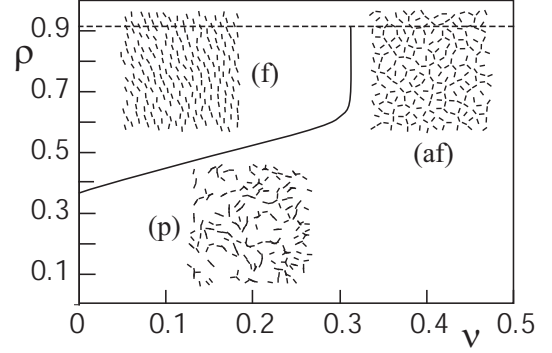


FIG. 24 Phase diagram for positionally disordered cells. At low values of the scaled cell density, ρ , an orientationally disordered (paraelastic) phase (p) prevails. At high cell density, orientational order sets in, with a nematic string like (ferroelastic) phase (f) at low values of Poisson ratio, ν , and a isotropic ringlike (antiferroelastic) phase (af) at large values. From Bischofs and Schwarz (2006).

cell density and Poisson ratio of the substrate. One interesting situation considered was that of an infinitely extended string of aligned force dipoles spaced at equal distances, a (Bischofs and Schwarz, 2005). An additional dipole is placed at a horizontal distance x and with a vertical offset y . Despite the long-ranged character of the elastic dipole interaction, the nearby dipoles in the string screen each other’s strain fields; thus, the effective interaction between an infinite string and a single dipole (or a second string) is short ranged and decays as an exponential function of x/a . The magnitude of the interaction depends strongly on the Poisson ratio of the substrate. The results suggest that long-ranged effects do not dominate structure formation at particle densities sufficiently large as to allow formation of strings of aligned dipoles.

The orientational interactions of dipoles at random spatial positions (but constrained to obey excluded volume) were considered; the elastic energies and noise were used to equilibrate the dipolar directions (Bischofs and Schwarz, 2006). At low density, the simulations show many short strings with few correlations (paraelastic phase) among them. At high density and small values of the Poisson ratio, spontaneous polarization occurs (ferroelastic or nematic), that results in a unidirectional contraction of the substrate. At large values of both the cell density and the Poisson ratio, the system becomes macroscopically isotropic again, with a local structure which is ringlike rather than string like (antiferroelastic). The predicted structures are shown in Fig. 24.

C. Myofibril registry modulated by substrate elasticity

We now summarize a model that shows that elastic interactions can tune the registry of long actomyosin fibers whose nematic (orientational) order is already well estab-

lished (Friedrich *et al.*, 2011). In a variety of cell types, various types of actomyosin bundles exhibit periodic internal structure with alternating localization of myosin filaments and the actin crosslinker α -actinin. Examples include striated stress fibers in fibroblasts and striated stress fiber-like actomyosin bundles in some developing muscle cells (Hotulainen and Lappalainen, 2006; Pellegrin and Mellor, 2007; Rhee *et al.*, 1994; Russell *et al.*, 2009). The striated architecture of these fibers is similar to the sarcomeric architecture of myofibrils in striated muscle, but is much less regular. In both adherent, non-muscle cells as well as in developing striated muscle cells, the striations of neighboring, but distinct fibers are often in registry, *i.e.*, the positions of the respective α -actinin and myosin bands match, see Fig. 25. This inter-fiber registry of striated fibers represents a further state of cytoskeletal order, which might be termed “smectic order” using liquid crystal terminology.

Experiments on cultured cells plated on flexible substrates have shown that substrate stiffness is one factor that can regulate cytoskeletal order in general, and myofibril assembly in particular (Engler *et al.*, 2004b, 2008; Jacot *et al.*, 2008; Majkut and Discher, 2012; Serena *et al.*, 2010). Relative sliding of striated actomyosin bundles into registry was previously reported in McKenna *et al.* (1986). In Engler *et al.* (2004b) the amount of striated myosin (which serves as a measure of myofibril condensation) depended on the stiffness of the matrix upon which various cells were cultured, with a pronounced maximum at an optimal stiffness of about $E_m \approx 10$ kPa. Interestingly, this value is close to the longitudinal stiffness of relaxed muscle.

The striated fibers are under constant tension due to the activity of myosin filaments that link actin filaments of opposite polarity, see figure 25. These actomyosin contractile forces strain the α -actinin-rich crosslinking regions (termed Z-bodies) of premyofibrils and nascent myofibrils in developing muscle cells. Because the crosslinking regions can be mechanically connected to the substrate by means of adhesive contacts, the tension generated in them may be transmitted to the substrate. Thus, the substrate underneath a striated fiber is strained with regions of expansion below the crosslinking bands and regions of compression in between. The strain fields induced by a single bundle of actomyosin propagate laterally towards its neighbors, inducing an effective elastic interaction between the fibers; this biases the spatial reorganization of fibers to favor registry, that results in smectic ordering of the crosslinkers and the myosin in neighboring bundles.

A minimal model for this effect (Friedrich *et al.*, 2011) considers the cell-substrate interface as the xy -plane with a single contractile fiber parallel to the x -axis. The forces transmitted by the fiber onto the substrate can be effectively described by a dipole distribution (with units of energy per unit area) $\Pi_{ij}(x, y) = \rho(x)\delta(y)\delta_{ix}\delta_{jx}$ of force

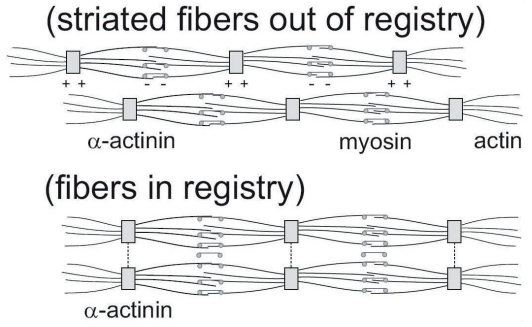


FIG. 25 Schematic view of two striated fibers. Striated stress fiber-like acto-myosin fibers form close to the cell-substrate interface of adherent, non-muscle cells. Each fiber is a bundle of aligned actin filaments that has a sarcomeric sub-architecture: Z-bodies (containing alpha-actinin) that crosslink actin filament barbed ends alternate with regions rich in myosin II in a periodic fashion. Striated fibers can slide past each other until their periodic structures are in phase. Adapted from Friedrich *et al.* (2011).

dipoles that are localized to the adhesive contacts whose lateral extension are on the order of 100 nm and are thus much smaller than the spacing $a \approx 1 \mu\text{m}$ of Z-bodies. Here, the force dipole density (with units of energy per unit length) $\rho(x)$ is a periodic function of x due to the sarcomeric (*i.e.*, periodic) architecture of a single striated fiber. For simplicity, the analysis focuses on the principal Fourier mode: $\rho(x) = \rho_0 + \rho_1 \cos(2\pi x/a)$ where a corresponds to the sarcomeric periodicity of the striated fiber.

The strain field $u_{ij}(x, y)$ at the surface of the substrate with Young's modulus E_m (and located at $z = 0$) that is induced by this periodic dipole “string” can be found from the Green's function of Eq. 57. The parallel strain component $u_{11}(x, y)$ can be written as a product of a “lateral propagation factor” Φ that characterizes the propagation of strain in the lateral y direction and a harmonic modulation in the x direction along the striated fiber

$$u_{11}(x, y) = \Phi(|y|/a, \nu) \frac{2\rho_1}{E_m a^2} \cos(2\pi x/a) \quad (68)$$

Thus the strain field u_{11} is periodic in the x -direction with period a reflecting the periodicity of the striated fiber. The factor Φ characterizes the propagation of strain in the lateral direction away from the centerline of the fiber; this depends on the distance from the fiber as well as the Poisson ratio. The interaction between two such strings of dipoles is described by the elastic interaction energy, which is the local product of the dipole and the strain. The energy which a given fiber (string of dipoles), must invest in order to deform the substrate is the sum of a “self-energy” of the first dipolar string, $W_{\text{self}} = \int d^2\mathbf{x} \Pi_{ij}^{(1)} u_{ij}^{(1)}$, which accounts for the substrate deformation energy in the absence of the second string of dipoles, and an interaction term

$W_{\text{int}} = \int d^2\mathbf{x} \Pi_{ij}^{(1)} u_{ij}^{(2)}$. The term W_{int} characterizes an effective, substrate-mediated interaction between the two contractile fibers and can guide their spatial reorganization.

Inserting the specific strain field induced by a single striated fiber, Eq. (68), into the general formula for elastic interactions, yields the elastic interaction energy between the two fibers (per mini-sarcomere) as a function of the phase shift Δx and the separation of their center-lines, d :

$$W_{\text{interaction}} = \Phi(d/a, \nu) \frac{\rho_1^2}{aE_m} \cos(2\pi\Delta x/a) \quad (69)$$

Here $W^* = \rho_1^2/(aE_m) \approx 10^{-18}\text{J} \approx 250 k_B T$ sets a typical energy of the elastic interactions. Registry of fibers with $\Delta x = 0$ is favoured for inter-bundle spacings where the propagation factor, $\Phi < 0$.

For incompressible substrates with Poisson ratio close to $\nu = 1/2$, such as those used in experiments (Buxboim *et al.*, 2010; Engler *et al.*, 2004b), it can be shown (Friedrich *et al.*, 2011) that the sign of the prefactor Φ of the elastic interaction energy is negative provided that the lateral fiber spacing is larger than some threshold $d/a > d^*/a \approx 0.247$. Hence, elastic interactions favor a configuration where neighboring fibers are in registry with $\Delta x = 0$. The opposite trend is found when $\nu \approx 0$ (Bischofs and Schwarz, 2005; Friedrich *et al.*, 2011). It is therefore possible that elastic interactions also set a preferred lateral spacing of striated fibers. Additionally, steric interactions may prevent neighboring fibers from getting too close and could enforce the condition $d > d^*$.

We previously discussed experiments and theory that demonstrated that cells tend to prefer rigid substrates where the elastic deformation energy cost is minimal. This also determines the optimal value of the cellular dipole magnitude in a simple model that balances the “cell activity” (described in Eq. 66 with zero applied field, $P_a = 0$) with the elastic energy cost of deforming the substrate (analogous to the expression in Eq. 64) (De *et al.*, 2007; Friedrich and Safran, 2012; Safran and De, 2009). In terms of the present model, this determines the optimal amplitude of the dipole string, ρ_1^* , from the force balance given by minimization with respect to the dipole amplitude, ρ_1 , of the sum of the two energies (per unit length of the bundle): the activity optimization, $W_{\text{active}} = \chi(\rho_1 - \rho_1^*)^2/2$ and the deformation energy, $W_{\text{deform}} \sim \rho_1^2/(2a^2 E_m)$ where E_m is the Young’s modulus of the substrate (Friedrich *et al.*, 2011). This predicts that $\rho_1 = \rho_1^* E_m/(E_m + E_m^*)$ where $E_m^* = 1/(a^2 \chi)$. The set-point value ρ_1^* corresponds to the amplitude ρ_1 of the dipole density on very stiff substrates with $E_m \gg E_m^*$. On soft substrates with $E_m \ll E_m^*$, however, ρ_1 can be considerably smaller than ρ_1^* .

Using this expression for the saturation of ρ_1 on substrate stiffness further predicts that the registry force

between two parallel striated fibers becomes a non-monotonic function of E_m with a Lorentzian form and has maximal magnitude for $E_m = E_m^* f_{\text{reg}} \sim -1/E_m \rho_1^2 \sim -E_m/(E_m^* + E_m)^2$. Here, it is assumed that the lateral spacing d of the fibers is larger than the critical distance d^* and independent of substrate stiffness.

The theory was compared with recent experimental studies of the inter-fiber registry in human mesenchymal stem cells that were plated on polymeric gels of different stiffness (ranging from 0.3 kPa to 40 kPa) (Friedrich *et al.*, 2011; Majkut and Discher, 2012). Well established, inter-fiber registry of adjacent striated fibers was observed primarily for cells that were cultured on 10 kPa gels as opposed to softer or more rigid substrates. Myosin bands perpendicular to the axis of nematic fiber organization were clearly visible and most likely connect neighboring actomyosin bundles in registry. Out of approximately 20 cells examined per gel, roughly 30%-50% exhibited aligned, striated fibers. The guidance mechanism for the registry of striated fibers by elastic interactions due to their elastic interactions predicts maximal registry at an “optimal” value of the substrate rigidity and represents a plausible mechanism for the establishment of inter-fiber registry observed in the experiments. Further experiments are needed to resolve the extent of striations within one acto-myosin bundle from the registry of striations in neighboring bundles; the theory presented here addresses the question of registry among bundles. It assumes that each bundle is well ordered; a possible mechanism for the development of such order was recently suggested in Friedrich *et al.* (2012).

VIII. CONCLUSIONS AND OUTLOOK

Research at the interface of physics and biology is an exciting adventure that has led and is still leading in several different directions. In this review with a theoretical focus, we have appropriately modified soft matter physics approaches to analyze how adherent cells mechanically interact with their environment through forces at the cell-material interface. Although passive soft matter systems such as droplets, fully elastic particles, vesicles and polymeric capsules are important reference cases for the adhesion of single cells, our discussion has shown that the main feature missing from such theoretical frameworks are active processes. In the context of force generation and sensing of adherent cells, the most prominent active processes are the polymerization of lamellipodia at the cell edge and the myosin II generated tensions in the actin cytoskeleton, including the contractile bundles (stress fibers) and networks that form during mature adhesion. These cytoskeletal processes are closely integrated with the dynamics of spatially localized sites of focal adhesions. Together, this system allows cells to sense and react to the mechanical properties of their envi-

ronment. Our review shows that the active and dynamic nature of cellular systems must be addressed on many different scales, from the modeling of nanometer-scale molecular association and dissociation events in adhesion clusters, to force generation in large supramolecular complexes and the shape and effective force balance at the 10 micrometer scale for animal cells. A further level of cooperativity arises if one considers the tissue scale at which cells can be further abstracted as discrete particles or defects. In the future, it is hoped that these different approaches will converge into a systems-level understanding of cellular systems that not only includes genetic and biochemical aspects (which were not the focus of this review), but also structural and mechanical ones; the latter are at least equally influential as biochemistry and genetics for the interactions of cells with their environment.

An important aspect of this review is to point out in which regard concepts from physics can be used to improve our understanding of cellular systems. By focusing on the physical constraints posed by the overall force balance in single myosin-minofilaments and cells, we arrived at the notion of force dipoles, which turns out to be a very powerful concept to rationalize many important aspects of the interactions of adherent cells with their physical environment. Motivated by pioneering experiments with adhesive micropatterns (Chen *et al.*, 1997) and soft elastic substrates (Pelham and Wang, 1997), during the last two decades or so, a growing body of research has addressed the physical understanding of how cells sense and respond to the physical properties of their surroundings, including adhesive geometry, topography and stiffness (Geiger *et al.*, 2009). The generic nature of the experimental observations (including the essential role of active contractility) suggests that measurements that focus on mesoscale (tens of nm to micrometers) behavior along with “coarse grained” models that capture the physics with only a small number of molecular parameters, can provide insight into the generic aspects of cell mechanosensitivity. In particular, we discussed models for the observed force dependence of the initial stages of cell adhesion in terms of either polymer-like elasticity or nucleation and growth. The genesis of the CSK in stem cells and its dependence on the rigidity of its elastic environment can be understood in terms of models that focus on the interactions of actomyosin force dipoles (within the cell) through the elastic deformations they induce in the cytoskeleton and the substrate. These deformations are long range and the ordering that develops in the CSK is therefore dependent on global boundary conditions such as the cell shape and the substrate rigidity. This can be demonstrated either by a rigorous treatment of the elasticity (that extends known results for passive inclusions to the case of active contractile elements) or by a simplified version based on the approximation of the cell as a thin, actively contractile film coupled to an elastic substrate. In the latter theory, the shape dependence

enters via moments of the Fourier transform of the lateral spatial dependence of the cell height. The response of cells to time varying, externally applied stresses can be understood in terms of either a specific elastic response of stress fibers or in terms of a generic theory that treats the entire cell as an elastic dipole that exerts forces on an elastic substrate. When the dipole dynamics (the formation and orientation of actomyosin bundles and their adhesions) are fast enough to follow the applied field, the cell is predicted to align parallel to the stress direction. However, if the applied strains or stresses vary too rapidly, the cell cannot adjust and orients its CSK in the zero strain or zero stress directions.

Despite some successes of these models in understanding and in some cases, predicting the experimental findings, many questions remain unresolved. Regarding the relation between focal adhesions, actin cytoskeleton and rigidity sensing, recent experimental progress has posed new challenges to theory. Quantitative studies with elastic substrates have shown that the size and traction force of focal adhesions can be very variable, depending on the history and internal structure of the adhesion (including a possible templating effect for growth by the actin cytoskeleton) (Stricker *et al.*, 2011). Studies of cell forces with microplates (Mitrossilis *et al.*, 2010) and pillar assays (Trichet *et al.*, 2012) have suggested that rigidity sensing is a more global process than formerly appreciated; however, models integrating focal adhesion dynamics over entire cells present a great challenge. Finally RNA-interference studies have revealed the regulatory complexity of rigidity sensing (Prager-Khoutorsky *et al.*, 2011), but a theoretical framework to integrate the biochemical, genetic and mechanical features of focal adhesions on a systems level is still missing.

Another important challenge is improving our understanding of cell behavior in three dimensions. The physiological environment of tissue cells in three dimensions is a viscoelastic porous matrix and it is thus not surprising that cell behavior in three dimensions tends to be different from the one on flat culture dishes (Baker and Chen, 2012; Cukierman *et al.*, 2001). Surprisingly, however, if one cultures cells in open three-dimensional scaffolds, many of the features known from two-dimensional scaffolds seem to be conserved (in particular arc-like stress fibers and focal adhesions) (Klein *et al.*, 2011, 2010). Recent experiments with three-dimensional hydrogels have shown that the dependence of cytoskeletal orientation on the matrix rigidity is similar in both two and three dimensions (Rehfeldt *et al.*, 2012). In the future, a careful quantitative comparison should be made of those factors that are substantially different in various experimental assays.

From the mechanical point of view, many of the theoretical models described here treat the CSK and the matrix as linear elastic materials in which the stresses are proportional to the strains. However, biopolymers that

are important in either the cytoskeleton or the extracellular matrix often show interesting non-linear responses to applied forces (Gardel *et al.*, 2004; Klotzsch *et al.*, 2009; Storm *et al.*, 2005) as discussed above. Generalizing the theory of stress generation, response and interactions of elastic dipoles to non-linear elastic environments, either within the CSK itself or via the coupling of actomyosin forces to non-linear substrates by focal adhesions, is thus an important future goal. Some experiments report that cells sense each other (most probably via elastic deformations) at distances on the order of $400\mu\text{m}$ (Winer *et al.*, 2009) on non-linear, elastic substrates. In addition, those observations report that cell spreading becomes independent of the (small-stress) elastic modulus, suggesting that a mechanical “tug-of-war” persists until neither the cell nor the non-linear substrate can increase its resistance (Winer *et al.*, 2009). A recent theory (Shokef and Safran, 2012a,b) of the deformations induced by force dipoles in non-linear elastic media predicts a linear-type response in the far-field regime, but with an amplitude that is magnified by the non-linearities important in the near-field where the stresses are large. The predicted amplification can be quite large even for modest forces applied by the dipole. This can also modify the interactions between dipoles. The theory suggests further quantitative measurements of the long-range effects reported in Winer *et al.* (2009) along with corresponding theoretical calculations of the interactions of force dipoles in non-linear elastic medium. An experimental hint of some non-linear effects was presented in Pompe *et al.* (2009) where a non-quadratic dependence of the deformation energy on the cellular force dipole moment was reported; linear elasticity would predict a quadratic dependence as in Eqs. 57 and 64.

Apart from making use of non-linear elasticity, another interesting avenue is the development of models for non-traditional mechanics, such as the actively contracting cable networks discussed in section V (Bischofs *et al.*, 2008; Guthardt Torres *et al.*, 2012). By focusing on two essential physical aspects of biological materials, namely the asymmetric mechanical response of filaments and the generation of tension by molecular motors, these models capture some of the essential physics but are still relatively easy to handle. This will allow the ideas to be used in new ways for detailed comparison with experiments on micropatterned and elastic substrates. Interestingly, these models also demonstrate a close relation between elasticity and tension (Bischofs *et al.*, 2008; Edwards and Schwarz, 2011; Guthardt Torres *et al.*, 2012; Mertz *et al.*, 2012a), which recently has been confirmed by experiments on cell layers (Mertz *et al.*, 2012a).

Although here we focused on the physical aspects of cellular systems, it is worth noting that some of the questions addressed in this framework come quite close to central questions currently studied in biology, for example stem cell differentiation and development. Experiments

that report genetic effects of substrate rigidity and their implications for stem cell differentiation (Engler *et al.*, 2006) are based on observations performed on the scale of several days while those that report the physical effects of CSK nematic order in response to rigidity changes (Zemel *et al.*, 2010b) are based on observations performed on the scale of hours. Are these two effects related and is CSK nematic order in stem cells and its optimization on substrates of particular rigidities a precursor of differential of stem cells into muscle cells? While it is true that muscle cells show highly developed nematic order of actomyosin bundles, it is not yet clear that the early-time development of nematic order in the same rigidity range triggers stem cell differentiation into muscle. Further experiments and models that explore how CSK stresses translate into nuclear stresses and possibly chromosomal rearrangements (Iyer *et al.*, 2012; Roopa *et al.*, 2008; Wang *et al.*, 2009; Zeng *et al.*, 2011) are needed before conclusions can be drawn.

Another, related area are the effects of elastic interactions, substrate rigidity, and applied stresses on development. Understanding the role of elastic stresses on development involves not only an interplay of genetic expression controlled by CSK and nuclear deformations within a single cell, but also the interactions of many developing cells via both chemical signals and elastic stresses. The spatial development of “order” as evidenced by differentiation within a developing tissue will be influenced by both the diffusion of signaling morphogens (Ben-Zvi *et al.*, 2008) as well as by the long-range elastic interactions explored here in simpler contexts. The connection to morphogen diffusion requires an understanding of the dynamical elastic interactions of cells and this may involve both their elastic (“speed of sound”) and viscous (damping) dynamics as well as a complete theory that may bridge the elastic nature of adherent cells to active-gel theories of cytoskeletal flow and cell motility (Julicher *et al.*, 2007; Kruse *et al.*, 2004; Liverpool and Marchetti, 2003; Marchetti *et al.*, 2013).

IX. ACKNOWLEDGEMENTS

The authors are grateful to L. Addadi, N. Balaban, M. Bastmeyer, A. Bershadsky, A. Besser, D. Ben-Yakov, I. Bischofs, A. Brown, A. Buxboim, K. Dasbiswas, R. De, D. Discher, C. Dunlop, T. Erdmann, J. Fredberg, B. Friedrich, F. Frischknecht, H. Gao, K. Garikpati, M. Gardel, B. Geiger, G. Genin, P. Guthardt Torres, B. Hoffmann, R. Kaunas, R. Kemkemer, M. Kozlov, E. Langbeheim, R. Merkel, D. Navajas, A. Nicolas, R. McMeeking, F. Rehfeldt, D. Riveline, B. Sabass, Y. Shokef, J. Spatz, X. Trepat, C. Waterman, J. Weichsel, Y. Yuval and A. Zemel for useful discussions and comments. USS is a member of the Heidelberg cluster of excellence CellNetworks and acknowledges support by the BMBF-

project MechanoSys and the EU-project MEHTRICS. SAS thanks the Israel Science Foundation, the Minerva Foundation, the Kimmel Stem Cell Institute and the U.S.-Israel Binational Science Foundation for its support.

REFERENCES

- Aegerter-Wilmsen, T., A. C. Smith, A. J. Christen, C. M. Aegerter, E. Hafner, and K. Basler (2010), Development **137** (3), 499.
- Albersdorfer, A., T. Feder, and E. Sackmann (1997), Biophysical Journal **73** (1), 245.
- Alberts, B., A. Johnson, P. Walter, J. Lewis, M. Raff, and K. Roberts (2007), *Molecular Biology of the Cell*, 5th ed. (Taylor & Francis).
- Ali, O., H. Guillou, O. Destaing, C. Albigs-Rizo, M. Block, and B. Fourcade (2011), Biophysical Journal **100** (11), 2595.
- Alliee, M., J.-C. Röper, K. P. Landsberg, C. Pentzold, T. J. Widmann, F. Julicher, and C. Dahmann (2012), Current Biology **22** (11), 967.
- Allioux-Guerin, M., D. Icard-Arcizet, C. Durieux, S. Henon, F. Gallet, J.-C. Mevel, M.-J. Masse, M. Tramier, and M. Coppey-Moisan (2009), Biophysical Journal **96** (1), 238.
- Ambrosi, D., G. Ateshian, E. Arruda, S. Cowin, J. Dumais, A. Goriely, G. Holzapfel, J. Humphrey, R. Kemkemer, E. Kuhl, J. Olberding, L. Taber, and K. Garikipati (2011), Journal of the Mechanics and Physics of Solids **59** (4), 863.
- Arfken, G., and H. Weber (1995), *Mathematical methods for physicists* (Academic Press).
- Baker, B. M., and C. S. Chen (2012), Journal of Cell Science **125** (13), 3015.
- Balaban, N. Q., U. S. Schwarz, D. Riveline, P. Goichberg, G. Tzur, I. Sabanay, D. Mahalu, S. Safran, A. Bershadsky, L. Addadi, and B. Geiger (2001), Nat. Cell Biol. **3**, 466.
- Banerjee, S., and M. C. Marchetti (2011), EPL (Europhysics Letters) **96** (2), 28003.
- Banerjee, S., and M. C. Marchetti (2012), Physical Review Letters **109** (10), 108101.
- Bar-Ziv, R., T. Tlusty, E. Moses, S. Safran, and A. Bershadsky (1999), Proceedings of the National Academy of Sciences USA **96** (18), 10140.
- Barnhart, E. L., K. Lee, K. Keren, A. Mogilner, and J. A. Theriot (2011), PLoS Biol **9** (5), e1001059.
- Basan, M., T. Risler, J. Joanny, X. Sastre-Garau, and J. Prost (2009), HFSP Journal **3** (4), 265.
- Bausch, A. R., and K. Kroy (2006), Nat Phys **2** (4), 231.
- de Beer, A., G. Majer, S. Roke, and J. Spatz (2010), Journal of Adhesion Science and Technology **24**, 2323.
- Beleggia, M., M. De Graef, and Y. Millev (2006), Philosophical Magazine **86** (16), 2451.
- Bell, G. (1978), Science **200** (4342), 618.
- Ben-Isaac, E., Y. Park, G. Popescu, F. Brown, G. NS, and S. Y (2011), Physical Review Letters **106**, 283103.
- Ben-Zvi, D., B. Shilo, A. Fainsod, and N. Barkai (2008), Nature **453**, 1205.
- Bershadsky, A., M. Kozlov, and B. Geiger (2006), Current Opinion in Cell Biology **18** (5), 472.
- Bershadsky, A. D., N. Q. Balaban, and B. Geiger (2003), Annual Review of Cell and Developmental Biology **19** (1), 677.
- Besser, A., J. Colombelli, E. H. K. Stelzer, and U. S. Schwarz (2011), Phys. Rev. E **83** (5), 051902.
- Besser, A., and S. Safran (2006), Biophysical Journal **90** (10), 3469.
- Besser, A., and U. S. Schwarz (2007), New J. Phys. **9**, 425.
- Besser, A., and U. S. Schwarz (2010), Biophys. J. **99**, L10.
- Bischofs, I. B., F. Klein, D. Lehnert, M. Bastmeyer, and U. S. Schwarz (2008), Biophys. J. **95**, 34883496.
- Bischofs, I. B., S. A. Safran, and U. S. Schwarz (2004), Phys. Rev. E **69**, 021911.
- Bischofs, I. B., S. S. Schmidt, and U. S. Schwarz (2009), Phys. Rev. Lett. **103**, 048101.
- Bischofs, I. B., and U. S. Schwarz (2003), Proc. Natl. Acad. Sci. USA **100**, 9274.
- Bischofs, I. B., and U. S. Schwarz (2005), Phys. Rev. Lett. **95**, 068102.
- Bischofs, I. B., and U. S. Schwarz (2006), Acta Biomaterialia **2**, 253.
- Boal, D. (2012), *Mechanics of the Cell*, 2nd ed. (Cambridge University Press).
- Brangwynne, C. P., F. C. MacKintosh, S. Kumar, N. A. Geisse, J. Talbot, L. Mahadevan, K. K. Parker, D. E. Ingber, and D. A. Weitz (2006), The Journal of Cell Biology **173** (5), 733.
- Bray, D. (2001), *Cell movements: from molecules to motility*, 2nd ed. (Garland, New York).
- Brown, R., R. Prajapati, D. McGrouther, I. Yannas, and M. Eastwood (1998), Journal of Cellular Physiology **175** (3), 323.
- Buehler, M. J., and S. Keten (2010), Reviews of Modern Physics **82** (2), 1459.
- Burridge, K., and E. S. Wittchen (2013), The Journal of Cell Biology **200** (1), 9.
- Bursac, P., G. Lenormand, B. Fabry, M. Oliver, D. Weitz, V. Viasnoff, J. Butler, and J. Fredberg (2005), Nature Materials **4**, 557.
- Butler, J. P., I. M. Toli-Nrrelykke, B. Fabry, and J. J. Fredberg (2002), American Journal of Physiology - Cell Physiology **282** (3), C595.
- Buxboim, A., I. Ivanovska, and D. Discher (2010), Journal of Cell Science **123** (3), 297.
- Califano, J. P., and C. A. Reinhart-King (2010), Cellular and molecular bioengineering **3** (1), 68.
- Cameron, A., J. Frith, and J. Cooper-White (2011), Biomaterials **32**, 5979.
- Camps, O., L. Mahadevan, and J. Joanny (2012), Biophysical Journal **102** (5), 1049.
- Canela-Xandri, O., F. Sagus, J. Casademunt, and J. Buceta (2011), PLoS Comput Biol **7** (9), e1002153.
- Canham, P. (1970), J. Theor. Biol. **26**, 61.
- Carlsson, A. (2003), Biophysical Journal **84** (5), 2907.
- Chaikin, P. M., and T. C. Lubensky (2000), *Principles of Condensed Matter Physics*, reprint ed. (Cambridge University Press).
- Chan, C., and D. Odde (2008), Science **322** (5908), 1687.
- Chen, C., R. Krishnan, E. Zhou, A. Ramachandran, D. Tambe, K. Rajendran, R. Adam, L. Deng, and J. Fredberg (2010a), PLoS One **5**, e12035.
- Chen, C. S. (2008), J. Cell Sci. **121**, 3285.
- Chen, C. S., M. Mrksich, S. Huang, G. M. Whitesides, and D. E. Ingber (1997), Science **276** (5317), 1425.
- Chen, D. T., Q. Wen, P. A. Janmey, J. C. Crocker, and A. G. Yodh (2010b), Annual Review of Condensed Matter Physics **1**, 301.

- Choquet, D., D. Felsenfeld, and M. Sheetz (1997), *Cell* **88** (1), 39.
- Chrzanowska-Wodnicka, M., and K. Burridge (1996), *The Journal of Cell Biology* **133** (6), 1403.
- Civelekoglu-Scholey, G., A. Wayne Orr, I. Novak, J.-J. Meister, M. Schwartz, and A. Mogilner (2005), *Journal of Theoretical Biology* **232** (4), 569.
- Cohen, M., D. Joester, B. Geiger, and L. Addadi (2004), *ChemBioChem* **5** (10), 1393.
- Collinsworth, A., C. Torgan, S. Nagda, R. Rajalingam, W. Kraus, and G. Truskey (2000), *Cell and Tissue Research* **302** (2), 243.
- Colombelli, J., A. Besser, H. Kress, E. Reynaud, P. Girard, E. Caussinus, U. Haselmann, J. Small, U. S. Schwarz, and E. Stelzer (2009), *J. Cell Sci.* **122**, 1665.
- Coughlin, M. F., and D. Stamenovic (2003), *Biophysical Journal* **84** (2), 1328.
- Crow, A., K. Webster, E. Hohlfeld, W. Ng, P. Geissler, and D. Fletcher (2012), *Biophysical Journal* **102** (3), 443.
- Cukierman, E., R. Pankov, D. R. Stevens, and K. M. Yamada (2001), *Science* **294** (5547), 1708.
- Cuvelier, D., M. Thery, Y. Chu, S. Dufour, J. Thiery, M. Bornens, P. Nassoy, and L. Mahadevan (2007), *Current Biology* **17** (8), 694.
- Dasanayake, N. L., P. J. Michalski, and A. E. Carlsson (2011), *Physical Review Letters* **107** (11), 118101.
- Davies, P., A. Robotewskyj, and M. Griem (1994), *Journal of Clinical Investigation* **93** (5), 2031.
- De, R., and S. Safran (2008), *Physical Review E* **78** (3).
- De, R., A. Zemel, and S. A. Safran (2007), *Nature Physics* **3** (9), 655.
- De, R., A. Zemel, and S. A. Safran (2008), *Biophysical Journal* **94** (5), L29.
- De, R., A. Zemel, and S. A. Safran (2010), *Methods in Cell Biology* **98C**, 143.
- Deibler, M., J. P. Spatz, and R. Kemkemer (2011), *PLoS ONE* **6** (8), e22941.
- Delano-Ayari, H., R. Al Kurdi, M. Vallade, D. Gulino-Debrac, and D. Riveline (2004), *Proceedings of the National Academy of Sciences of the United States of America* **101** (8), 2229.
- Delano-Ayari, H., J. P. Rieu, and M. Sano (2010), *Physical Review Letters* **105** (24), 248103.
- Dembo, M., and Y. Wang (1999), *Biophysical Journal* **76** (4), 2307.
- Deng, L., X. Trepat, J. P. Butler, E. Millet, K. G. Morgan, D. A. Weitz, and J. J. Fredberg (2006), *Nature Materials* **5** (8), 636.
- Deshpande, V. S., R. M. McMeeking, and A. G. Evans (2006), *Proceedings of the National Academy of Sciences* **103** (38), 14015.
- Deshpande, V. S., R. M. McMeeking, and A. G. Evans (2007), *Proceedings of the Royal Society A: Mathematical, Physical and Engineering Science* **463** (2079), 787.
- Diamant, H., and D. Andelman (1996), *J. Phys. Chem.* **100**, 13732.
- Dill, K. A., and S. Bromberg (2010), *Molecular Driving Forces: Statistical Thermodynamics in Chemistry and Biology*, revised ed. (Garland Pub.).
- Discher, D., D. Mooney, and P. Zandstra (2009), *Science* **324** (5935), 1673.
- Discher, D. E., P. Janmey, and Y.-l. Wang (2005), *Science* **310** (5751), 1139.
- Dogterom, M., and B. Yurke (1997), *Science* **278** (5339), 856.
- Doi, M. (1996), *Introduction to polymer physics* (Oxford Uni).
- DuFort, C. C., M. J. Paszek, and V. M. Weaver (2011), *Nat Rev Mol Cell Biol* **12** (5), 308.
- Duke, T. a. J. (1999), *Proceedings of the National Academy of Sciences* **96** (6), 2770.
- Eastwood, M., V. Mudera, D. McGrath, and R. Brown (1998), *Cell Motility and the Cytoskeleton* **40** (1), 13.
- Edwards, C. M., and U. S. Schwarz (2011), *Phys. Rev. Lett.* **107**, 128101.
- Engler, A., L. Bacakova, C. Newman, A. Hategan, M. Griffin, and D. Discher (2004a), *Biophysical Journal* **86** (1), 617.
- Engler, A., M. Griffin, S. Sen, C. Bonnet, H. Sweeney, and D. Discher (2004b), *Journal of Cell Biology* **166** (6), 877.
- Engler, A., S. Sen, H. Sweeney, and D. Discher (2006), *Cell* **126** (4), 677.
- Engler, A. J., C. Carag-Krieger, C. P. Johnson, M. Raab, H.-Y. Speicher, T. D. W. J. W. Sanger, J. M. Sanger, and D. E. Discher (2008), *J. Cell Sci.* **121**, 3794.
- Erdmann, T., and U. S. Schwarz (2004a), *Phys. Rev. Lett.* **92**, 108102.
- Erdmann, T., and U. S. Schwarz (2004b), *J. Chem. Phys.* **121**, 8997.
- Erdmann, T., and U. S. Schwarz (2012), *Phys. Rev. Lett.* **108**, 188101.
- Eshelby, J. D. (1957), *Proc. R. Soc. London, Ser. A* **241**, 376.
- Eshelby, J. D. (1959), *Proc. R. Soc. London, Ser. A* **252**, 561.
- Evans, E., and K. Ritchie (1997), *Biophysical Journal* **72** (4), 1541.
- Evans, E. A., and D. A. Calderwood (2007), *Science* **316** (5828), 1148.
- Farhadifar, R., J. Roper, B. Algouy, S. Eaton, and F. Julicher (2007), *Current Biology* **17** (24), 2095.
- Faust, U., N. Hampe, W. Rubner, N. Kirchgessner, S. Safran, B. Hoffmann, and R. Merkel (2011), *PLoS ONE* **6** (12), e28963.
- Fernandez, P., and A. Bausch (2009), *Integrative Biology* **1** (3), 252.
- Fery, A., and R. Weinkamer (2007), *Polymer* **48** (25), 7221.
- Filippov, A. E., J. Klafter, and M. Urbakh (2004), *Physical Review Letters* **92** (13), 135503.
- Fink, J., N. Carpi, T. Betz, A. Betard, M. Chebah, A. Azioune, M. Bornens, C. Sykes, L. Fetler, D. Cuvelier, and M. Piel (2011), *Nature Cell Biology* **13** (7), 771.
- Fletcher, D., and P. Geissler (2009), *Annual Review of Physical Chemistry* **60**, 469.
- Fletcher, D. A., and R. D. Mullins (2010), *Nature* **463** (7280), 485.
- Fletcher, D. A., and J. A. Theriot (2004), *Physical Biology* **1** (1), T1.
- Friedrich, B., E. Fischer-Friedrich, N. Gov, and S. SA (2012), *PLoS Com* **8**, e1002544.
- Friedrich, B. M., A. Buxboim, D. E. Discher, and S. A. Safran (2011), *Biophysical Journal* **100**, 2706.
- Friedrich, B. M., and S. A. Safran (2011), *EPL (Europhysics Letters)* **93** (2), 28007.
- Friedrich, B. M., and S. A. Safran (2012), *Soft Matter* **8** (11), 3223.
- Fu, J., Y. Wang, M. T. Yang, R. A. Desai, X. Yu, Z. Liu, and C. S. Chen (2010), *Nat Meth* **7** (9), 733.
- Fung, Y. C. (1993), *Biomechanics: mechanical properties of living tissues* (Springer Verlag, New York).
- Gao, H., J. Qian, and B. Chen (2011), *Journal of The Royal Society Interface* **8** (62), 1217.

- Gardel, M., J. Shin, F. MacKintosh, L. Mahadevan, P. Matsudaira, and D. Weitz (2004), *Science* **304** (5675), 1301.
- Gardel, M. L., K. E. Kasza, C. P. Brangwynne, J. Liu, and D. A. Weitz (2008a), *Methods in Cell Biology* **89**, 487.
- Gardel, M. L., B. Sabass, L. Ji, G. Danuser, U. S. Schwarz, and C. M. Waterman (2008b), *The Journal of Cell Biology* **183** (6), 999.
- Gauthier, N. C., M. A. Fardin, P. Roca-Cusachs, and M. P. Sheetz (2011), *Proceedings of the National Academy of Sciences* **108** (35), 14467.
- Gavara, N., P. Roca-Cusachs, R. Sunyer, R. Farre, and D. Navajas (2008), *Biophysical Journal* **95** (1), 464.
- Geiger, B., J. P. Spatz, and A. D. Bershadsky (2009), *Nat Rev Mol Cell Biol* **10** (1), 21.
- de Gennes, P. (1992), *Angewandte Chemie-international Edition in English* **31** (7), 842.
- de Gennes, P. G. (1979), *Scaling concepts in polymer physics* (Cornell University Press).
- de Gennes, P. G. (1985), *Reviews of Modern Physics* **57** (3), 827.
- de Gennes, P. G., and J. Prost (1995), *Physics of liquid crystals*, 2nd ed. (Oxford University Press).
- Gonzalez-Rodriguez, D., K. Guevorkian, S. Douezan, and F. Brochard-Wyart (2012), *Science* **338** (6109), 910.
- Gov, N. (2004), *Physical Review Letters* **93** (26), 10.1103/PhysRevLett.93.268104.
- Gov, N. S. (2006), *Physical Review Letters* **97**, 018101.
- Guo, M., and D. Weitz (2012), unpublished.
- Guthardt Torres, P., I. B. Bischofs, and U. S. Schwarz (2012), *Phys. Rev. E* **85**, 011913.
- Gurin, T., J. Prost, P. Martin, and J. Joanny (2010), *Current Opinion in Cell Biology* **22** (1), 14.
- Haken, H. (1983), *Synergetics, an Introduction: Nonequilibrium Phase Transitions and Self-Organization in Physics, Chemistry, and Biology* (Springer—Verlag).
- Hanggi, P., P. Talkner, and M. Borkovec (1990), *Reviews of Modern Physics* **62** (2), 251.
- Hayakawa, K., N. Sato, and T. Obinata (2001), *Experimental Cell Research* **268** (1), 104.
- Head, D. A., A. J. Levine, and F. C. MacKintosh (2003a), *Physical Review Letters* **91** (10), 108102.
- Head, D. A., A. J. Levine, and F. C. MacKintosh (2003b), *Physical Review E* **68** (6), 061907.
- Heil, P., and J. Spatz (2010), *Journal of Physics: Condensed Matter* **22**, 194108.
- Helfrich, W. (1973), *Z. Naturforsch. C* **28**, 693.
- Heussinger, C., and E. Frey (2006), *Physical Review Letters* **96** (1), 017802.
- Heussinger, C., B. Schaefer, and E. Frey (2007), *Physical Review E* **76** (3), 031906.
- Hoffman, B. D., C. Grashoff, and M. A. Schwartz (2011), *Nature* **475** (7356), 316.
- Hoffmann, M., and U. S. Schwarz (2013), *BMC Systems Biology* **7**, 2.
- Hotulainen, P., and P. Lappalainen (2006), *The Journal of Cell Biology* **173** (3), 383.
- Howard, J. (2001), *Mechanics of motor proteins and the cytoskeleton* (Sinauer Associates, Sunderland, Massachusetts).
- Hsu, H.-J., C.-F. Lee, and R. Kaunas (2009), *PLOS ONE* **4** (3).
- Huang, S., and D. Ingber (1999), *Nature Cell Biology* **1** (5), E131.
- Huber, F., J. Schnauss, S. Ronicke, P. Rauch, K. Muller, C. Futterer, and J. Kas (2013), *Advances in Physics* **62** (1), 1.
- Hufnagel, L., A. Teleman, H. Rouault, S. Cohen, and B. Shraiman (2007), *Proceedings of the National Academy of Sciences USA* **104** (10), 3835.
- Hur, S. S., Y. Zhao, Y. Li, E. Botvinick, and S. Chien (2009), *Cellular and Molecular Bioengineering* **2** (3), 425.
- Huxley, A. (1957), *Prog. Biophys. Chem.* **7**, 255.
- Ingber, D. (1993), *Journal of Cell Science* **104**, 613.
- Ingber, D. E. (2003), *Ann. Med.* **35**, 1.
- Isenberg, B., P. DiMilla, M. Walker, S. Kim, and J. Wong (2009), *Biophys. J.* **97**, 1313.
- Israelachvili, J. N. (2011), *Intermolecular and surface forces*, 3rd ed. (Academic Press, Waltham).
- Iyer, K. V., S. Maharana, S. Gupta, A. Libchaber, T. Tlusty, and G. V. Shivashankar (2012), *PLoS ONE* **7** (10), e46628.
- Jacot, J. G., A. D. McCulloch, and J. H. Omens (2008), *Biophysical journal* **95** (7), 3479.
- Janmey, P., S. Hydrt, J. Lamb, and T. Stossel (1990), *Nature* **345** (6270), 89.
- Janmey, P., J. Winer, M. Murray, and Q. Wen (2009), *Cell Motility and the Cytoskeleton* **66** (8), 597.
- Janmey, P. A., and R. T. Miller (2011), *Journal of Cell Science* **124** (1), 9.
- Johnson, K. L. (1985), *Contact mechanics* (Cambridge University Press, Cambridge).
- Johnson, K. L., K. Kendall, and A. D. Roberts (1971), *Proc. R. Soc. Lond. A* **324**, 301.
- Jones, R. A. (2002), *Soft Condensed Matter* (Oxford University Press).
- Julicher, F., K. Kruse, J. Prost, and J. Joanny (2007), *Physics Reports* **449** (1-3), 3.
- Julicher, F., and J. Prost (1995), *Physical Review Letters* **75** (13), 2618.
- Jungbauer, S., H. Gao, J. Spatz, and R. Kemkemer (2008), *Biophysical Journal* **95** (7), 3470.
- van Kampen, N. G. (1992), *Stochastic processes in physics and chemistry* (Elsevier, Amsterdam).
- Kaunas, R., H. J. Hsu, and S. Deguchi (2011), *Cell Health and Cytoskeleton* **3**, 13.
- Kaunas, R., P. Nguyen, S. Usami, and S. Chien (2005), *Proceedings of the National Academy of Sciences of the United States of America* **102** (44), 15895.
- Kawakami, K., H. Tatsumi, and M. Sokabe (2001), *Journal of Cell Science* **114** (17), 3125.
- Kilian, K., B. Bugarija, B. Lahn, and M. Mrksich (2010), *Proceedings of the National Academy of Sciences USA* **107** (11), 4872.
- Klein, F., B. Richter, T. Striebel, C. M. Franz, G. v. Freymann, M. Wegener, and M. Bastmeyer (2011), *Advanced Materials* **23** (11), 1341.
- Klein, F., T. Striebel, J. Fischer, Z. Jiang, C. M. Franz, G. von Freymann, M. Wegener, and M. Bastmeyer (2010), *Advanced Materials* **22** (8), 868.
- Klotzsch, E., M. L. Smith, K. E. Kubow, S. Muntwyler, W. C. Little, F. Beyeler, D. Gourdon, B. J. Nelson, and V. Vogel (2009), *Proceedings of the National Academy of Sciences of the United States of America* **106** (43), 18267.
- Klumpp, S., and R. Lipowsky (2005), *Proceedings of the National Academy of Sciences of the United States of America* **102** (48), 17284.
- Knoche, S., and J. Kierfeld (2011), *Physical Review E* **84** (4), 046608.

- Koenderink, G. H., Z. Dogic, F. Nakamura, P. M. Bendix, F. C. MacKintosh, J. H. Hartwig, T. P. Stossel, and D. A. Weitz (2009), Proceedings of the National Academy of Sciences **106** (36), 15192.
- Kohler, S., V. Schaller, and A. R. Bausch (2011), Nat Mater **10** (6), 462.
- Kollmannsberger, P., C. M. Bidan, J. W. C. Dunlop, and P. Fratzl (2011), Soft Matter **7** (20), 9549.
- Kollmannsberger, P., and B. Fabry (2011), Annu. Rev. Mater. Res. **41**, 75.
- Komura, S., K. Tamura, and T. Kato (2005), The European Physical Journal E: Soft Matter and Biological Physics **18** (3), 343.
- Korff, T., and H. Augustin (1999), Journal of Cell Science **112** (19), 3249.
- Kovar, D. R. (2006), Current Opinion in Cell Biology **18**, 11.
- Krishnan, R., C. Park, Y. Lin, M. J. R. Jaspers, X. Trepaut, G. Lenormand, D. Tambe, A. Smolensky, A. Knoll, J. Butler, and F. JJ (2009), Plos One **4**, e5486.
- Kruse, K., J. Joanny, F. Julicher, J. Prost, and K. Sekimoto (2004), Physical Review Letters **92** (7).
- Kruse, K., and F. Julicher (2000a), Physical Review Letters **85** (8), 1778.
- Kruse, K., and F. Julicher (2000b), Physical Review Lett **85**, 1778.
- Kruse, K., and F. Julicher (2003), Physical Review E **67** (5).
- Kruse, K., A. Zumdieck, and F. Julicher (2003), Europhysics **64**, 716722.
- Kumar, S., I. Z. Maxwell, A. Heisterkamp, T. R. Polte, T. P. Lele, M. Salanga, E. Mazur, and D. E. Ingber (2006), Biophysical Journal **90** (10), 3762.
- Kuo, J., X. Han, C. Hsiao, J. R. Yates III, and C. M. Waterman (2011), Nat Cell Biol **13** (4), 383.
- Kurpinski, K., J. Chu, C. Hashi, and S. Li (2006), PNAS **103** (44), 16095.
- Ladoux, B., and A. Nicolas (2012), Reports on Progress in Physics **75** (11), 116601.
- Landau, L. D., and E. M. Lifshitz (1970), *Theory of elasticity*, 2nd ed., Course of Theoretical Physics, Vol. 7 (Pergamon Press, Oxford).
- Landsberg, K. P., R. Farhadifar, J. Ranft, D. Umetsu, T. J. Widmann, T. Bittig, A. Said, F. Jlicher, and C. Dahmann (2009), Current Biology **19** (22), 1950.
- Lau, K., and W. Kohn (1977), Surface Science **65** (2), 607.
- Lauffenburger, D. A., and A. F. Horwitz (1996), Cell **84** (3), 359.
- Lecuit, T., and P. Lenne (2007), Nat Rev Mol Cell Biol **8** (8), 633.
- Lee, K., and A. J. Liu (2009), Biophysical Journal **97** (5), 1295.
- Legant, W. R., C. K. Choi, J. S. Miller, L. Shao, L. Gao, E. Betzig, and C. S. Chen (2013), Proceedings of the National Academy of Sciences **110** (3), 881.
- Lele, T. P., J. Pendse, S. Kumar, M. Salanga, J. Karavitis, and D. E. Ingber (2006), Journal of Cellular Physiology **207** (1), 187.
- Lenne, P.-F., and A. Nicolas (2009), Soft Matter **5** (15), 2841.
- Lenz, M., T. Thoresen, M. Gardel, and D. AR (2012), Physical Review Letters **108**, 238107.
- Li, Y., P. Bhimalapuram, and A. R. Dinner (2010), Journal of Physics: Condensed Matter **22**, 194113.
- Lieleg, O., M. Claessens, Y. Luan, and A. Bausch (2008), Phys. Rev. Lett. **101**, 108101.
- Lim H. W., G., M. Wortis, and R. Mukhopadhyay (2002), Proceedings of the National Academy of Sciences **99** (26), 16766.
- Lipowsky, R. (1996), Physical Review Letters **77** (8), 1652.
- Liverpool, T., and M. Marchetti (2003), Physical Review Letters **90** (13).
- Lo, C., H. Wang, M. Dembo, and Y. Wang (2000), Biophysical Journal **79** (1), 144.
- Lobkovsky, A., S. Gentges, H. Li, D. Morse, and T. A. Witten (1995), Science **270** (5241), 1482.
- Loosli, Y., R. Luginbuehl, and J. G. Snedeker (2010), Philosophical Transactions of the Royal Society A: Mathematical, Physical and Engineering Sciences **368** (1920), 2629.
- Lu, L., Y. Feng, W. Hucker, S. Oswald, G. Longmore, and F. Yin (2008), Cell Motility and the Cytoskeleton **65**, 281.
- Luo, Y., X. Xu, T. Lele, S. Kumar, and D. Ingber (2008), Journal of Biomechanics **41** (11), 2379.
- Macdonald, A., A. R. Horwitz, and D. A. Lauffenburger (2008), Cell Adhesion & Migration **2** (2), 95.
- MacKintosh, F. (2006), in *Soft Condensed Matter Physics in Molecular and Cell Biology* (CRC Press).
- MacKintosh, F. C., and C. F. Schmidt (2010), Current Opinion in Cell Biology **22** (1), 29.
- Maier, W., and A. Saupe (1959), Z. Naturforschg. **14**, 882.
- Majkut, S. F., and D. E. Discher (2012), Biomechanics and Modeling in Mechanobiology **11** (8), 1219.
- Manneville, J., P. Bassereau, S. Ramaswamy, and J. Prost (2001), Physical Review E **64** (2).
- Marchetti, M. C., J. F. Joanny, S. Ramaswamy, T. B. Liverpool, J. Prost, M. Rao, and R. A. Simha (2013), Rev. Mod. Phys. **85**, 1143.
- Marcq, P., N. Yoshinaga, and J. Prost (2011), Biophysical Journal **101** (6), L33.
- Marcy, Y., J.-F. Joanny, J. Prost, and C. Sykes (2007), New Journal of Physics **9** (11), 431.
- Marcy, Y., J. Prost, M. Carlier, and C. Sykes (2004), Proceedings of the National Academy of Sciences of the United States of America **101** (16), 5992.
- Marko, J., and E. Siggia (1995), Macromolecules **28**, 8759.
- McGarry, J. P., J. Fu, M. T. Yang, C. S. Chen, R. M. McMeeking, A. G. Evans, and V. S. Deshpande (2009), Philosophical Transactions of the Royal Society A: Mathematical, Physical and Engineering Sciences **367** (1902), 3477.
- McKenna, N. M., C. S. Johnson, and Y. L. Wang (1986), The Journal of cell biology **103** (6 Pt 1), 2163.
- McMahon, T. A. (1984), *Muscles, reflexes, and locomotion* (Princeton University Press, Princeton, New Jersey).
- Menes, R., and S. A. Safran (1997), Physical Review E **56** (2), 1891.
- Mertz, A. F., S. Banerjee, Y. Che, G. K. German, Y. Xu, C. Hyland, M. C. Marchetti, V. Horsley, and E. R. Dufresne (2012a), Physical Review Letters **108** (19), 198101.
- Mertz, A. F., Y. Che, S. Banerjee, J. M. Goldstein, K. A. Rosowski, S. F. Revilla, C. M. Niessen, M. C. Marchetti, E. R. Dufresne, and V. Horsley (2012b), Proceedings of the National Academy of Sciences .
- Miao, L., U. Seifert, M. Wortis, and H. Dbereiner (1994), Physical Review E **49** (6), 5389.
- Mitra, S. K., D. A. Hanson, and D. D. Schlaepfer (2005), Nature Reviews Molecular Cell Biology **6** (1), 56.
- Mitragotri, S., and J. Lahann (2009), Nat Mater **8** (1), 15.

- Mitrossilis, D., J. Fouchard, A. Guiroy, N. Desprat, N. Rodriguez, B. Fabry, and A. Asnacios (2009), Proceedings of the National Academy of Sciences **106** (43), 18243.
- Mitrossilis, D., J. Fouchard, D. Pereira, F. Postic, A. Richert, M. Saint-Jean, and A. Asnacios (2010), Proceedings of the National Academy of Sciences **107** (38), 16518.
- Mizuno, D., C. Tardin, C. F. Schmidt, and F. C. MacKintosh (2007), Science **315** (5810), 370.
- Mogilner, A. (2006), Current Opinion in Cell Biology **18** (1), 32.
- Mogilner, A., and K. Keren (2009), Current Biology **19**, R762.
- Mogilner, A., and B. Rubinstein (2005), Biophysical Journal **89** (2), 782.
- Mura, T. (1991), *Micromechanics of defects* (Kluwer Academic, Dordrecht).
- Murrell, M. P., and M. L. Gardel (2012), Proceedings of the National Academy of Sciences **109** (51), 20820.
- Nekouzadeh, A., K. M. Pryse, E. L. Elson, and G. M. Genin (2008), Journal of Biomechanics **41** (14), 2964.
- Nelson, C., R. Jean, J. Tan, W. Liu, N. Sniadecki, A. Spector, and C. Chen (2005), Proceedings of the National Academy of Sciences of the United States of America **102** (33), 11594.
- Nicolas, A., A. Besser, and S. A. Safran (2008), Biophysical Journal **95** (2), 527.
- Nicolas, A., B. Geiger, and S. Safran (2004), Proceedings of the National Academy of Sciences of the United States of America **101** (34), 12520.
- Nicolas, A., and S. Safran (2006a), Biophysical Journal **91** (1), 61.
- Nicolas, A., and S. Safran (2006b), Biophysical Journal **91** (1), 61.
- Nicolas, A., and S. A. Safran (2004), Phys. Rev. E **69**, 051902.
- Nobuhiko Sait, K. T., and Y. Yunoki (1967), Journal of the Physical Society of Japan **22**, 219.
- Noguchi, H., and G. Gompper (2005), Proceedings of the National Academy of Sciences of the United States of America **102** (40), 14159.
- Olberding, J., M. Thouless, E. Arruda, and K. Garikipati (2010), PLoS ONE **5**, e12043.
- Paluch, E., and C. Heisenberg (2009), Current Biology **19** (17), R790.
- Parekh, S. H., O. Chaudhuri, J. A. Theriot, and D. A. Fletcher (2005), Nat Cell Biol **7** (12), 1219.
- Parker, K. K., A. L. Brock, C. Brangwynne, R. J. Mannix, N. Wang, E. Ostuni, N. A. Geisse, J. C. Adams, G. M. Whitesides, and D. E. Ingber (2002), The FASEB Journal **16** (10), 1195.
- Pate, E., G. Wilson, M. Bhimani, and R. Cooke (1994), Biophysical Journal **66** (5), 1554.
- Pathak, A., V. Deshpande, R. McMeeking, and A. Evans (2008), Journal of The Royal Society Interface **5** (22), 507.
- Patla, I., T. Volberg, N. Elad, V. Hirschfeld-Warneken, C. Grashoff, R. Fassler, J. P. Spatz, B. Geiger, and O. Medalia (2010), Nat Cell Biol **12** (9), 909.
- Paul, R., P. Heil, J. P. Spatz, and U. S. Schwarz (2008), Biophys. J. **94**, 1470.
- Pearson, H. (2008), Nature **453**, 150.
- Pelham, R., and Y. Wang (1997), Proceedings of the National Academy of Sciences of the United States of America **94** (25), 13661.
- Pellegrini, S., and H. Mellor (2007), Journal of Cell Science **120** (20), 3491.
- Peterson, L. J., Z. Rajfur, A. S. Maddox, C. D. Freel, Y. Chen, M. Edlund, C. Otey, and K. Burridge (2004), Molecular Biology of the Cell **15** (7), 3497.
- Phillips, R., J. Kondev, and J. Theriot (2008), *Physical Biology of the Cell*, 1st ed. (Taylor & Francis).
- Pieranski, P. (1983), Contemporary Physics **24** (1), 25.
- Pinto, I. M., B. Rubinstein, A. Kucharavy, J. R. Unruh, and R. Li (2012), Developmental Cell **22**, 12471260.
- Pirentis, A., and P. Lazopoulos (2009), Arch. Appl. Mech. **77**, 263.
- Pirentis, A., E. Peruski, A. Jordan, and D. Stamenovic (2011), Cellular and Molecular Bioengineering **4**, 67.
- Placais, P., M. Balland, T. Gurin, J. Joanny, and P. Martin (2009), Physical Review Letters **103** (15), 158102.
- Plotnikov, S. V., A. M. Pasapera, B. Sabass, and C. M. Waterman (2012), Cell **151** (7), 1513.
- Pollard, T. D., and J. Berro (2009), Journal of Biological Chemistry **284** (9), 5433.
- Pollard, T. D., and G. G. Borisy (2003), Cell **112** (4), 453.
- Pollard, T. D., and J. A. Cooper (2009), Science **326** (5957), 1208.
- Pompe, T., S. Glorius, T. Bischoff, I. Uhlmann, M. Kauffmann, S. Brenner, and C. Werner (2009), Biophysical Journal **97** (8), 2154.
- Ponti, A., M. Machacek, S. L. Gupton, C. M. Waterman-Storer, and G. Danuser (2004), Science **305** (5691), 1782.
- Powers, T. R. (2010), Reviews of Modern Physics **82** (2), 1607.
- Pozrikidis, C., and C. Pozrikidis (2003), *Modeling and Simulation of Capsules and Biological Cells* (CRC Press).
- Prager-Khoutorsky, M., A. Lichtenstein, R. Krishnan, K. Rajendran, A. Mayo, Z. Kam, B. Geiger, and A. D. Bershadsky (2011), Nat Cell Biol **13** (12), 1457.
- Prass, M., K. Jacobson, A. Mogilner, and M. Radmacher (2006), The Journal of Cell Biology **174** (6), 767.
- Pullarkat, P. A., P. Dommersnes, P. Fernández, J. Joanny, and A. Ott (2006), Physical Review Letters **96** (4), 048104.
- Qian, J., J. Wang, and H. Gao (2008), Langmuir **24** (4), 1262.
- Ramaswamy, S. (2010), Annual Review of Condensed Matter Physics **1** (1), 323.
- Ranft, J., M. Basan, J. Elgeti, J.-F. Joanny, J. Prost, and F. Julicher (2010), PNAS **107** (49), 20863.
- Rauzi, M., P. Verant, T. Lecuit, and P. Lenne (2008), Nature Cell Biology **10** (12), 1401.
- Rehfeldt, F., A. Brown, M. Raab, S. Cai, A. Zajac, A. Zemel, and D. DE (2012), Integrative Biology **4**, 422430.
- Reinhart-King, C. A., M. Dembo, and D. A. Hammer (2008), Biophysical Journal **95** (12), 6044.
- Rhee, D., J. M. Sanger, and J. W. Sanger (1994), Cell motility and the cytoskeleton **28** (1), 1.
- Ridley, A. J. (2011), Cell **145** (7), 1012.
- Riehl, B., J.-H. Park, I. Kwon, and J. Lim (2012), Tissue Engineering Part B **18**, 288.
- Riveline, D., E. Zamir, N. Q. Balaban, U. S. Schwarz, T. Ishizaki, S. Narumiya, Z. Kam, B. Geiger, and A. D. Bershadsky (2001), J. Cell Biol. **153** (6), 1175.
- Roopa, T., A. Mazumder, A. Basu, M. L., and S. GV (2008), Biophysical Journal **95**, 3028.
- Rubinstein, M., and R. Colby (2003), *Polymer Physics* (Oxford U.).
- Russell, R. J., S. Xia, R. B. Dickinson, and T. P. Lele (2009), Biophysical Journal **97** (6), 1578.

- Sabass, B., M. L. Gardel, C. M. Waterman, and U. S. Schwarz (2008), *Biophys. J.* **94**, 207.
- Sabass, B., and U. S. Schwarz (2010), *Journal of Physics: Condensed Matter* **22**, 194112.
- Saez, A., A. Buguin, P. Silberzan, and B. Ladoux (2005), *Biophysical Journal* **89** (6), L52.
- Saez, A., M. Ghibaudo, A. Buguin, P. Silberzan, and B. Ladoux (2007), *Proceedings of the National Academy of Sciences of the United States of America* **104** (20), 8281.
- Safran, S. (2003), *Statistical Thermodynamics of Surfaces, Interfaces, and Membranes*, reprint ed. (Westview Pr).
- Safran, S., and R. De (2009), *Physical Review E* **80** (6).
- Safran, S., and D. Hamann (1979), *Physical Review Letters* **42** (21), 1410.
- Safran, S. A. (1999), *Advances in Physics* **48** (4), 395.
- Samuel, J., and H. Vandenburg (1990), *In Vitro Cellular & Developmental Biology* **26** (9), 905.
- Savir, Y., E. Noor, R. Milo, and T. Tlusty (2010), *PNAS* **107** (8), 3475.
- Schallamach, A. (1963), *Wear* **6**, 375.
- Schreiber, C. H., M. Stewart, and T. Duke (2010), *Proceedings of the National Academy of Sciences* **107** (20), 9141.
- Schwarz, U. S. (2007), *Soft Matter* **3**, 263.
- Schwarz, U. S., N. Q. Balaban, D. Riveline, A. Bershadsky, B. Geiger, and S. A. Safran (2002), *Biophys. J.* **83**, 1380.
- Schwarz, U. S., and I. B. Bischofs (2005), *Med. Eng. Phys.* **27**, 763.
- Schwarz, U. S., T. Erdmann, and I. B. Bischofs (2006), *BioSystems* **83**, 225.
- Schwarz, U. S., and M. L. Gardel (2012), *J. Cell Sci.* **125**, 3051.
- Schwarz, U. S., and G. Gompper (2002), in *Morphology of Condensed Matter: Physics and Geometry of Spatially Complex Systems*, Lecture Notes in Physics, Vol. 600, edited by K. R. Mecke and D. Stoyan (Springer, Heidelberg) pp. 107–151.
- Schwarz, U. S., S. Komura, and S. A. Safran (2000), *Europhys. Lett.* **50**, 762.
- Schwarz, U. S., and S. A. Safran (2002), *Phys. Rev. Lett.* **88**, 048102.
- Seifert, U. (1997), *Advances in Physics* **46** (1), 13.
- Seifert, U., K. Berndl, and R. Lipowsky (1991), *Physical Review A* **44** (2), 1182.
- Seifert, U., and R. Lipowsky (1990), *Physical Review A* **42** (8), 4768.
- Serena, E., S. Zatti, E. Reghelin, A. Pasut, E. Cimetta, and N. Elvasorre (2010), *Integr. Biol.* **2**, 193.
- Shao, D., W.-J. Rappel, and H. Levine (2010), *Physical Review Letters* **105** (10), 108104.
- Shemesh, T., A. Bershadsky, D., and M. M. Kozlov (2012), *Biophysical Journal* **102** (8), 1746.
- Shemesh, T., B. Geiger, A. Bershadsky, and M. Kozlov (2005), *Proceedings of the National Academy of Sciences of the United States of America* **102** (35), 12383.
- Shemesh, T., A. B. Verkhovsky, T. M. Svitkina, A. D. Bershadsky, and M. M. Kozlov (2009), *Biophysical Journal* **97** (5), 1254.
- Shirinsky, V., A. Antonov, K. Birukov, A. Sobolevsky, Y. Romanov, N. Kabaeva, G. Antonova, and V. Smirnov (1989), *Journal of Cell Biology* **109** (1), 331.
- Shokef, Y., and S. A. Safran (2012a), *Physical Review Letters* **109**, 169901.
- Shokef, Y., and S. A. Safran (2012b), *Physical Review Letters* **108** (17), 178103.
- Shraiman, B. (2005), *Proceedings of the National Academy of Sciences of the United States of America* **102** (9), 3318.
- Shtengel, G., J. A. Galbraith, C. G. Galbraith, J. Lippincott-Schwartz, J. M. Gillette, S. Manley, R. Sougrat, C. M. Waterman, P. Kanchanawong, M. W. Davidson, R. D. Fetter, and H. F. Hess (2009), *Proceedings of the National Academy of Sciences* **106** (9), 3125.
- Siems, R. (1968), *Physica Status Solidi* **30** (2), 645.
- Silva, M. S. e., M. Depken, B. Stuhrmann, M. Korsten, F. C. MacKintosh, and G. H. Koenderink (2011), *Proceedings of the National Academy of Sciences* **108** (23), 9408.
- Smith, A., and U. Seifert (2005), *Physical Review E* **71** (6), 061902.
- Smith, A., K. Sengupta, S. Goennenwein, U. Seifert, and E. Sackmann (2008), *Proceedings of the National Academy of Sciences* **105** (19), 6906.
- Solon, J., I. Levental, K. Sengupta, P. C. Georges, and P. A. Janmey (2007), *Biophysical Journal* **93** (12), 4453.
- Srinivasan, M., and S. Walcott (2009), *Physical Review E* **80** (4).
- Stachowiak, M., P. McCall, T. Thoresen, H. Balciooglu, L. Kasiewicz, M. Gardel, and B. O'Shaughnessy (2012), *Biophysical Journal* **103** (6), 1265.
- Stachowiak, M. R., and B. O'Shaughnessy (2008), *New Journal of Physics* **10**, 025002.
- Stachowiak, M. R., and B. O'Shaughnessy (2009), *Biophysical Journal* **97** (2), 462.
- Stamenovic, D., and D. E. Ingber (2009), *Soft Matter* **5** (6), 1137.
- Stamenovic, D., S. Mijailovich, I. Tolic-Norrelykke, J. Chen, and N. Wang (2002), *American Journal of Physiology-Cell Physiology* **282** (3), C617.
- Stamenovic, D., N. Rosenblatt, M. Montoya-Zavala, B. D. Matthews, S. Hu, B. Suki, N. Wang, and D. E. Ingber (2007), *Biophysical Journal* **93** (8), L39.
- Storm, C., J. Pastore, F. MacKintosh, T. Lubensky, and P. Janmey (2005), *Nature* **435** (7039), 191.
- Stricker, J., Y. Aratyn-Schaus, P. W. Oakes, and M. L. Gardel (2011), *Biophysical Journal* **100** (12), 2883.
- Stricker, J., T. Falzone, and M. L. Gardel (2010), *Journal of Biomechanics* **43** (1), 9.
- Svitkina, T. M., and G. G. Borisy (1999), *The Journal of Cell Biology* **145** (5), 1009.
- Takakuda, K., and H. Miyairi (1996), *Biomaterials* **17**, 1393.
- Tan, J. L., J. Tien, D. M. Pirone, D. S. Gray, K. Bhadriraju, and C. S. Chen (2003), *Proceedings of the National Academy of Sciences* **100** (4), 1484.
- Tang, X., P. Bajaj, R. Bashir, and T. A. Saif (2011), *Soft Matter* **7** (13), 6151.
- Tawada, K., and K. Sekimoto (1991), *Journal of Theoretical Biology* **150** (2), 193.
- Tempel, M., G. Isenberg, and E. Sackmann (1996), *Physical Review E* **54** (2), 1802.
- Thery, M., A. Jimenez-Dalmaroni, V. Racine, M. Bornens, and F. Julicher (2007), *Nature* **447** (7143), 493.
- Thery, M., A. Pepin, E. Dressaire, Y. Chen, and M. Bornens (2006), *Cell Motility and the Cytoskeleton* **63** (6), 341.
- Thompson, D. W. (1992), *On Growth and Form*, abridged ed. (Cambridge University Press).
- Thoresen, T., M. Lenz, and M. L. Gardel (2011), *Biophysical Journal* **100** (11), 2698.
- Thoresen, T., M. Lenz, and M. L. Gardel (2013), *Biophysical Journal* **104** (3), 655.

- Tondon, A., H. Hsu, and R. Kaunas (2012), Journal of Biomechanics **45** (5), 728.
- Trappmann, B., J. E. Gautrot, J. T. Connelly, D. G. T. Strange, Y. Li, M. L. Oyen, M. A. C. Stuart, H. Boehm, B. Li, V. Vogel, J. P. Spatz, F. M. Watt, and W. T. S. Huck (2012), Nature Materials **11** (7), 642.
- Trepat, X., L. Deng, S. An, D. Navajas, D. Tschumperlin, W. Gerthoffer, J. Butler, and J. Fredberg (2007), Nature **447**, 592.
- Trepat, X., M. Grabulosa, F. Puig, Maksym, GN., D. Navajas, and R. Farre (2004), American Journal of Physiology **287**, L1025.
- Trepat, X., F. Puig, N. Gavara, J. Fredberg, R. Farre, and D. Navajas (2006), American Journal of Physiology **290**, L1104.
- Trichet, L., J. Le Digabel, R. J. Hawkins, S. R. K. Vedula, M. Gupta, C. Ribrault, P. Hersen, R. Voituriez, and B. Ladoux (2012), Proceedings of the National Academy of Sciences .
- Tseng, Q., E. Duchemin-Pelletier, A. Deshiere, M. Balland, H. Guillou, O. Filhol, and M. Thry (2012), Proceedings of the National Academy of Sciences **109** (5), 1506.
- Urban, E., S. Jacob, M. Nemethova, G. P. Resch, and J. V. Small (2010), Nat Cell Biol **12** (5), 429.
- Veigel, C., J. E. Molloy, S. Schmitz, and J. Kendrick-Jones (2003), Nat Cell Biol **5** (11), 980.
- Verkhovsky, A. B., and G. G. Borisy (1993), The Journal of Cell Biology **123** (3), 637.
- Vianay, B., J. Kafer, E. Planus, M. Block, F. Graner, and H. Guillou (2010), Physical Review Letters **105** (12).
- Vilfan, A., and T. Duke (2003), Biophysical Journal **85** (2), 818.
- Vliegenthart, G. A., and G. Gompper (2006a), Nature Materials **5** (3), 216.
- Vliegenthart, G. A., and G. Gompper (2006b), Biophysical Journal **91** (3), 834.
- Vogel, V., and M. Sheetz (2006), Nat Rev Mol Cell Biol **7** (4), 265.
- Vogel, V., and M. Sheetz (2009), Current Opinion in Cell Biology **21** (1), 38.
- Wagner, H., and H. Horner (1974), Advances in Physics **23** (4), 587.
- Walcott, S., D. Kim, D. Wirz, and S. X. Sun (2011), Biophysical Journal **101** (12), 2919.
- Walcott, S., and S. Sun (2010), Proceedings of the National Academy of Sciences of the United States of America **107** (17), 7757.
- Wang, J., P. Goldschmidt-Clermont, J. Wille, and F. Yin (2001), Journal of Biomechanics **34** (12), 1563.
- Wang, J., and E. Grood (2000), Connective Tissue Research **41** (1), 29.
- Wang, N., J. Tytell, and D. Ingber (2009), Nat. Reviews MCB **10**, 75.
- Wei, Z., V. Deshpande, R. McMeeking, and E. AG (2008), J. Biomed. Eng. **130**, 031009.
- Weichsel, J., and U. S. Schwarz (2010), Proc. Natl. Acad. Sci. USA **107**, 6304.
- Weichsel, J., E. Urban, J. V. Small, and U. S. Schwarz (2012), Cytometry Part A **81A**, 496.
- Weikl, T. R., and R. Lipowsky (2001), Physical Review E **64** (1), 011903.
- von Wichert, G., B. Haimovich, G. Feng, and M. Sheetz (2003), EMBO Journal **22**, 5023.
- Wilhelm, J., and E. Frey (2003), Physical Review Letters **91** (10), 108103.
- Winer, J., S. Oake, and J. PA (2009), PLOS One **4**, e6382.
- Wolfenson, H., A. Bershadsky, Y. I. Henis, and B. Geiger (2011), Journal of Cell Science **124** (9), 1425 .
- Wottawah, F., S. Schinkinger, B. Lincoln, R. Ananthakrishnan, M. Romeyke, J. Guck, and J. Kas (2005), Physical Review Letters **94** (9), 098103.
- Xu, J., D. Wirtz, and T. Pollard (1998), Journal of Biological Chemistry **273** (16), 9570.
- Yeung, T., P. Georges, L. Flanagan, B. Marg, M. Ortiz, M. Funaki, N. Zahir, W. Ming, V. Weaver, and P. Janmey (2005), Cell Motility and the Cytoskeleton **60** (1), 24.
- Yoshinaga, N., J. Joanny, J. Prost, and P. Marcq (2010), Physical Review Letters **105** (23), 238103.
- Zahn, J., I. Louban, S. Jungbauer, M. Bissinger, D. Kauffmann, R. Kemkemer, and J. Spatz (2011), Small **7**, 1480.
- Zaidel-Bar, R., C. Ballestrem, Z. Kam, and B. Geiger (2003), Journal of Cell Science **116** (22), 4605.
- Zaidel-Bar, R., S. Itzkovitz, A. Ma'ayan, R. Iyengar, and B. Geiger (2007), Nat Cell Biol **9** (8), 858.
- Zand, M. S., and G. Albrecht-Buehler (1989), Cell Motility and the Cytoskeleton **13** (3), 195.
- Zemel, A., I. Bischofs, and S. Safran (2006), Physical Review Letters **97** (12).
- Zemel, A., F. Rehfeldt, A. E. X. Brown, D. E. Discher, and S. A. Safran (2010a), Journal of Physics-Condensed Matter **22**, 194110.
- Zemel, A., F. Rehfeldt, A. E. X. Brown, D. E. Discher, and S. A. Safran (2010b), Nature Physics **6** (6), 468.
- Zemel, A., and S. A. Safran (2007), Phys. Rev. E **76**, 021905.
- Zeng, Y., A. Yip, S.-K. Teo, and K.-H. Chiam (2011), Biomech Model Mechanobiol **11**, 49.
- Zhao, X., C. Laschinger, P. Arora, K. Szàszi, A. Kapus, and M. CA (2007), J. Cell **120**, 1801.
- Ziebert, F., S. Swaminathan, and I. S. Aranson (2012), Journal of The Royal Society Interface **9** (70), 1084.
- Ziebert, F., and W. Zimmermann (2004), Physical Review E **70** (2), 022902.
- Zilman, A., and S. Safran (2003), Europhysics Letters **63**, 139.
- Zimmermann, J., C. Brunner, M. Enculescu, M. Goegler, A. Ehrlicher, J. Kas, and M. Falcke (2012), Biophysical Journal **102** (2), 287.
- Zuckerman, D., and R. Bruinsma (1995), Physical Review Letters **74** (19), 3900.